Computing Some Critical Multiscale Phenomena in Fluids and Combustion

Ahmed F. Ghoniem

Massachusetts Institute of Technology

Applied Modeling & Simulation (AMS) Seminar Series

NASA Ames Research Center, 30 March 2015

MITMECHE

RGD Group, 2013

Motivation: CO_2 & Global Warming

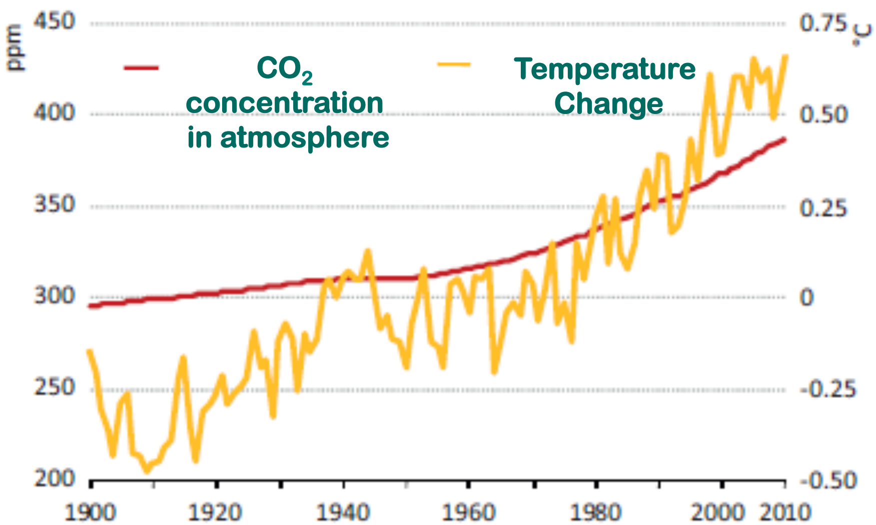

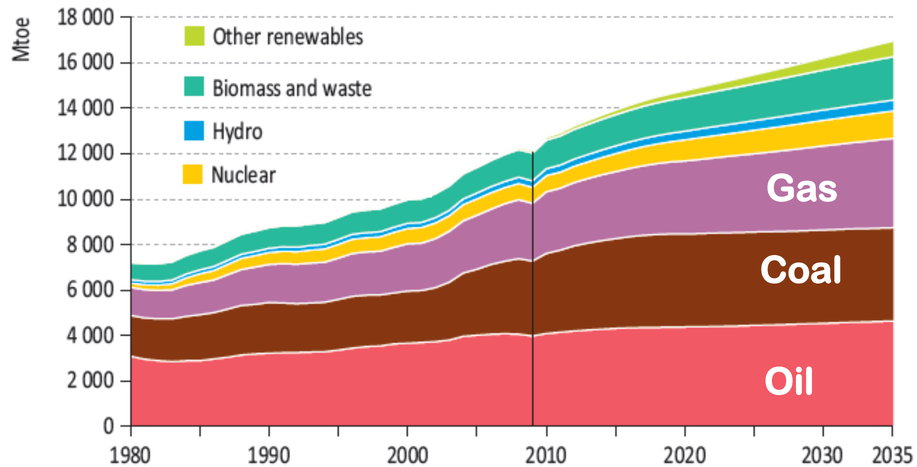

Facts:

1. Global Warming is attributed to CO_2
2. Fossil fuel combustion will remain the major energy supplier in the near future
3. Power generation with fossil fuels emits 1/3 CO_2 of overall emissions

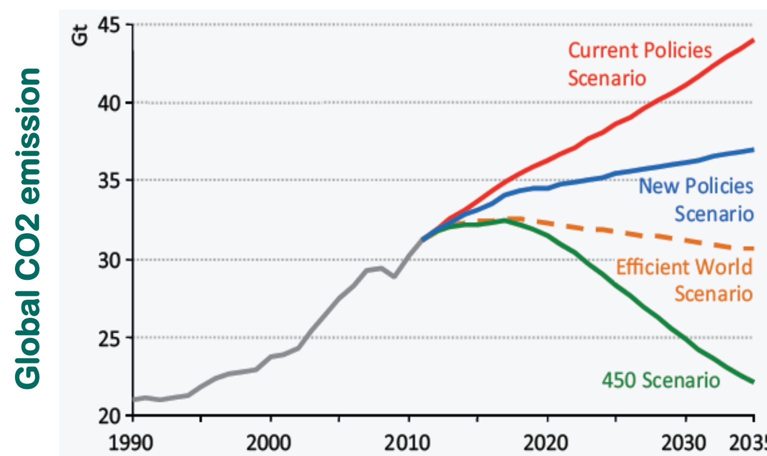

Actions to control CO_2 emissions

*2011 World Energy Outlook IEA

What do we do?

GASIFICATION
EF & FB

OXY-COMBUSTION

ITM, Chemical Looping & SOFC

CARBON CAPTURE, H_2, syngas and Synfuels RESEARCH:

OPTICAL DIAGNOSTICS

MATERIAL SCIENCE

CENTER FOR ENERGY AND PROPULSION RESEARCH
Reacting Gas Dynamics Lab

MULTISCALE SIMULATION

SYSTEM ANALYSIS

EFFICIENCY and FUEL FLEXIBILITY:

RENEWABLES

COMBUSTION DYNAMICS & CONTROL

CLEAN FUELS

WATER

HYBRID CSP

Biomass To Liquid

Massachusetts Institute of Technology

Estimated (in 2013) Levelized Cost of Electricity Generation 2018

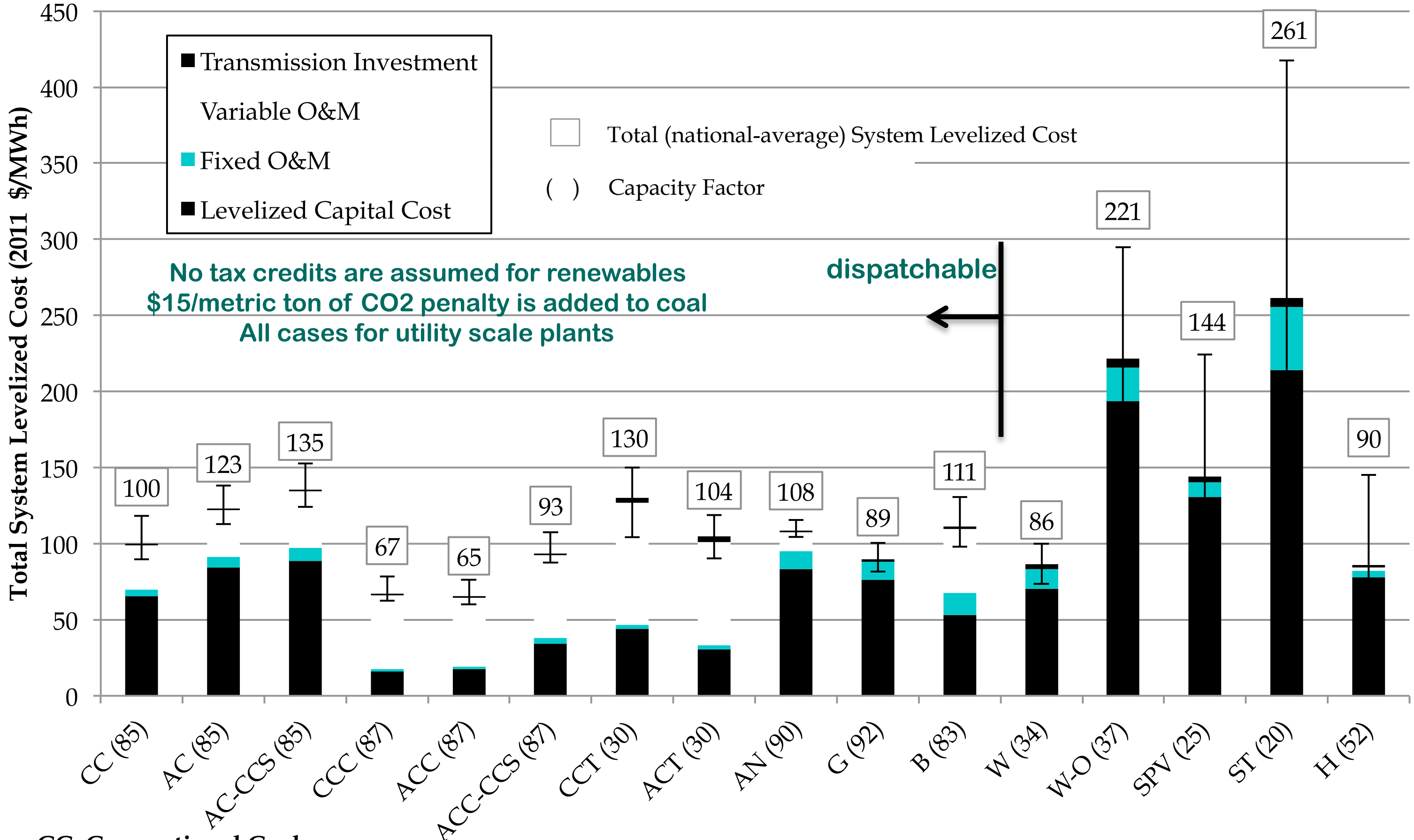

CC: Conventional Coal
AC: Advanced Coal
AC-CCS: Advanced Coal with CCS
CCC: Conventional Combined Cycle
ACC: Advanced Combined Cycle
ACC-CCS: Advanced Combined Cycle with CCS

CCT: Conventional Combustion Turbine
ACT: Advanced Combustion Turbine
AN: Advanced Nuclear
G: Geothermal
B: Biomass

W: Wind
W-O: Wind Offshore
SPV: Solar PV
ST: Solar Thermal
H: Hydro

U.S. Energy Information Administration, Annual Energy Outlook 2013, Dec. 2012, DOE/EIA-0383(2012)

Simulation of Supercritical Fluid Transport and Mixing

Energy Applications:

- Production of clean fuels (desulfurization, upgrade)
- Production of bio-oils
- Supercritical CO_2 transport for storage, and hypercritical CO_2 cycle

Computational Challenges:

- Complex equation of state (PR), and phase equilibrium (PPR-78)
- Complex transport (formation and dissolution of interfaces @ UCST)
- Complex transport (fugacity and nonideal fluid, diffusion)
- Complex dynamics (strong density gradients and jumps)

Timko, M.T., Ghoniem, A.F. and Green, W.H., Upgrading and desulfurization of heavy oils by supercritical water, *Journal of Supercritical Fluids*, Vol. 96 (2015), pp. 114-123.
http://dx.doi.org/10.1016/j.supflu.2014.09.015

MITMECHE

$$\sum_{j\neq i}\frac{x_i x_j}{D_{ij}}\left(\frac{\boldsymbol{J}_j}{\rho y_j}-\frac{\boldsymbol{J}_i}{\rho y_i}\right)=\boldsymbol{d}_i-\sum_{j\neq i}\frac{x_i x_j}{D_{ij}}\left(\frac{D_j^T}{\rho y_j}-\frac{D_i^T}{\rho y_i}\right)\nabla \ln T$$

$$cRT\boldsymbol{d}_i = c x_i RT\sum_{j=1}^{n}\left[\frac{\partial \ln(x_i\hat{\varphi}_i)}{\partial x_j}\right]_{T,P}\nabla x_j+(c x_i\bar{V}_i-y_i)\nabla P$$

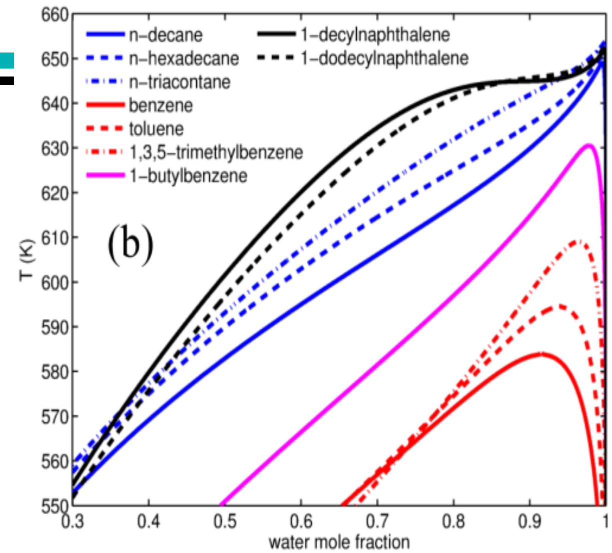

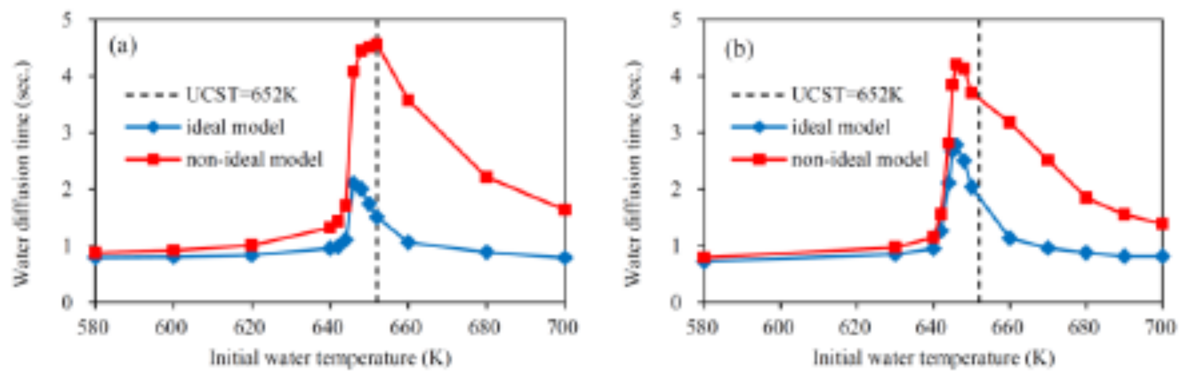

Figure 19. Water diffusion times for mixing of (a) a HC droplet of 1-decylnaphthalene (re-presenting Fig. 14a for comparison), and (b) a HC droplet of 50% benzene and 50% 1-decylnaphthalene with water at different initial water temperatures $T_{W,0}$ using ideal (blue) and non-ideal (red) diffusive driving forces (the dashed line show the UCST).

Mixing (single HC)

below and above the Upper Critical Solution Temperature

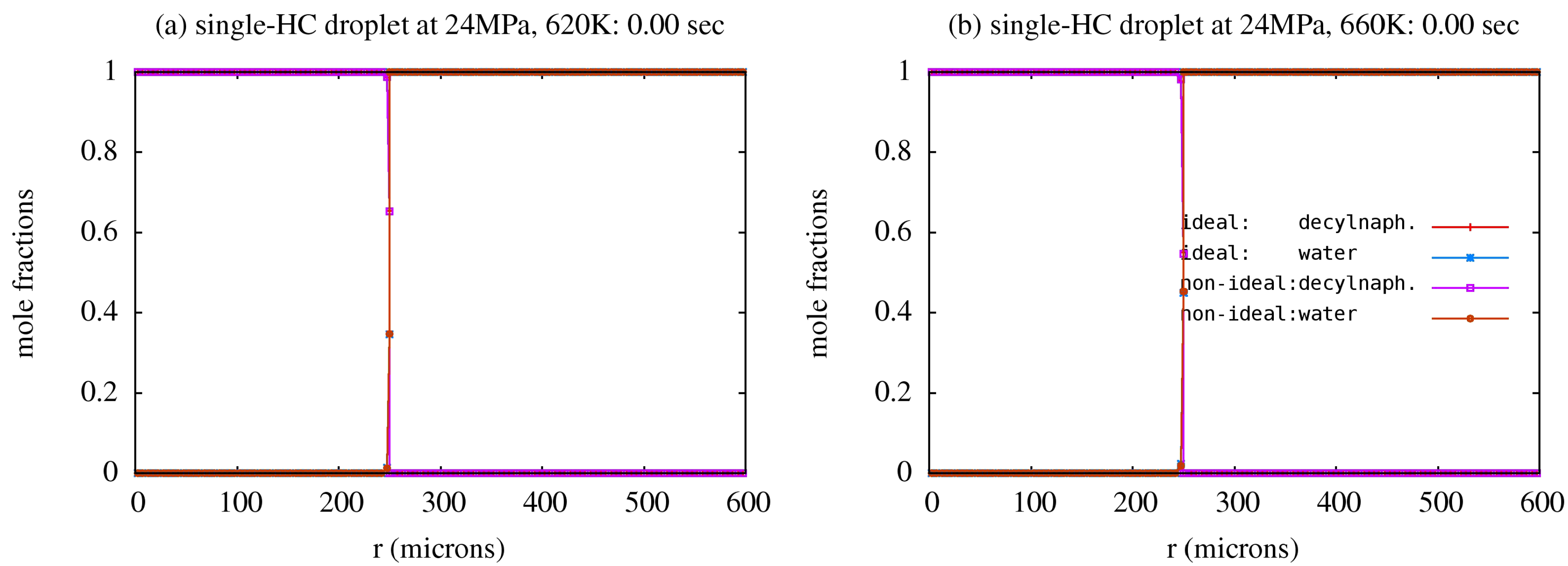

Dabiri, S., Wu, G., Timko, M. and Ghoniem, A.F., Mixing of single component hydrocarbon droplets in supercritical water, *J Supercritical Fluids*, 67 (2012) 29-40. http://dx.doi.org/10.1016/j.supflu.2012.02.014

Mixing (two HCs)

$UCST_1 < T < UCST_2$ and $T > UCST_2$

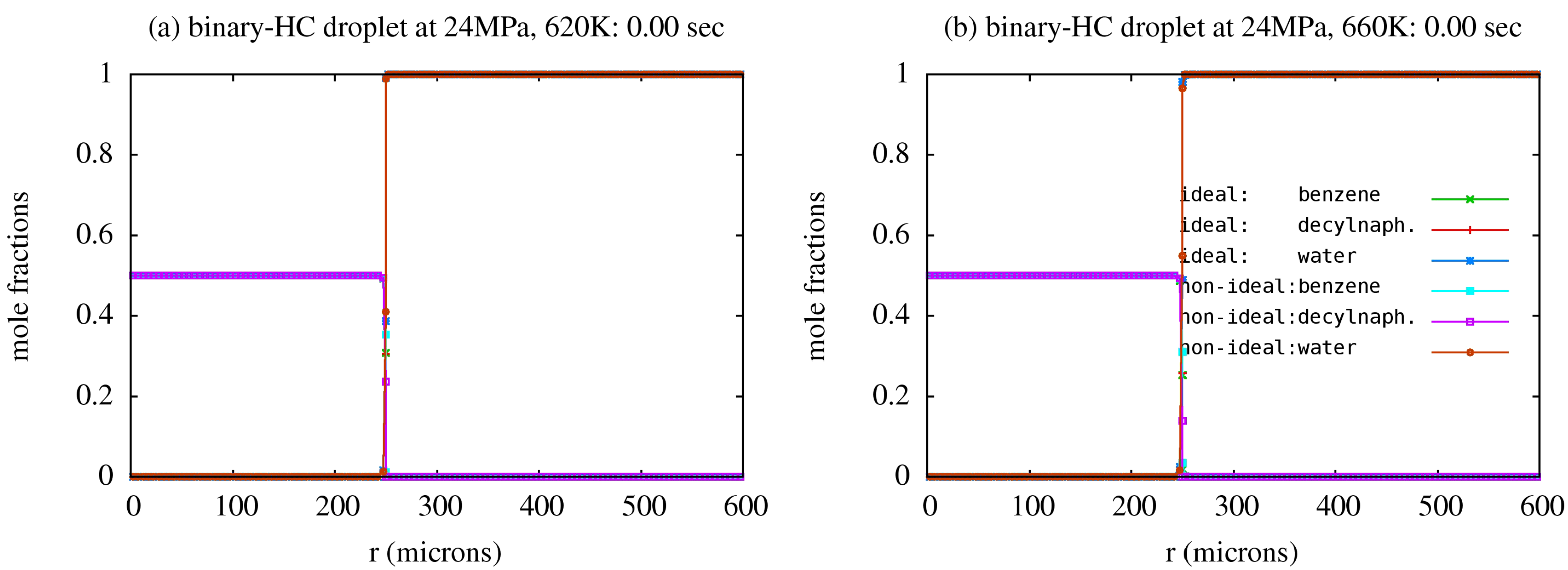

Wu, G., Dabiri, S., Timko, M.T., and Ghoniem, A.F., Fractionation of multicomponent hydrocarbon droplet in water at supercritical and near-critical conditions. *J. Supercritical Fluids*, 72 (2012) 150-160. [ttp://dx.doi.org/10.1016/j.supflu.2012.08.021](http://dx.doi.org/10.1016/j.supflu.2012.08.021)

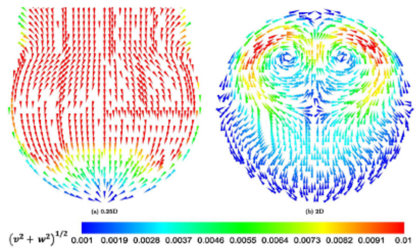

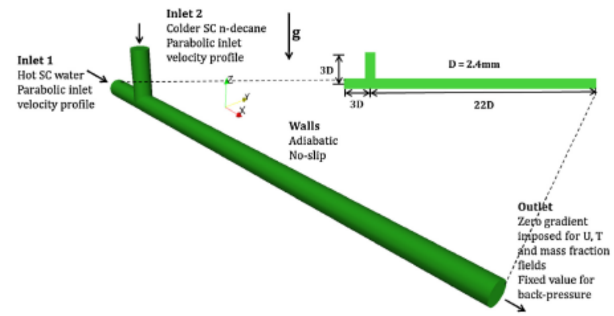

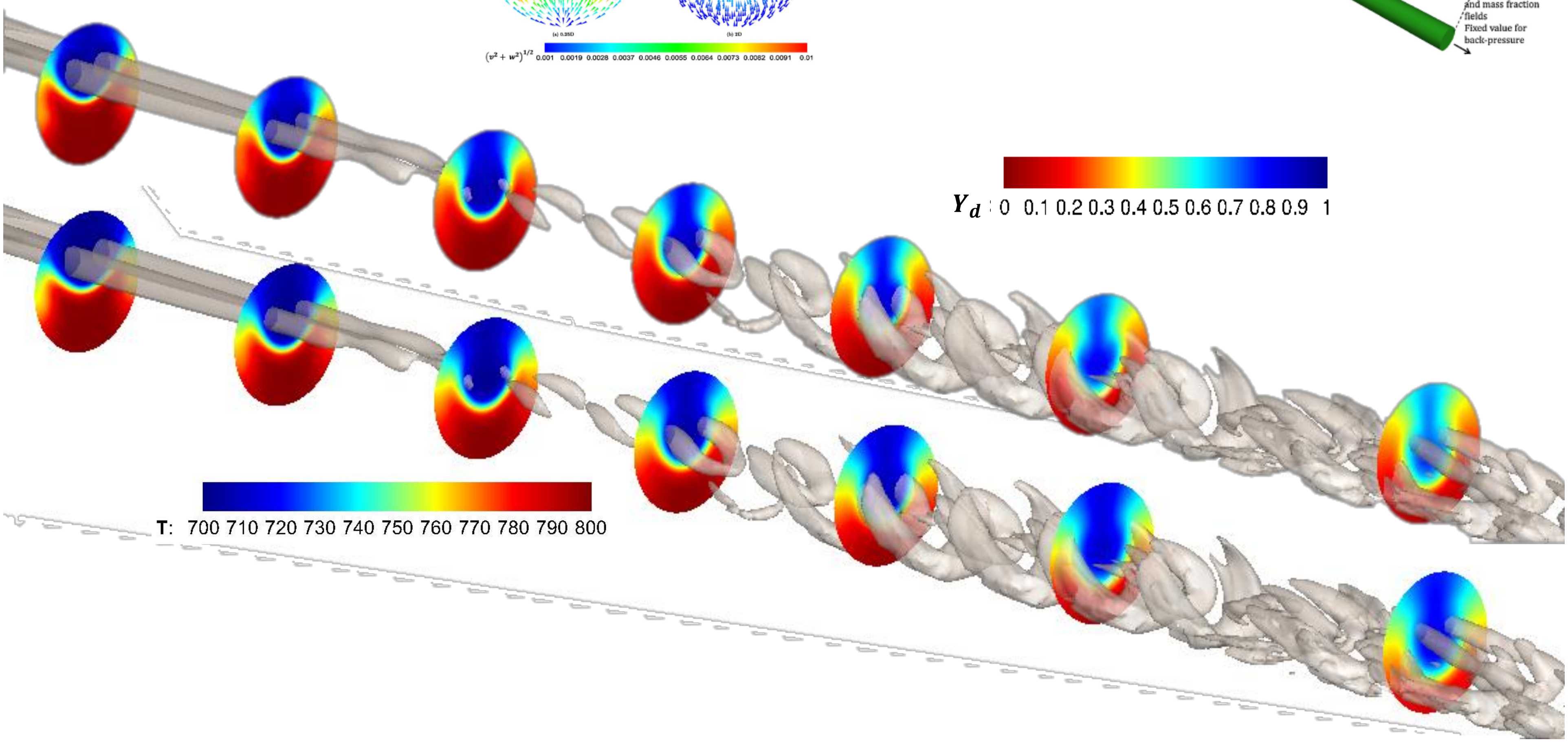

Ragavan, A, and Ghoniem, A.F., *J. Supercritical Fluids*, 2014, 92 (2014) 31-46.
Ragavan, A, and Ghoniem, A.F., Simulation of supercritical water-hydrocarbon mixing in a cylindrical Tee junction at intermediate Reynolds number: Impact of temperature difference between streams, *J. Supercritical Fluids*, 95 (2014) 325-338.

Simulations of Dense Multiphase flows

Energy Applications:

- Fluidized beds for biomass (and waste) gasification
- Novel designs of some FT and similar reactors

Computational Challenges

- Time and storage (especially for discrete particle or element approaches)
- Same for fully Eulerian (2FM) especially @ full scale
- Closure models for the 2FM (drag models and wall BCs)
- Extracting relevant data (bubble statistics and circulations times)
- Scale up (coarse graining)
- Coupling with particle gasification thermochemistry

Bakshi, A., Altantzis, C. and Ghoniem, A.F., Towards Accurate multidimensional simulations of dense multiphase flows using cylindrical coordinates, *Powder Technology*, 264 (2014) 242-255. Bakshi, A., Altantizis, C., Bates, R.B. and Ghoniem, A.F., Eulerian-Eulerian simulation of dense solid-gas cylindrical fluidized beds; wall boundary condition and its impact on fluidization. *Powder Tech.,* 277 (2015) 47-62.

Fluidization Regimes

Rectangular reactor in slugging regime

$$Ar = \frac{\rho_g g \left(\rho_s - \rho_g\right) d_p^3}{\mu_g^2}$$

Solids motion generated by bubble motion

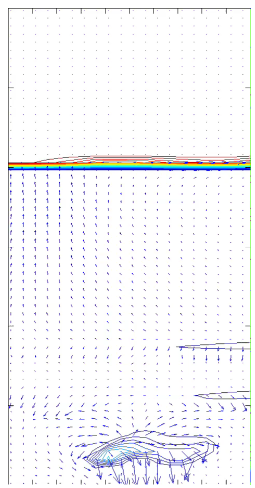

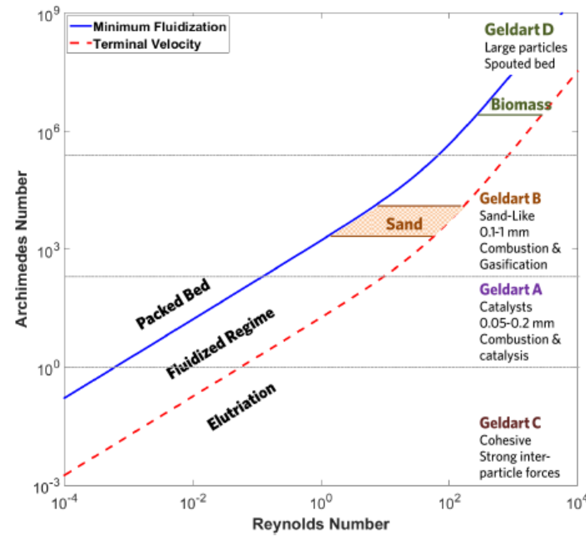

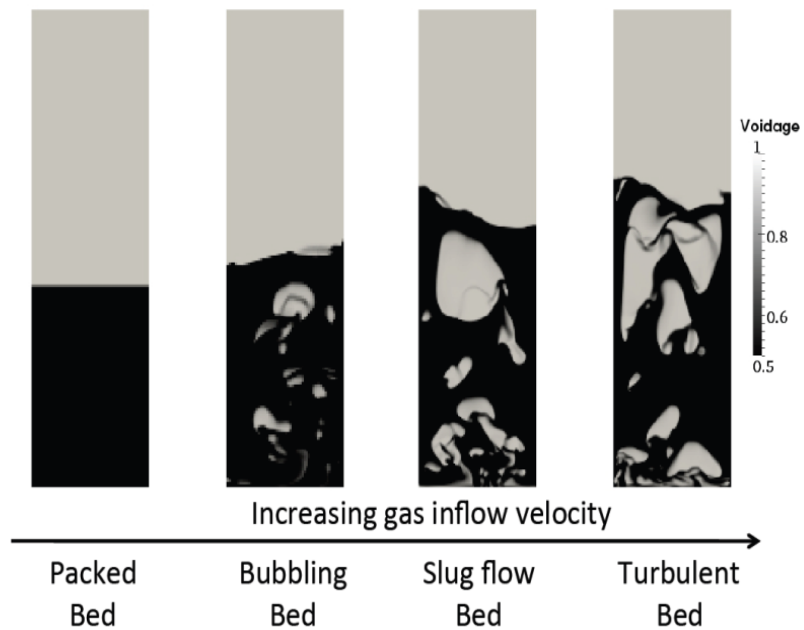

Fluidization Metrics

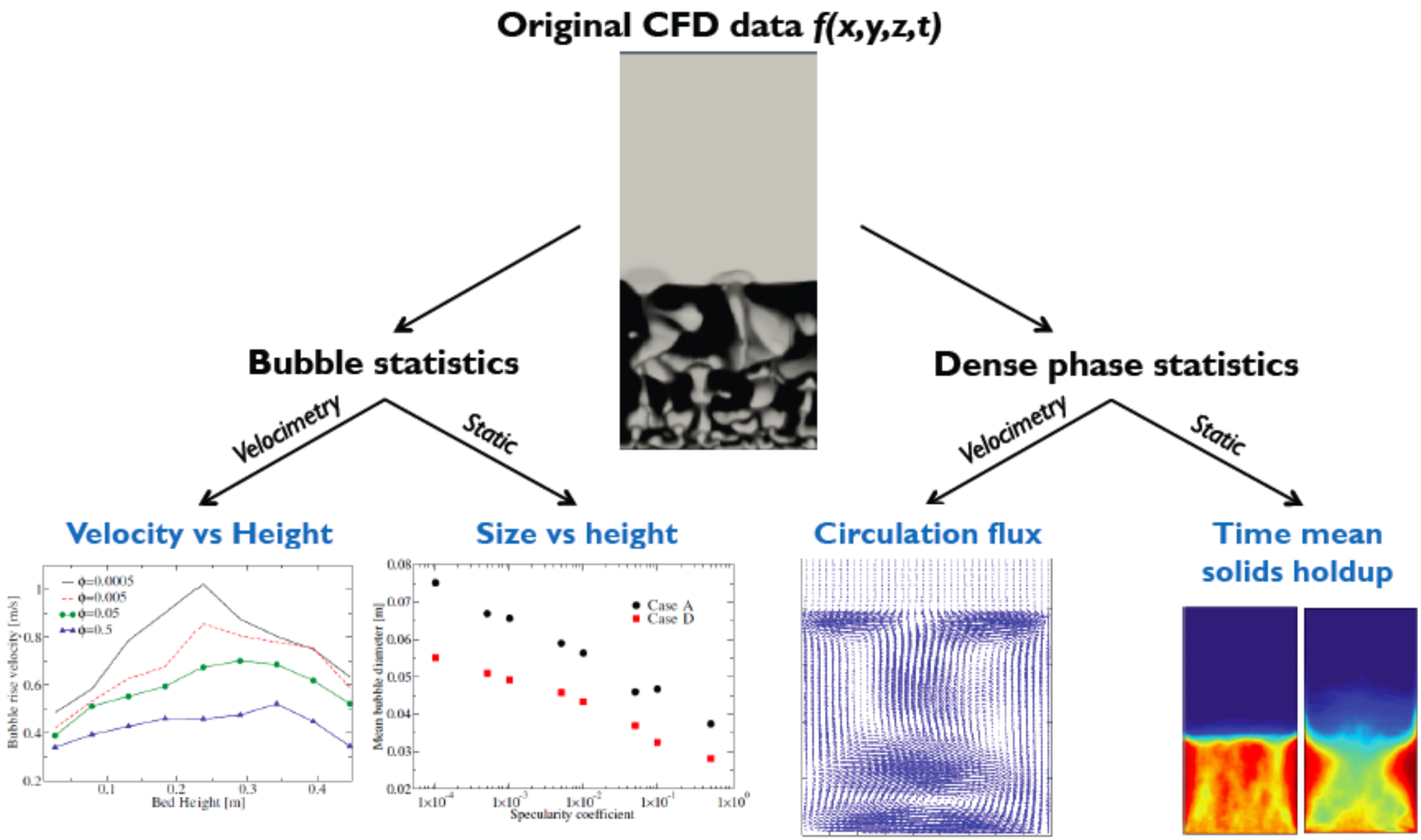

Altantzis, C., Bates, R.B. and Ghoniem, A.F. Estimating the specularity coefficient and its effect on bubble dynamics and circulation time in a thin rectangular fluidized bed, *Powder Technology,* 2015, 270 (2015) 256-270

Solid Circulation Pattern, and Validations

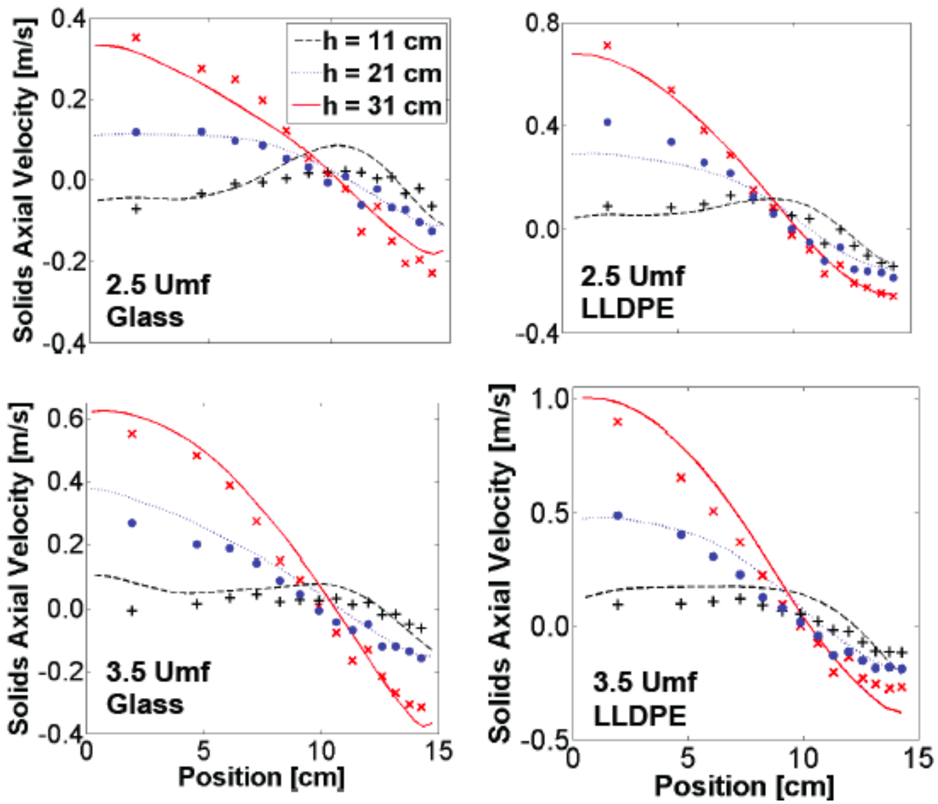

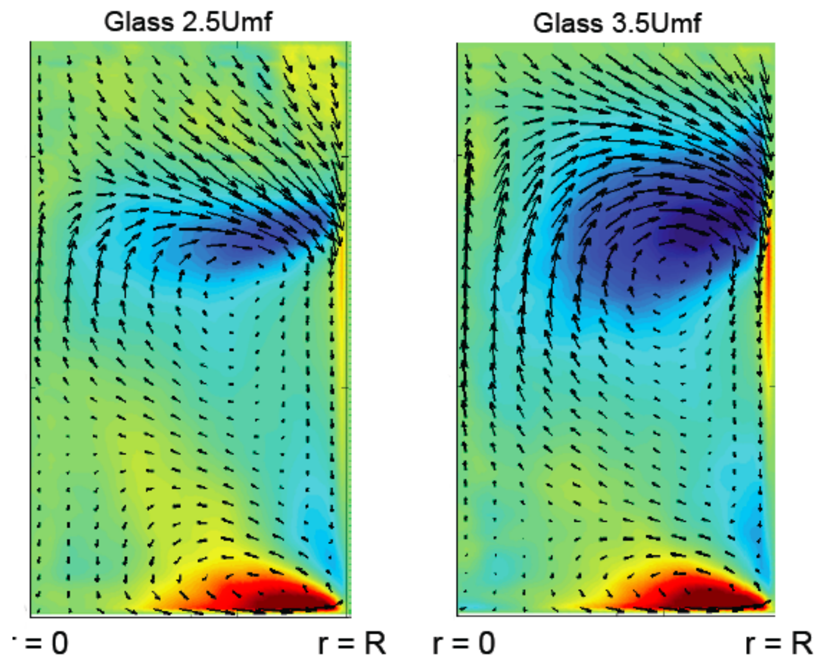

[1] Li et al, *Chemical Eng. Sc.* 2014
[2] Laverman et al, *Powder Technology* 2012

The Two-Fluid Model

- Solid and gas phases described using fully interpenetrating continua
- Particles are not individually tracked => Computationally efficient
- Constitutive relations requi[illegible] for particle-particle, particle-gas and particle-wall interactions
- Gas $k = g$, Solids $k = m$ and $\delta_{ki} = 1$ if $k = i$, else 0

$$\frac{\partial}{\partial t}\underline{(\varepsilon_k \rho_k)} + \nabla \cdot \left(\varepsilon_k \rho_k \vec{V}_k\right) = 0$$

Apparent density = Volume fraction x real density

$$\frac{\partial}{\partial t}\left(\varepsilon_k \rho_k \vec{V}_k\right) + \nabla \cdot \left(\varepsilon_k \rho_k \vec{V}_k \vec{V}_k\right) = \underline{\nabla \cdot \overline{\overline{S}}_k} - \varepsilon_k \nabla P_g + \varepsilon_k \rho_k \vec{g} + \underline{\left(\delta_{km} \vec{I}_{gm} - \delta_{kg} \vec{I}_{gm}\right)}$$

Solids Stress Tensor
particle-particle interactions

Drag Model
particle-gas interactions

Constitutive Relations

Solid Phase Stress Tensor

- Stress tensor represents particle-particle interactions through collisions (viscous) and friction (plastic)
- Reaction forces to maintain incompressibility, numerical stability
- Viscous regime based on Kinetic Theory of Granular Flow (KTGF), plastic regime more empirical

$$\overline{\overline{S}}_m = \begin{cases} -P_m^p \overline{\overline{I}} + \overline{\overline{\tau}}_m^p & \text{if}\, \varepsilon_g \le \varepsilon_g^* \\ -P_m^v \overline{\overline{I}} + \overline{\overline{\tau}}_m^v & \text{if}\, \varepsilon_g > \varepsilon_g^* \end{cases}$$

Plastic Flow (Frictional Theory)

Viscous Flow (KTGF)

Granular Energy

- Solids stress tensor = f(ε_m, Θ_m, d_p, ρ_m, g_0)
- Granular temperature measure of the random fluctuating component of the solids velocity
- Total Energy = Thermal energy + KE (mean velocity) + 'pseudo thermal' energy (fluctuations)

$$\frac{3}{2}\left(\frac{\partial(\varepsilon_m \rho_m \Theta_m)}{\partial t} + \nabla \cdot (\varepsilon_m \rho_m \mathbf{V}_m \Theta_m)\right) = \underbrace{\boldsymbol{S}_m : \nabla \mathbf{V}_m}_{\text{production}} + \underbrace{\nabla \cdot \mathbf{q}_{\Theta_m}}_{\text{diffusion}} \underbrace{- \gamma_{\Theta_m} + \phi_{gm}}_{\text{dissipation}}$$

Constitutive Relations

Gidaspow Drag Model[1]

- Combination of empirical models for packed and homogenously fluidized beds

$$\vec{I}_{gm} = \beta\left(\vec{V}_g - \vec{V}_m\right)$$

$$\beta = \begin{cases} 150\dfrac{\varepsilon_m^2 \mu_g}{\varepsilon_g d_p^2} + 1.75\dfrac{\varepsilon_m \rho_g |\vec{V}_m - \vec{V}_g|}{d_p} & \text{if } \varepsilon_g \leq 0.8 \\ \dfrac{3}{4} C_d \varepsilon_g^{-2.65} \dfrac{\varepsilon_m \varepsilon_g \rho_g |\vec{V}_m - \vec{V}_g|}{d_p} & \text{if } \varepsilon_g > 0.8 \end{cases}$$

Syamlal-O'Brien Drag Model[2]

- Derived from terminal velocity correlations in liquid-solid beds corrected to retrieve exp. U_{mf}

$$I_{gm} = \frac{3\varepsilon_m \varepsilon_g \rho_g}{4(V_{rm})^2 d_p} C_{Ds}\left(\frac{Re}{V_{rm}}\right) |\vec{V}_m - \vec{V}_g|$$

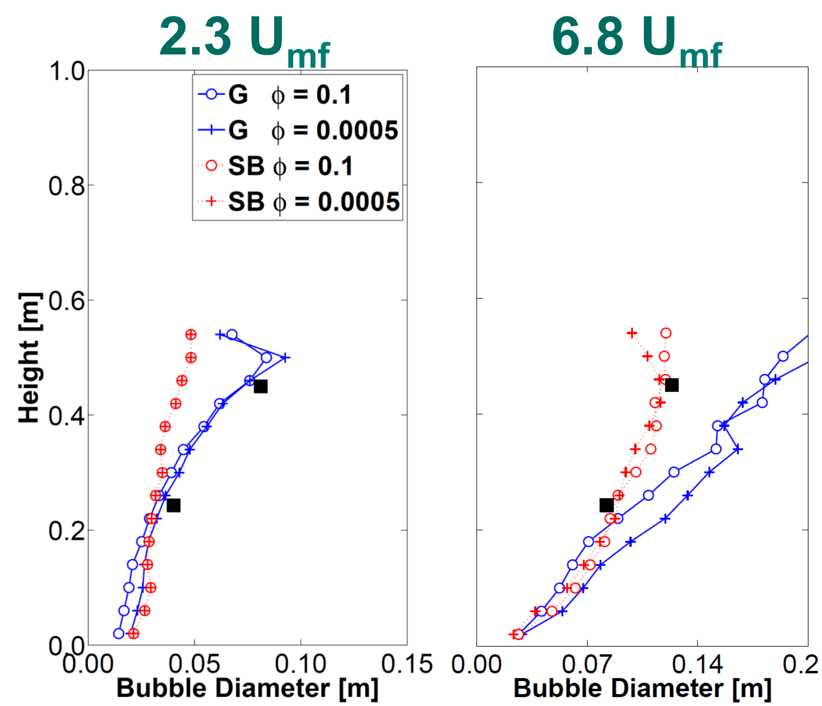

1 D. Gidaspow, *Multiphase Flow and Fluidization: Continuum and Kinetic Theory Descriptions.*, 1994
2 MFIX Documentation - Theory Guide

Wall Boundary Condition

Particle-Wall Interactions

- Johnson-Jackson model[1] computes solids slip velocity at wall by accounting for stress of solids approaching walls and momentum loss through collisions and friction

$$\vec{n} \cdot \mu_m \nabla \vec{V}_{sl} = -\frac{\pi \phi \varepsilon_m \rho_m \vec{V}_{sl} g_0 \sqrt{3\Theta}}{6\varepsilon_{m,max}}$$

- Specularity coefficient Φ = fraction of particle momentum lost through collisions and friction
- Indicative of wall roughness; affected by particle size, fluidization regime
- Φ = 0 => minimum hindrance and specular reflections, Φ = 1 => maximum hindrance

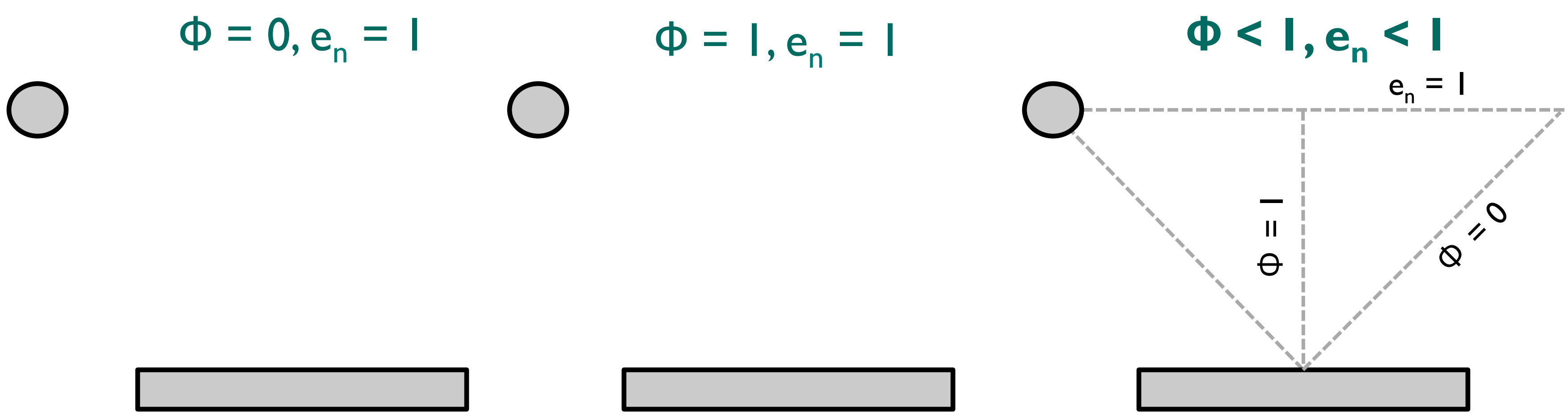

1 Johnson and Jackson, *J. Fluid Mech.*, 1987

Determining ϕ

- Range – 1.25-6.80 U_{mf}, 860-2500 kg/m^3, 0.289-1.1 mm
- Bubble diameter comparisons show higher values of ϕ (0.01-0.3) more suitable for dense flows
- Low sensitivity of metrics (solids / bubbles) for suitable ϕ

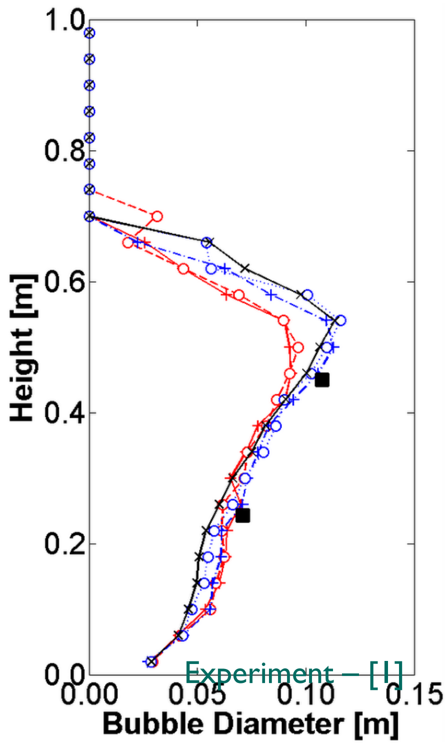

Alumina
1350 kg/m^3, 0.289 mm
Bed Dia = 14.5 cm
U=4.6 U_{mf}

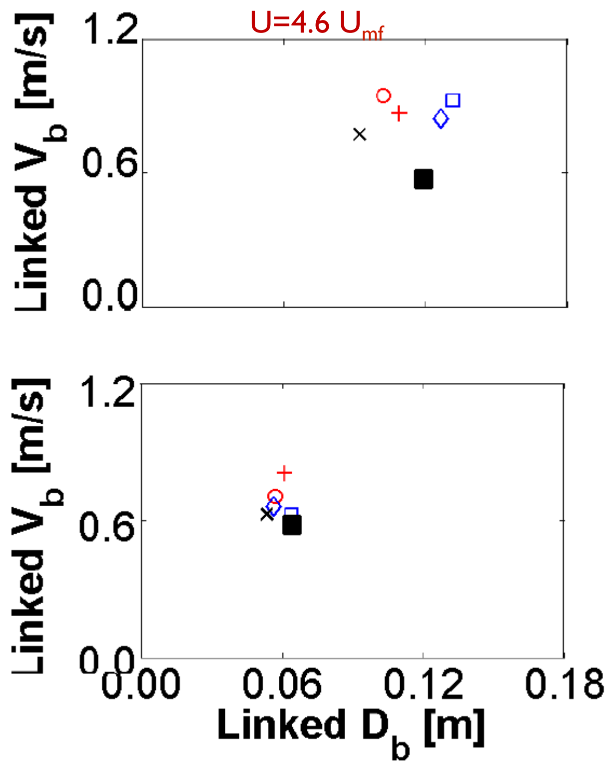

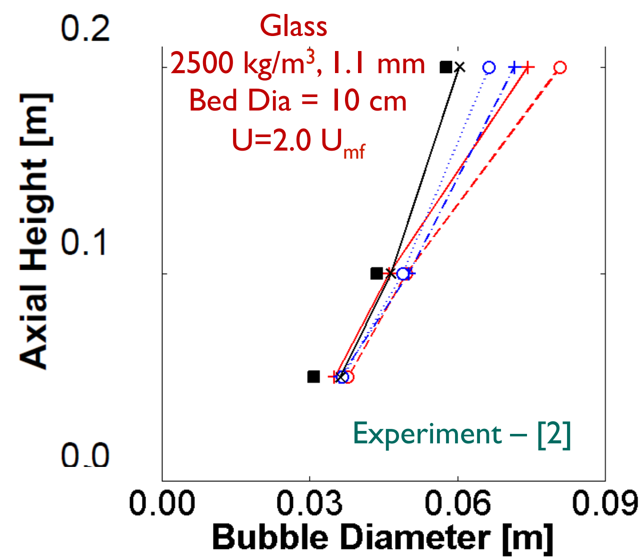

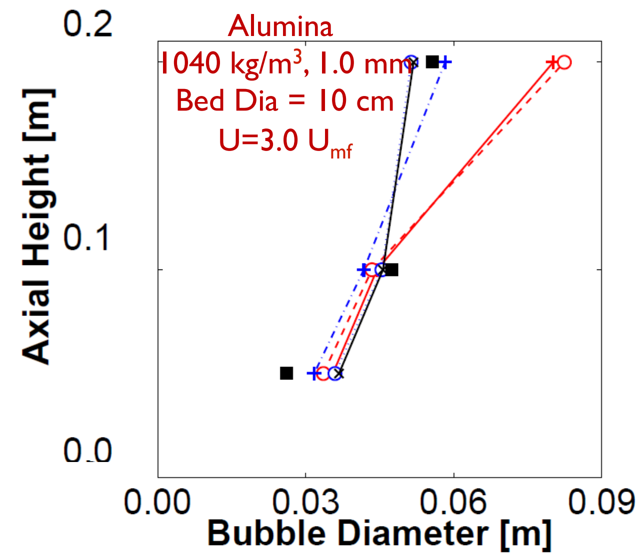

[1] Rüdisüli et al. *Chem. Eng. Sci.*, 2012
[2] Verma et al, *AIChE J.* 2014

MITMECHE

Computational complexity & scaling to practical size rectors

Computational time

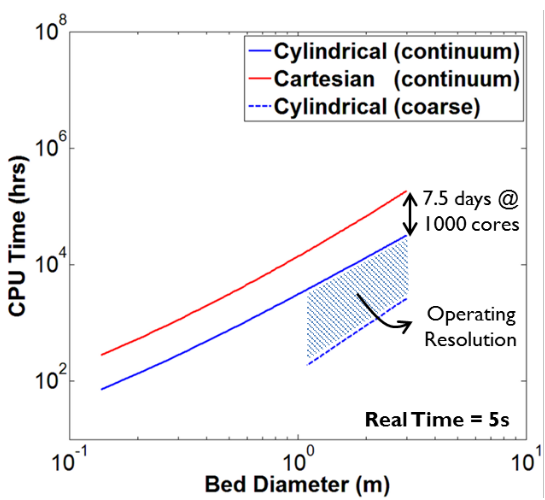

Impact of resolution …

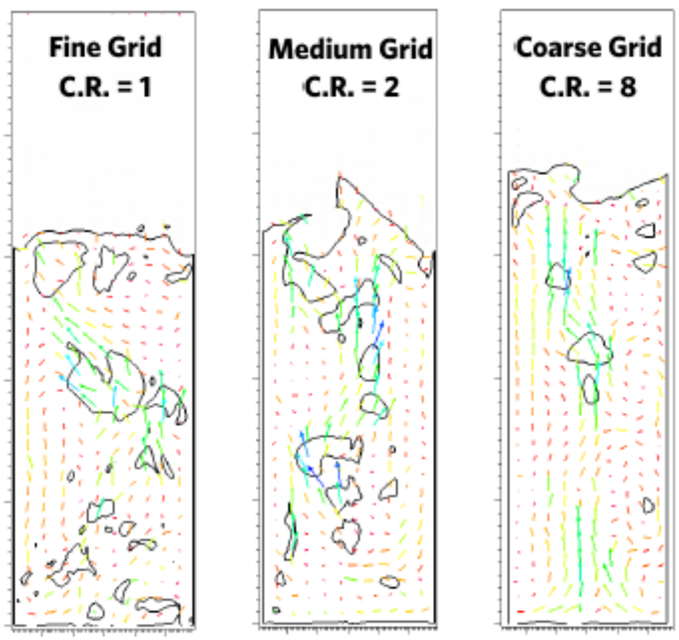

Mixing (3FM)

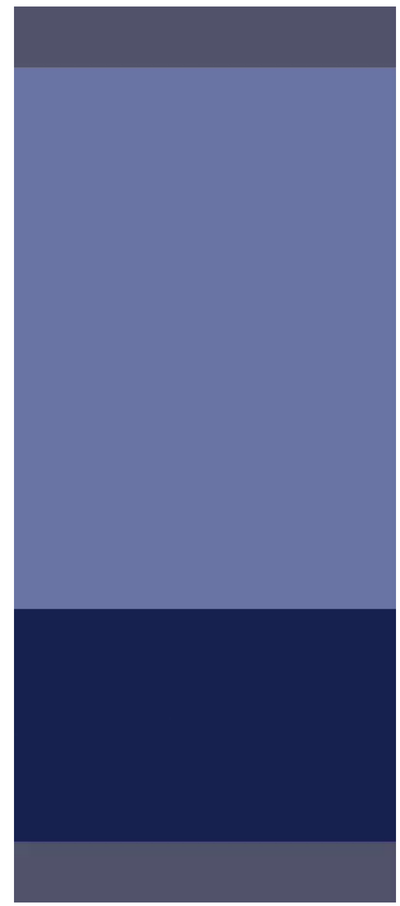

MITMECHE

KAUST
King Abdullah University of Science and Technology

Hybrid Eulerian/Lagrangian 3D Methods for High Reynolds Number Transverse Jets

Wee, D.H., and Ghoniem, A.F., “Modified interpolation kernels and treating diffusion and remeshing in vortex methods,” *J. Comput. Phys.,* 213, 2006, pp. 239-263.

Marzouk, Y.M. and Ghoniem, A.F., “Vorticity structure and evolution in a transverse jet,” *J. Fluid Mech.,* 575:267-305, 2007.

Schlegel, F., Wee, D.H, and Ghoniem, A.F., “A fast 3d particle method for simulations of buoyant flows”, *J. Computational Physics*, 227, 21, 2008, pp. 9063-9090.

Schlegel, F., Wee, Dh, Marzouk, Y.M. and Ghoniem, A.F., Contributions of the wall boundary layer to the formation of counter-rotating vortex pair in transverse jets, *J. Fluid Mechanics*, Vol. 676, 2011, pp. 461-490.

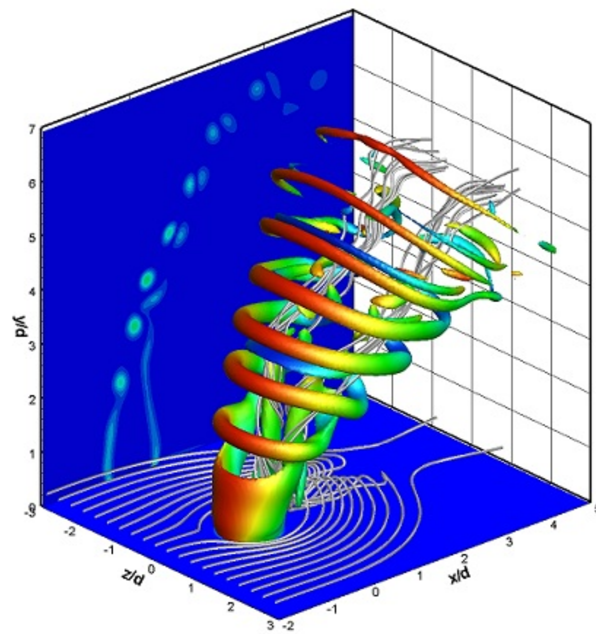

Motivation

Combustion:
industrial burners,
aircraft engines.

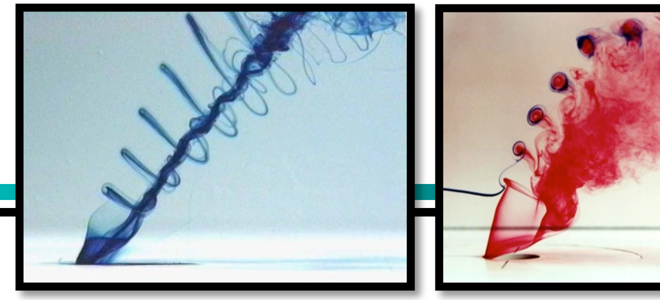

Kelso, 1996

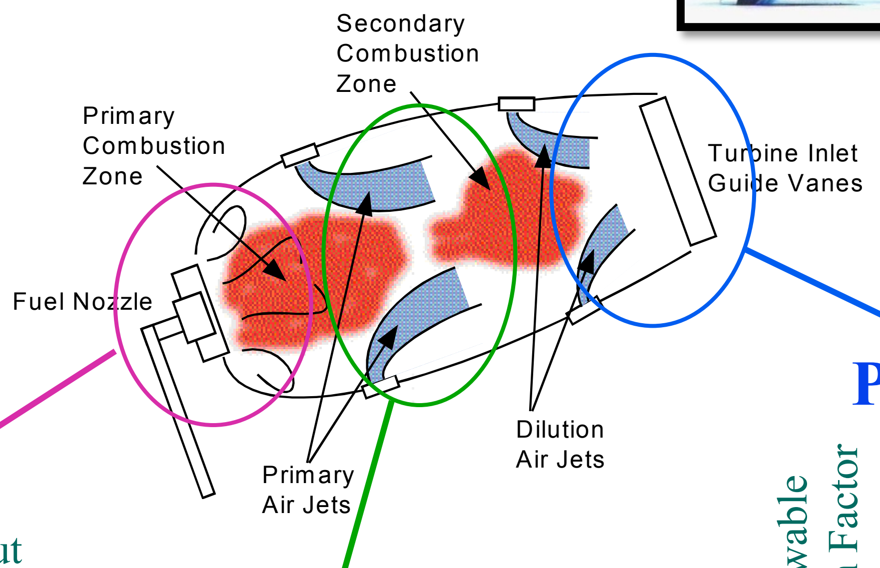

Turndown Ratio

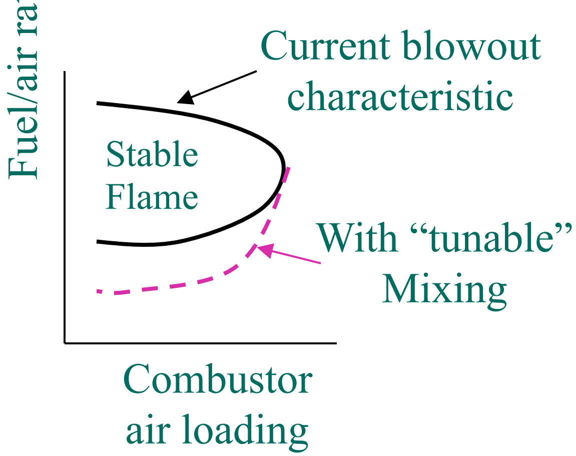

Better operability

Emissions

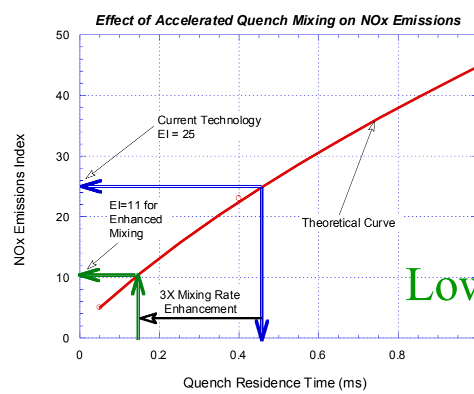

Lower NO_x, CO, UHC

Pattern Factor

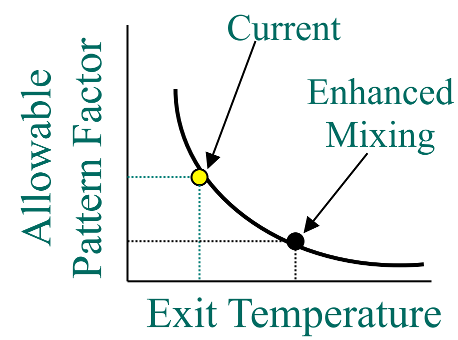

Higher thrust

How to set up a simulation to capture these images? And what do we learn from the massive calculation?

Non reactive structure in semi-infinite domain

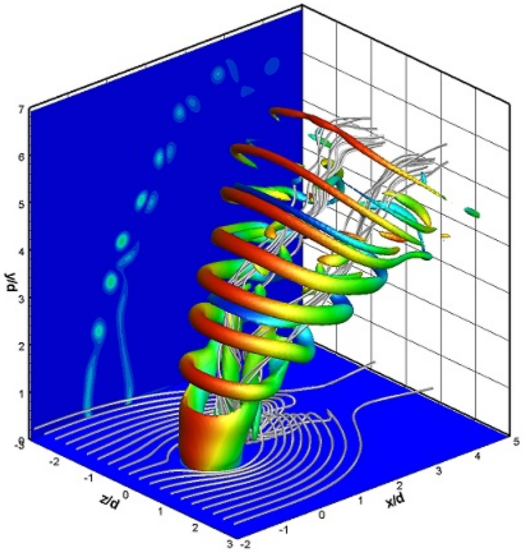

$$\omega = \nabla \wedge u$$

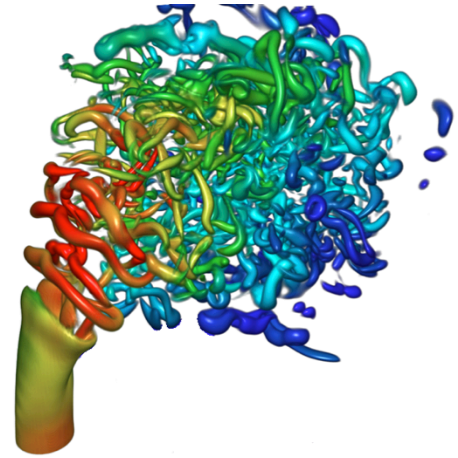

Flame stabilization, Combustion under no premixed conditions

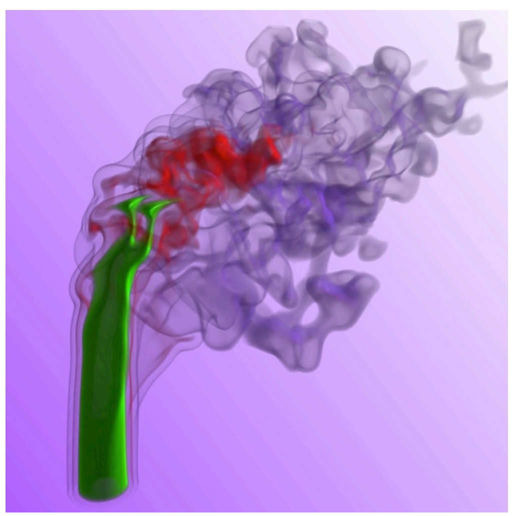

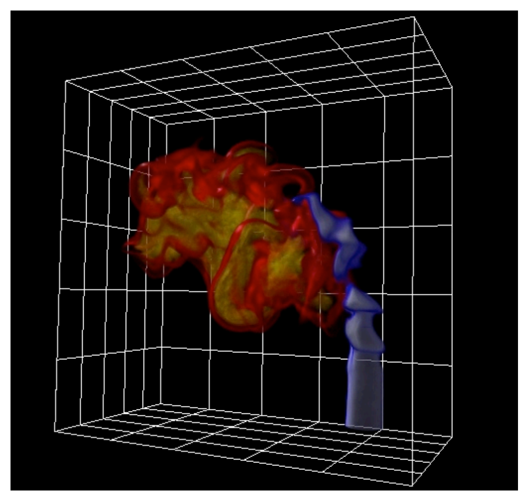

Physics of Transverse Jets

- Flow field dominated by *vortical structures*. (Better prospects for control!)

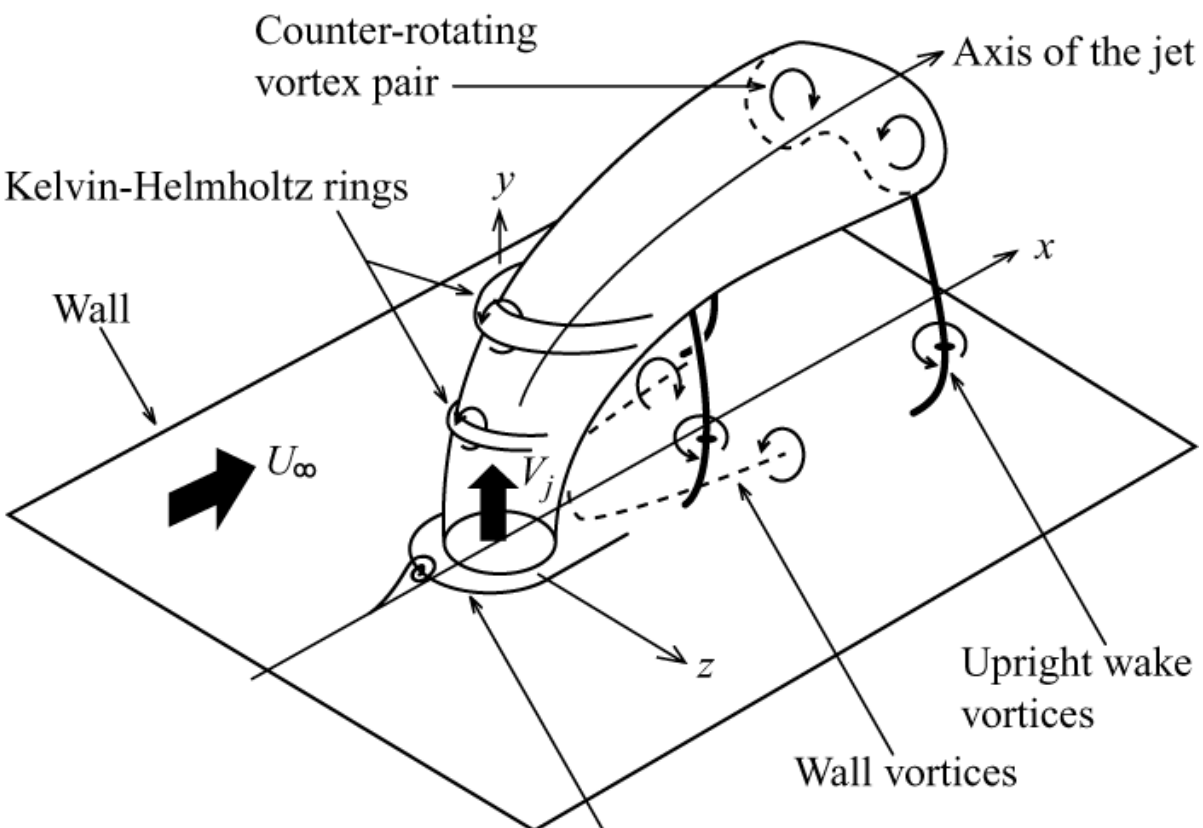

Modified from the schematic
drawing by Kelso *et al.*, JFM (1996)

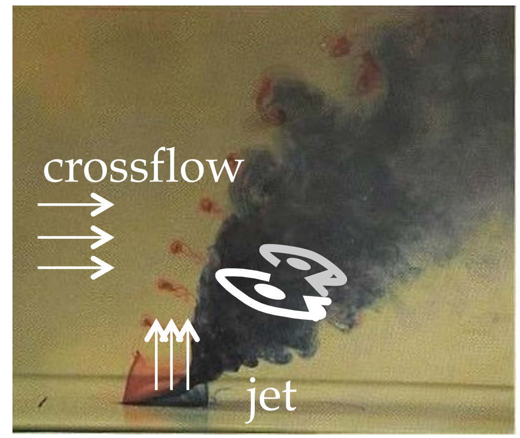

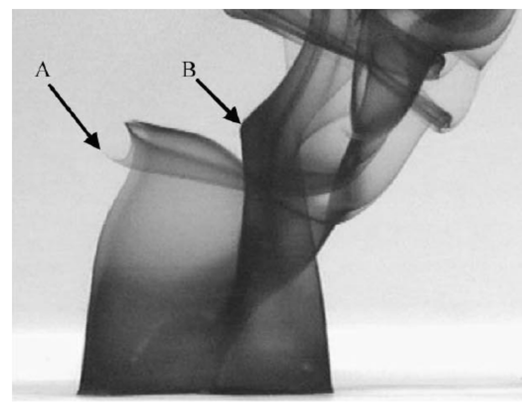

Dimensionless Parameters: Re, $r = V_j / U_\infty$

Overall flow features, reduced model

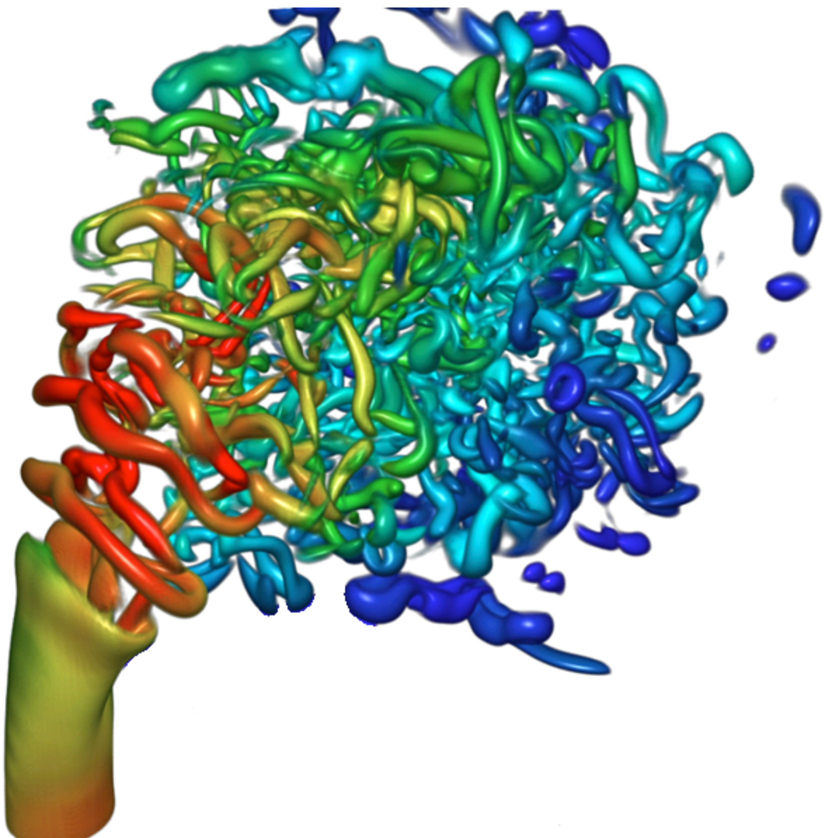

Graphics Plotting program: Bruno Jobard, Pau University

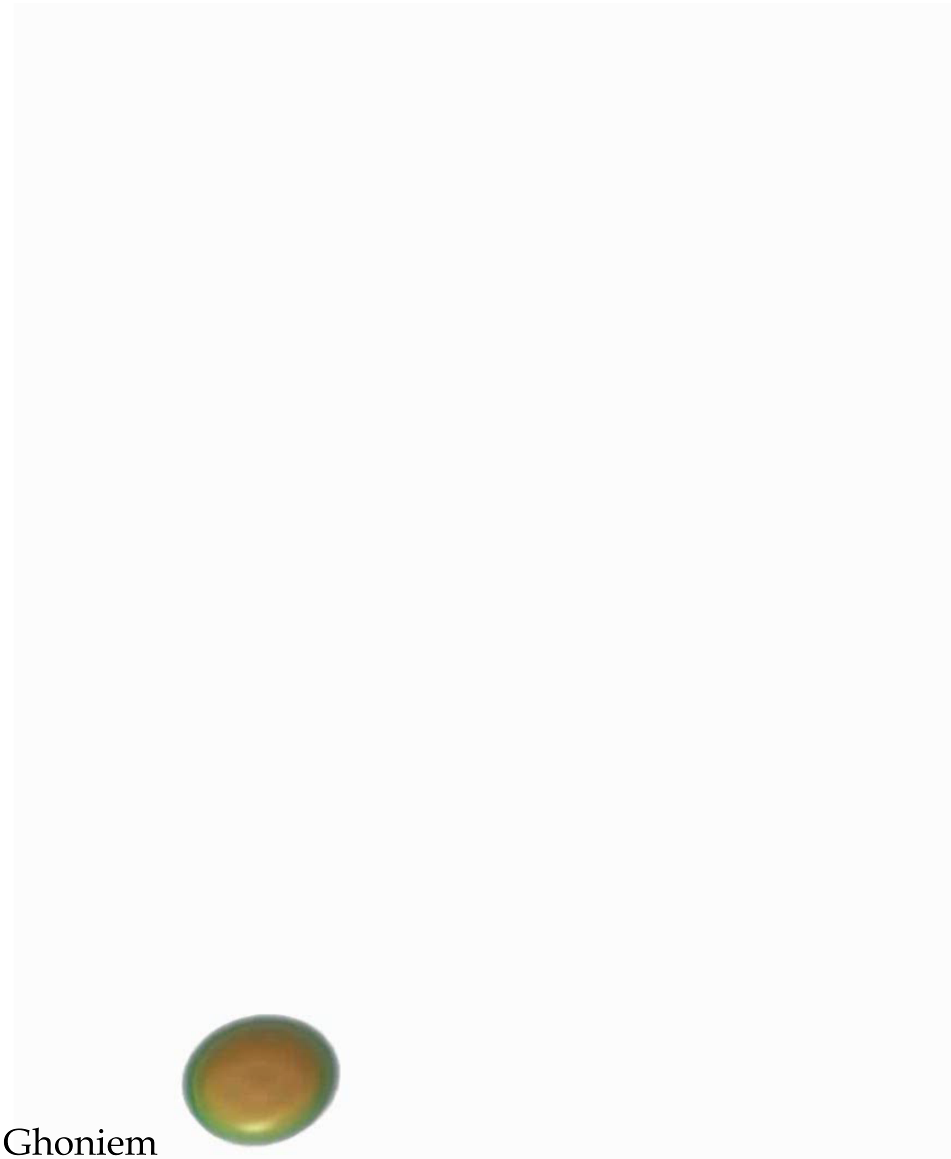

Overall flow features

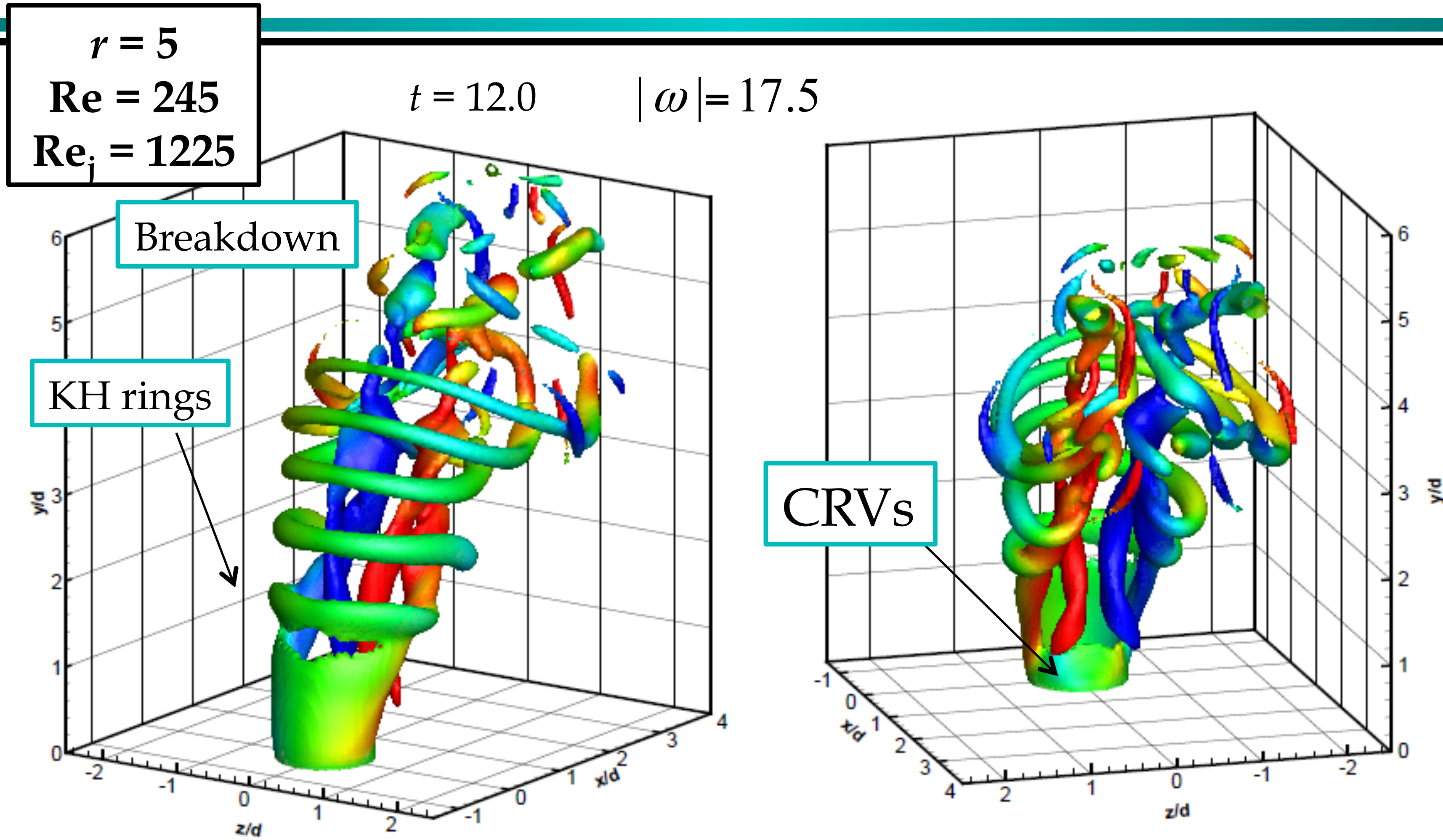

(a) windward side

(b) lee side

- Schlegel, F., Wee, Dh, Marzouk, Y.M. and Ghoniem, A.F., Contributions of the wall boundary layer to the formation of counter-rotating vortex pair in transverse jets, *J. Fluid Mechanics*, Vol. 676, 2011, pp. 461-490.

Overall flow features, vorticity organizes itself first then breaks down

r = 5
Re = 245
Re_j = 1225

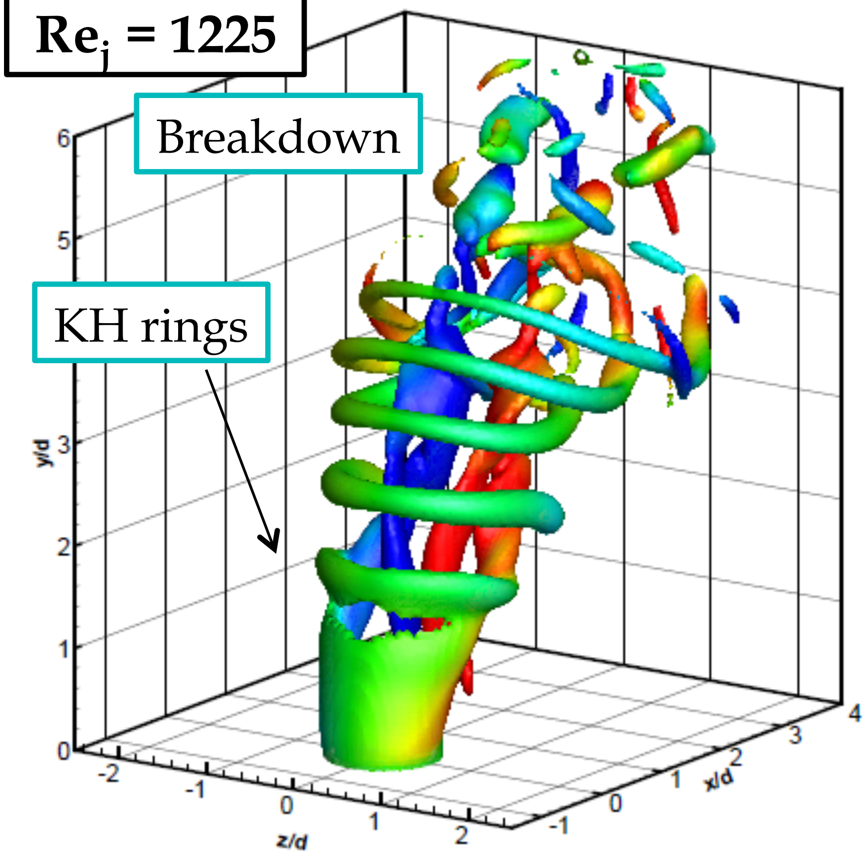

(a) windward side

$t = 12.0 \quad |\omega| = 17.5$

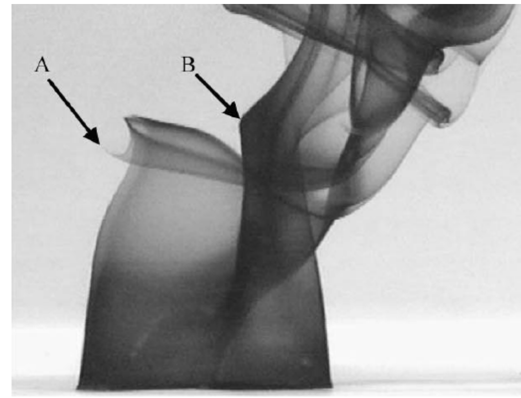

Notice that there are 2 vertical vortices

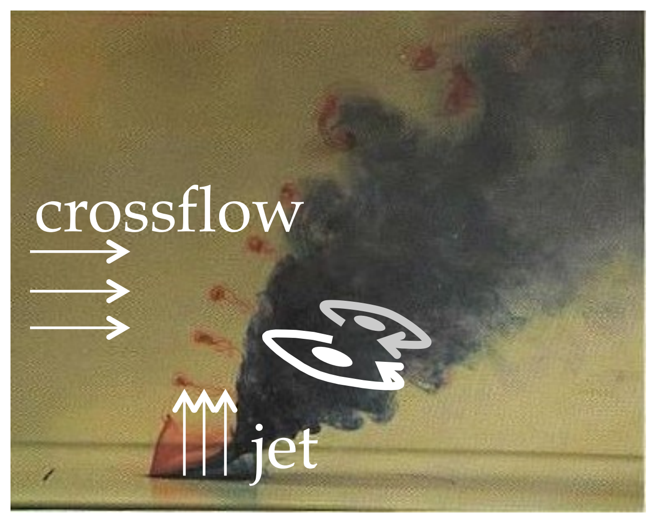

Overall flow features, vorticity organizes itself first then breaks down

$r = 5$
$Re = 245$
$Re_j = 1225$

Time-Averaged Vorticity

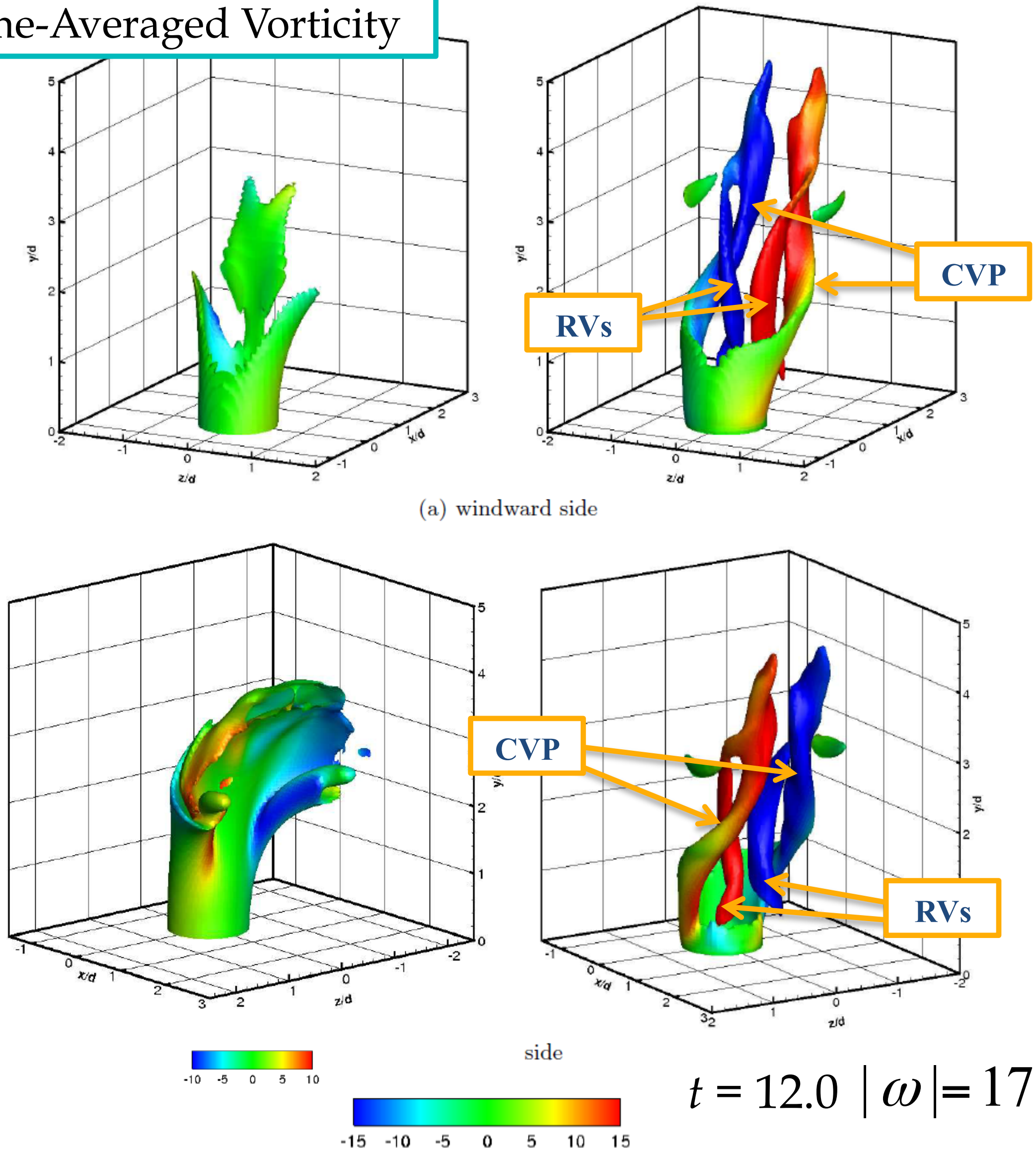

(a) windward side

side

$t = 12.0 \quad |\omega| = 17.5$

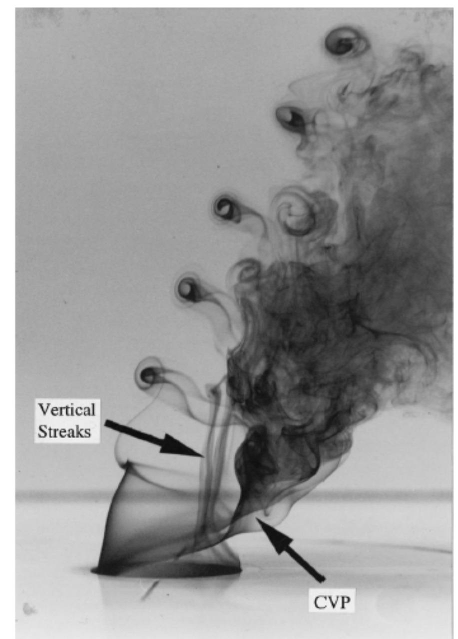

FIG. 3. Flow pattern obtained when dye is injected from a small injection hole below the edge of the pipe exit into the upstream side of the shear layer, and also from a circumferential slit to mark evenly the cylindrical shear layer of the jet. The Reynolds number is about 750 and the velocity ratio is about 5. The CVP and ''vertical streaks'' are indicated by the arrows.

Contribution to the total circulation; nozzle vorticity

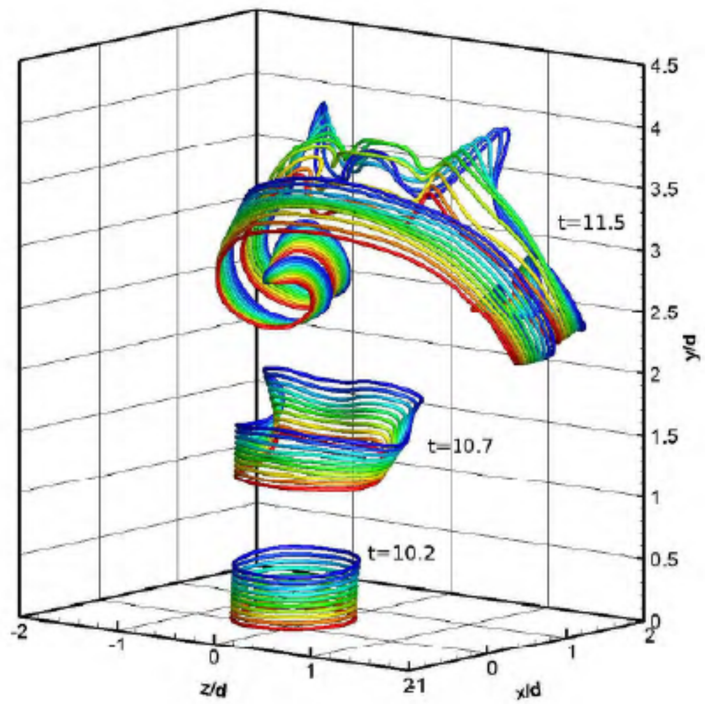

Classical view: vorticity from the nozzle BL (larger contributor because of velocity) folds on itself to form two crescents connected along the streamwise direction.

Not a complete picture as we show next

Schlegel, F., Wee, Dh, Marzouk, Y.M. and Ghoniem, A.F., Contributions of the wall boundary layer to the formation of counter-rotating vortex pair in transverse jets, *J. Fluid Mechanics*, Vol. 676, 2011, pp. 461-490.

MITMECHE

Contribution to the total circulation; wall vorticity

Lagrangian tracking

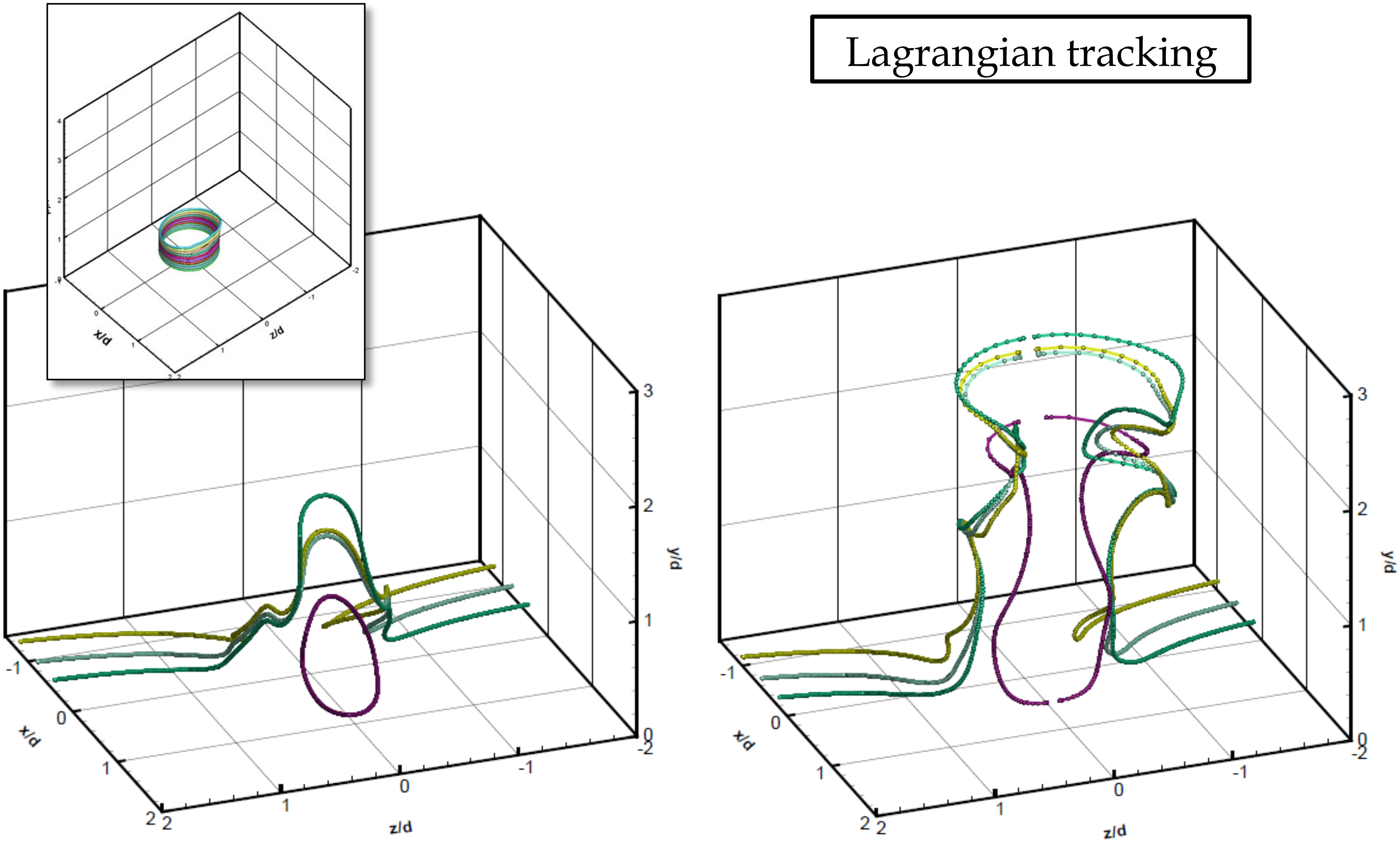

(a) $t = 10.0$

(b) $t = 10.5$

Near-wall CRV evolution

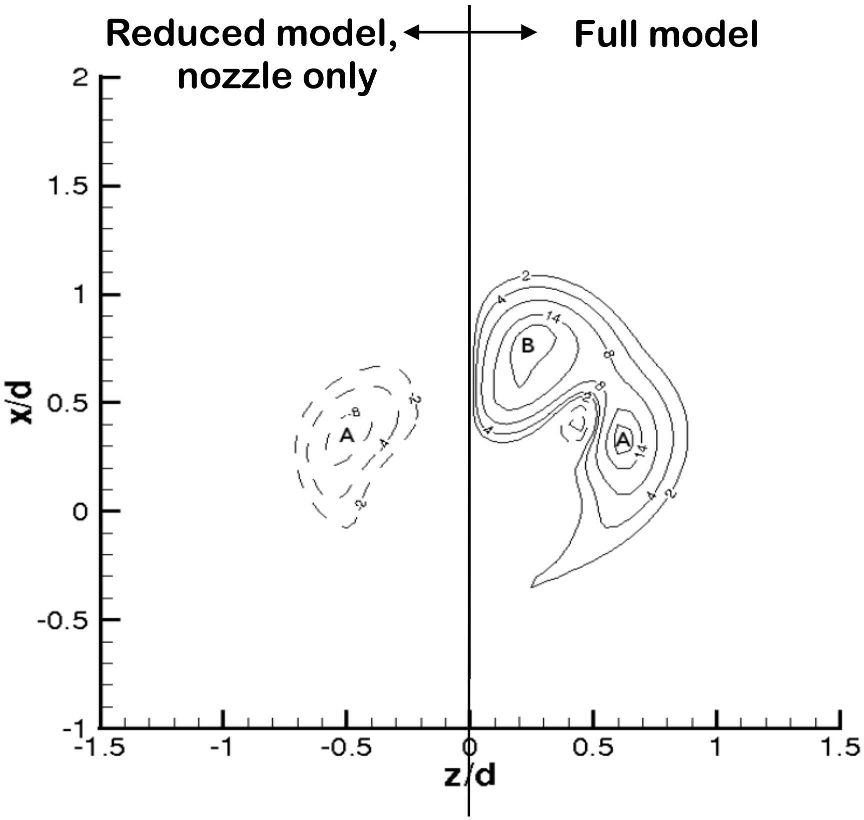

(b) $y/d = 1$.

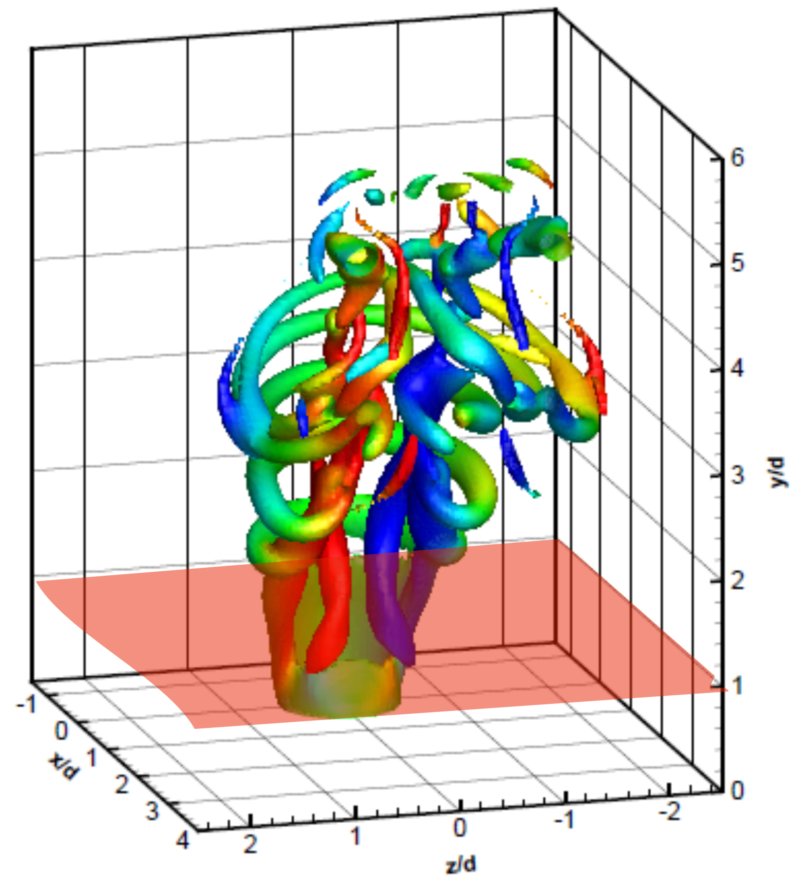

- Schlegel, F., Wee, Dh, Marzouk, Y.M. and Ghoniem, A.F., Contributions of the wall boundary layer to the formation of counter-rotating vortex pair in transverse jets, *J. Fluid Mechanics*, Vol. 676, 2011, pp. 461-490.

Near-wall structures #2

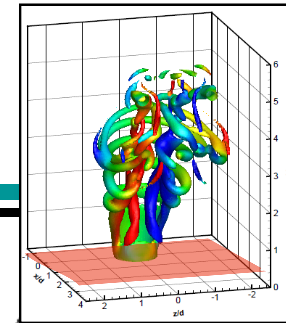

136 R. M. Kelso, T. T. Lim and A. E. Perry

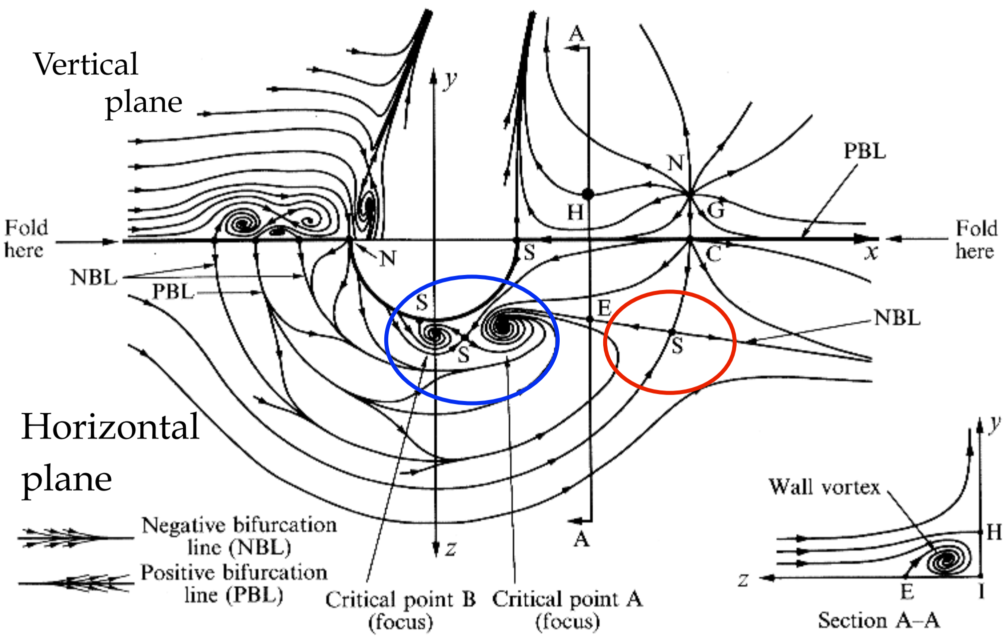

FIGURE 24. Composite streamline pattern. The horseshoe vortices are not included in section A-A. S denotes a saddle point and N denotes a node on the flat wall (x, z-plane) and centre-plane (x, y-plane).

Re=440, r = 6.0 (Kelso *et al.*)

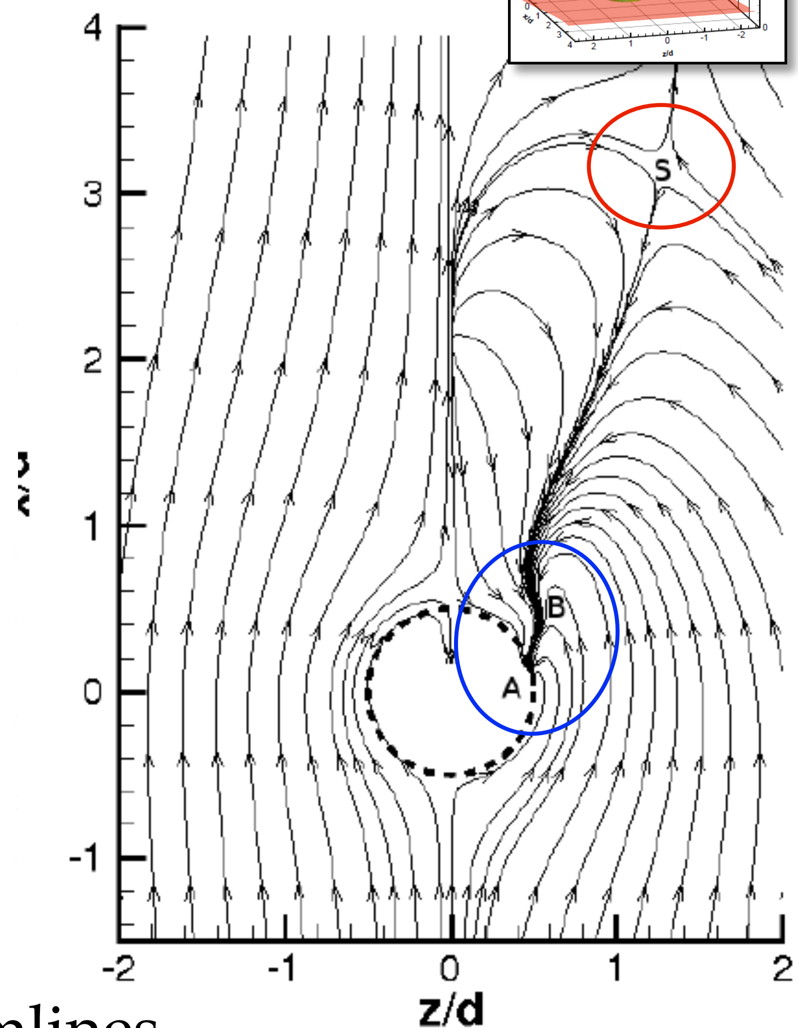

(a) $y/d = 0.2$

Instantaneous streamlines
at t = 10.0 on y=0.2

Importance of near-wall CRV formations

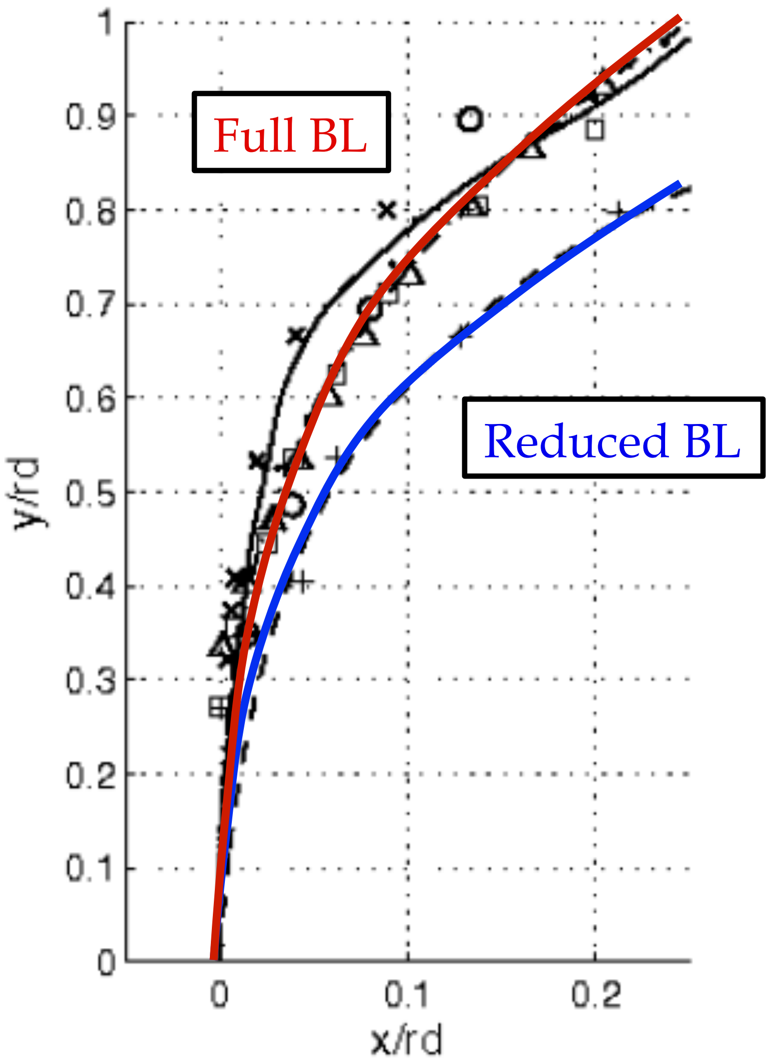

The wall boundary layer clearly contributes to the formation of near-wall CRVs.

⇨ The jet penetrates deeper

Inclusion of **feedback** and **separation** is **critical** to understand jet behaviors near the nozzle exit.

FIGURE 9. Computed trajectories verses experimental observations. Solid and dashed curves represent jet centre streamlines from the time-averaged velocity fields $t \in [10.0, 11.5]$ in Case II and $t \in [10.0, 11.5]$ in Case I, respectively. Upright crosses, squares, triangles, and slanted crosses represent the experimental data with $r = 4$, $r = 6$, $r = 8$, and $r = 10$ obtained by Keffer & Baines (1962), respectively. Circles show the data with $r = 7.72$ obtained by Kamotani & Greber (1972). Dots show the data with $r = 10$ obtained by Smith & Mungal (1998). The dash-dotted line represents an experimental correlation (3.1) for $r = 7$ from Margason (1968).

Actuation

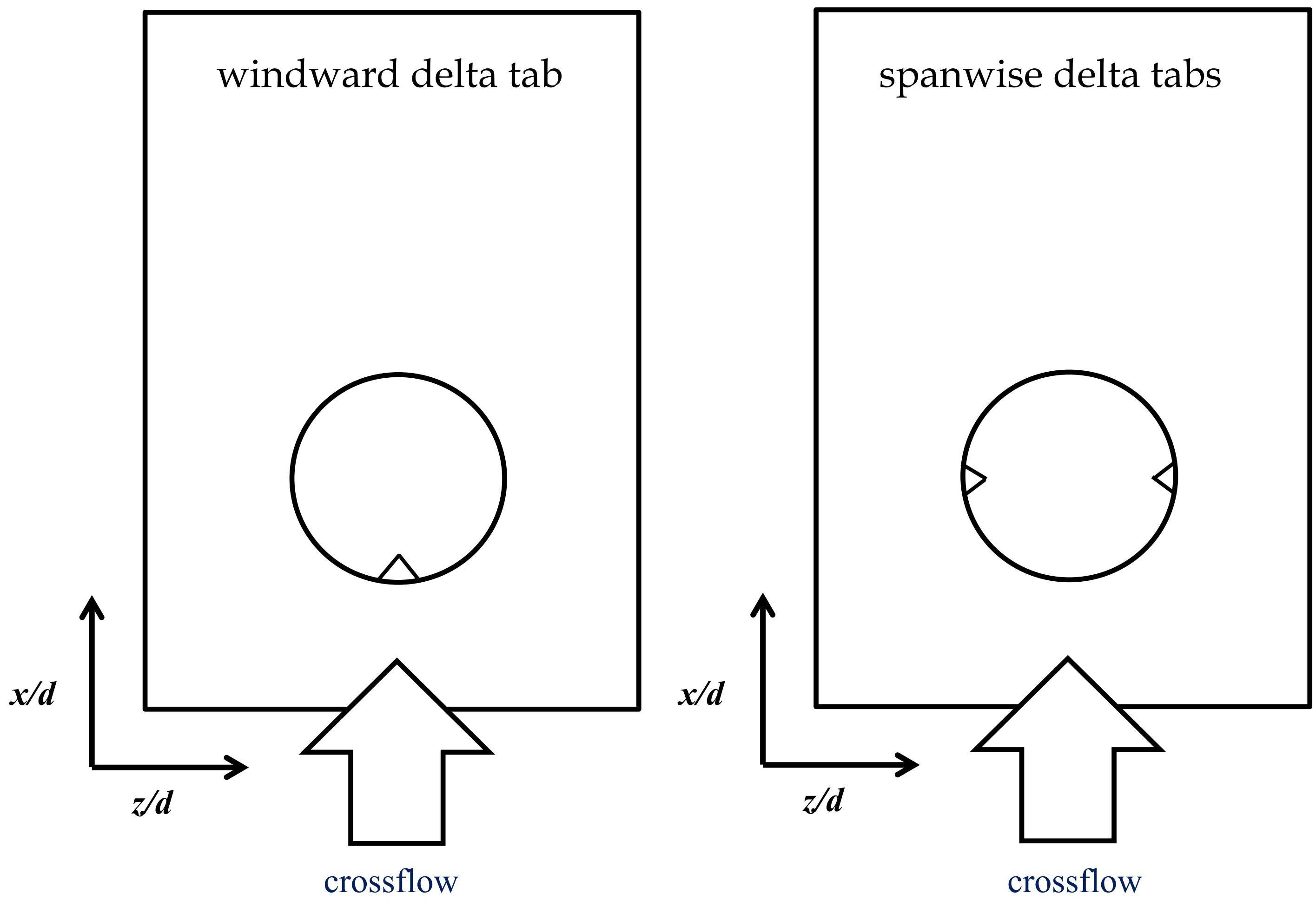

Tabs are oriented 45 degrees upwards with respect to the wall.

Delta tabs

$r = 7$
Re = 245
$Re_j = 1715$

Unforced jet

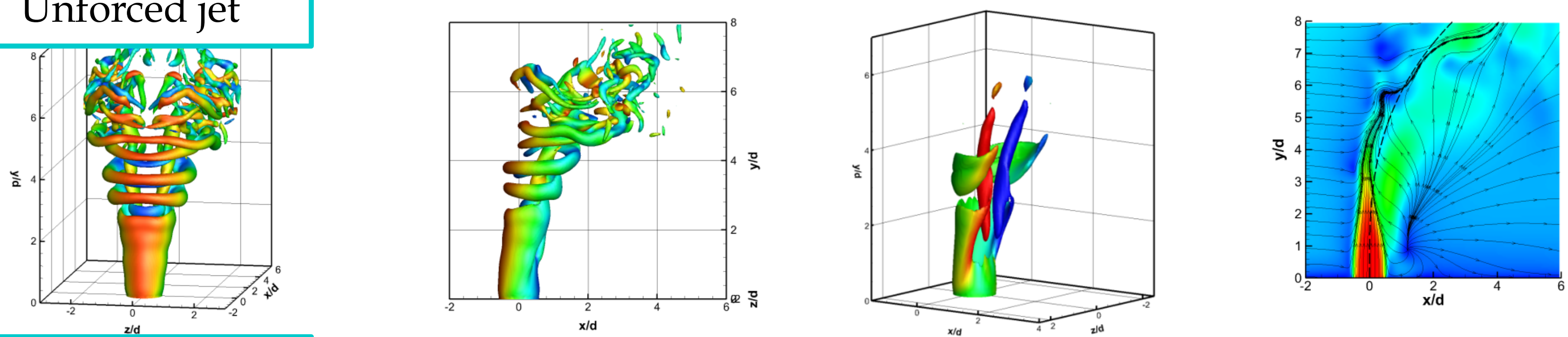

Windward tab

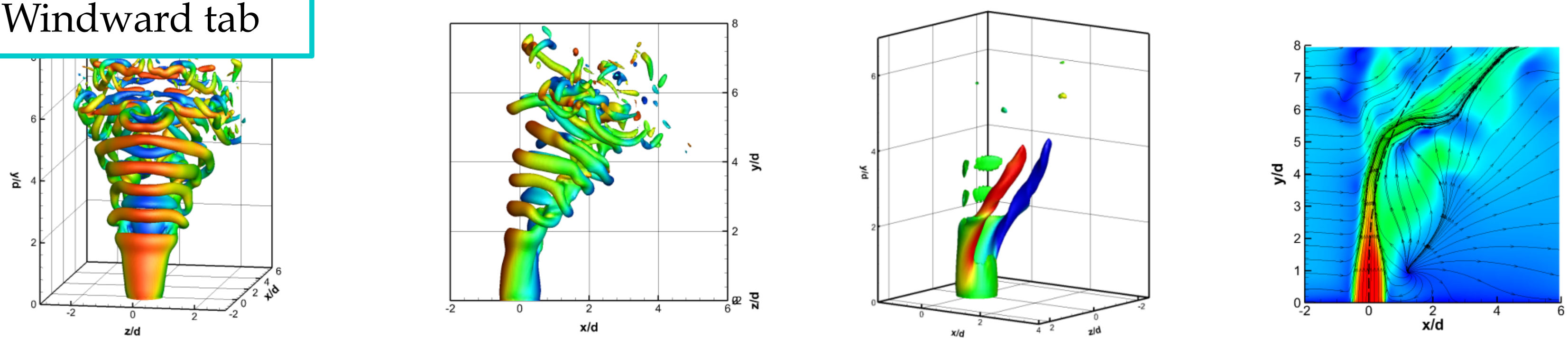

Lateral tabs

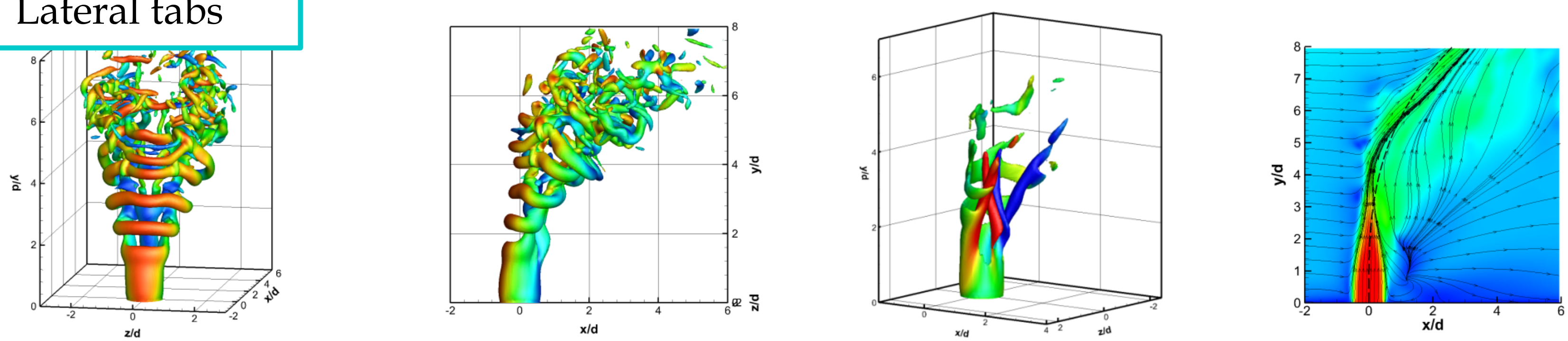

Bifurcating jets

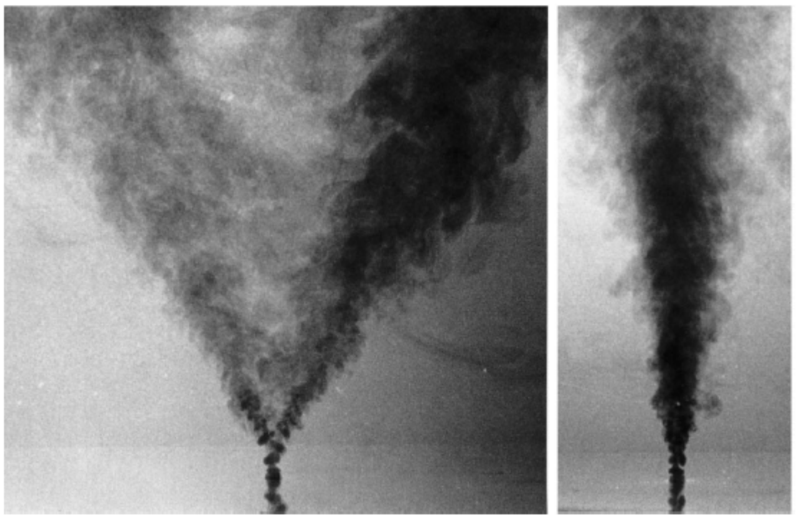

Figure 9 Bifurcating water jet at $Re \approx 20{,}000$ showing flow to $x/D \approx 80$: (*left*) bifurcation; (*right*) side view of the bifurcation. From Reynolds 1984.

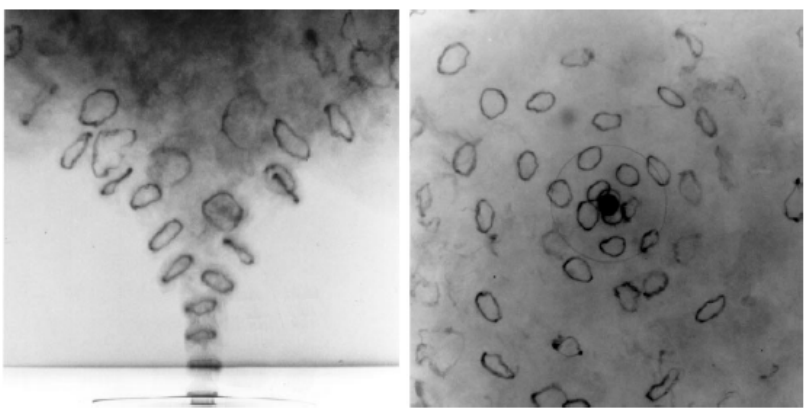

Figure 12 Side and axial views of a blooming water jet at $Re = 4300$, $r_f = 2.4$. Disturbances as in Figure 5. From Lee & Reynolds (1985a).

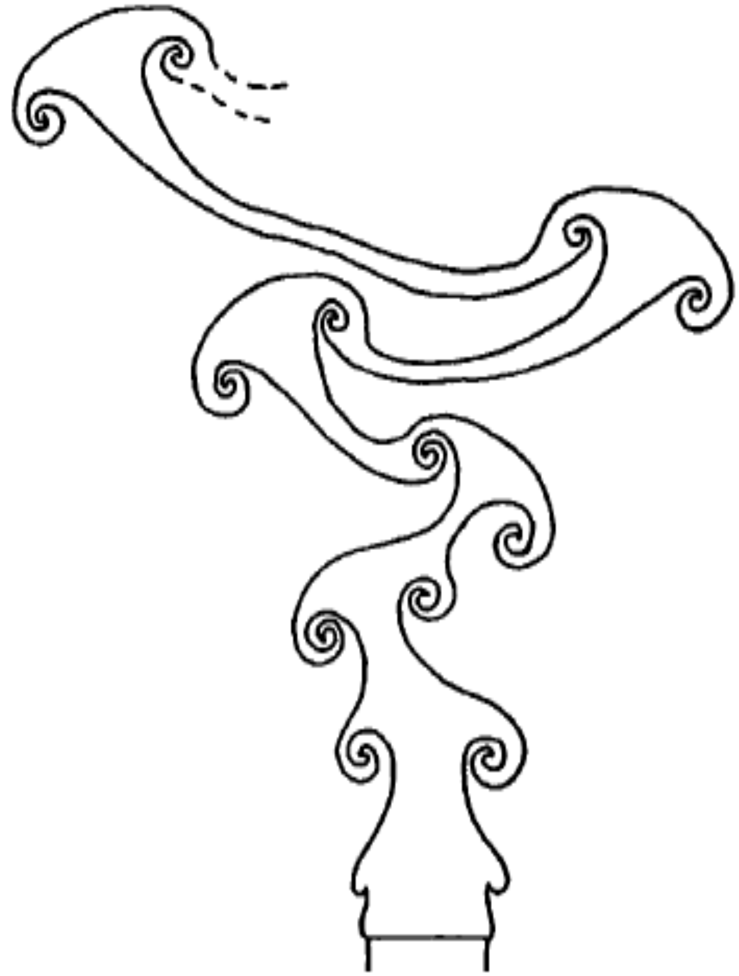

Flapping forcing

r = 7
Re = 245
Re_j =1715

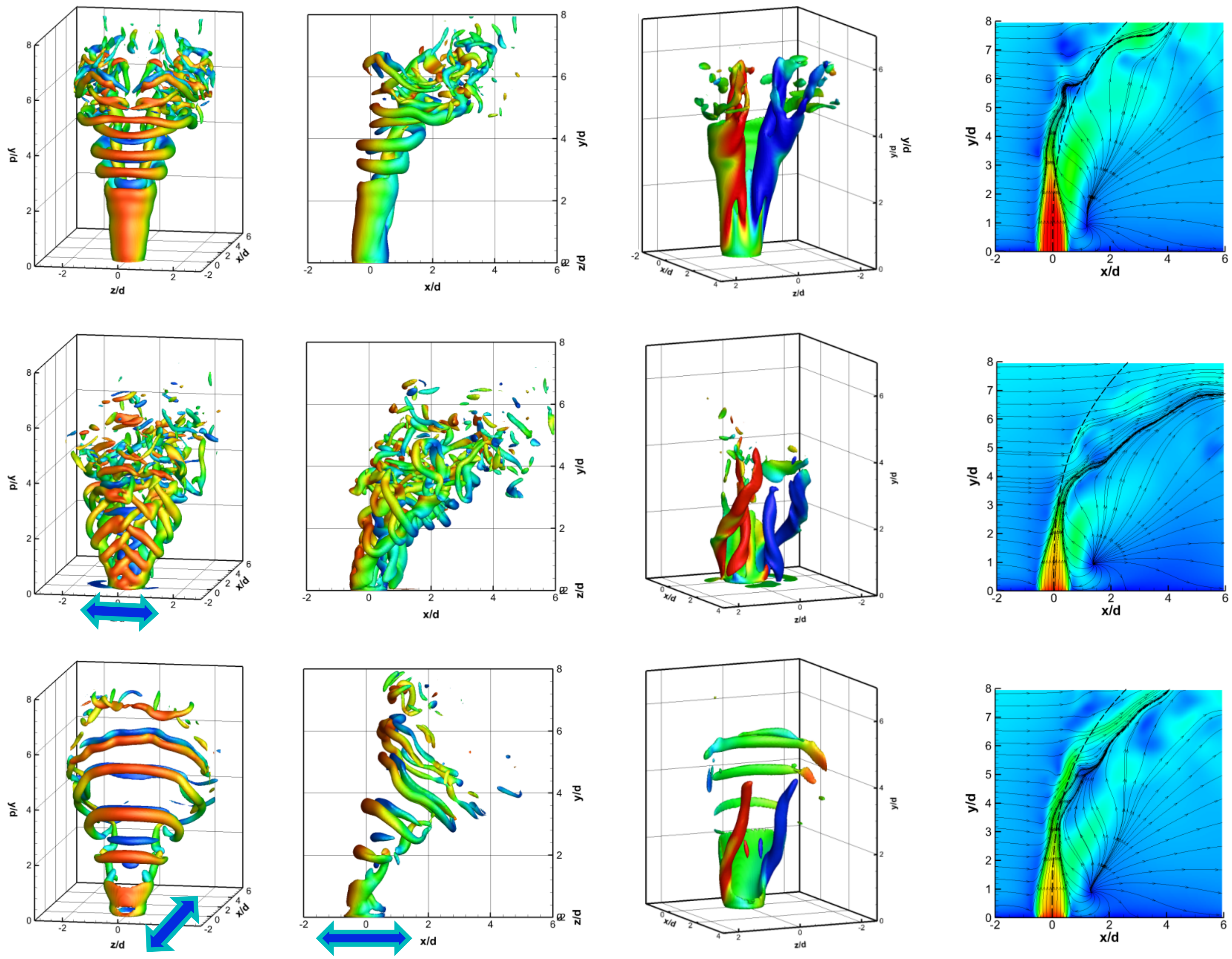

t=12.0

Spanwise flapping motions:

- Earlier breakdown into small scales
- Jet widened in the spanwise direction
- Initially upright, then bends quickly

Streamwise flapping motions:

- Delayed breakdown

$|\omega|= 20$

Reactive NS with Finite rate chemistry: Governing equations

Mass Continuity

$$\frac{\partial \rho}{\partial t} + \nabla.(\rho \mathbf{u}) = 0$$

$$\boxed{\varepsilon = -\frac{1}{\rho}\frac{D\rho}{Dt}}$$

Velocity-vorticity equation

$$\frac{\partial \omega}{\partial t} + \mathbf{u}.\nabla \omega = \omega.\nabla \mathbf{u} + (\frac{D\mathbf{u}}{Dt} - \mathbf{g}) \times \frac{\nabla \rho}{\rho} + \frac{1}{\rho}(\mu \Delta \omega - \nabla \mu \times (\nabla \times \omega) + \frac{4}{3}(\nabla \mu \times \nabla(\nabla.\mathbf{u})))$$

Thermal Energy

$$\rho c_p (\frac{\partial T}{\partial t} + \mathbf{u}.\nabla T) = \nabla.(\lambda \nabla T) - \sum_{k=1}^{K} c_{pk} \mathbf{j}_k.\nabla T - \sum_{k=1}^{K} h_k \dot{\omega}_k W_k + \Phi$$

Species continuity

$$\rho(\frac{\partial Y_k}{\partial t} + \mathbf{u}.\nabla Y_k) = -\nabla.\mathbf{j}_k + \dot{\omega}_k W_k$$

MITMECHE

LagrangianVortex Element Methods

Vortex simulations $\omega = \nabla \times \mathbf{u}$

Vorticity $\boldsymbol{\omega}$ instead of velocity $\mathbf{u}$:

$$\boxed{\frac{\partial \omega}{\partial t} + \mathbf{u}.\nabla \omega = \omega.\nabla \mathbf{u} + \frac{1}{\mathrm{Re}} \Delta \omega}$$

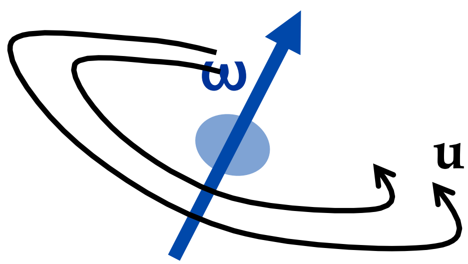

$$\boldsymbol{\omega}(\mathbf{x},t) \approx \sum_{1}^{N_\omega} \boldsymbol{\omega}_i(t) f_\sigma(\mathbf{x} - \chi_i(t))$$

$$\frac{d\chi_i}{dt} = \mathbf{u}(\chi_i, \mathrm{t})$$

$$\frac{d\boldsymbol{\omega}_i}{dt} = \boldsymbol{\omega}_i(t).\nabla \mathbf{u}(\chi_i, \mathrm{t})$$

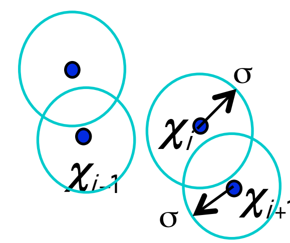

$$u_\omega(x) = \sum_i^N K_\sigma(x - \chi_i) \times \alpha_i$$

An element described by a discrete node point $\{\chi, \omega\}$

- **Inherent adaptivity with compact support of vorticity**
- **Less restrictive stability margins and low numerical diffusion**
- **No need for a pressure solver in semi-infinite domain**

Treecode for Fast Particle interactions

- Start with serial treecode, velocity from low order Rosenhead-Moore kernel (algebraic smoothing):

$$\mathbf{u}(\mathbf{x}_j) = \sum_{i=1}^{N} K_\delta^{RM}(\mathbf{x}_j, \mathbf{y}_i) \times \boldsymbol{\omega}_i$$

$$\mathbf{K}_\delta^{RM}(\mathbf{x},\mathbf{y}) = -\frac{1}{4\pi} \frac{\mathbf{x}-\mathbf{y}}{\left(|\mathbf{x}-\mathbf{y}|^2 + \delta^2\right)^{3/2}}$$

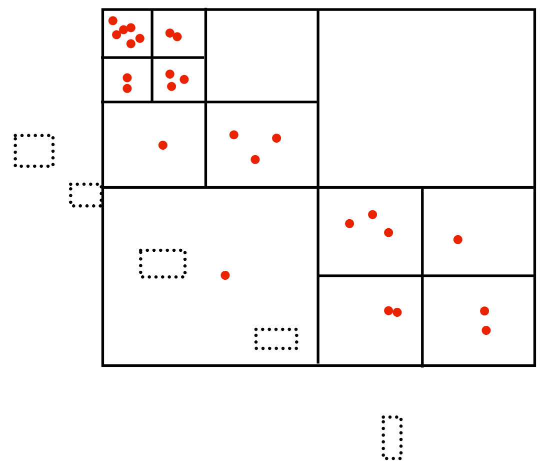

  - Constructs an adaptive oct-tree
  - Particle-particle to particle-cluster
  - Stop at leaf satisfying error:

$\Rightarrow$ use Taylor expansion of kernel in Cartesian:

$$\mathbf{u}(\mathbf{x}_{target}) = \sum_{i=1}^{N_c} \sum_p \frac{1}{p!} \underbrace{D_y^p K_\delta(\mathbf{x}_{target}, \mathbf{y}_c)}_{\text{Taylor coefficients, computed with recurrence relation}} \underbrace{(\mathbf{y}_i - \mathbf{y}_c)^p \times \boldsymbol{\omega}_i}_{\text{Cell moments, stored for re-use}}$$

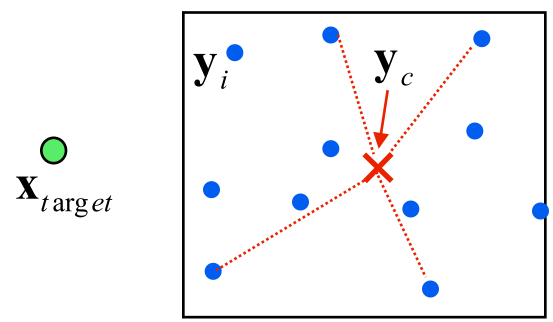

MITMECHE

Develop similar construction for a Second order kernel

– Winckelmans-Leonard kernel (**2nd-order** algebraic smoothing σ):

$$\mathbf{u}(\mathbf{x}_j)=\sum_{i=1}^{N}K_\delta^{WL}(\mathbf{x}_j,\mathbf{y}_i)\times\omega_i \qquad \mathbf{K}_\delta^{WL}(\mathbf{x},\mathbf{y})=-\frac{1}{4\pi}\frac{|\mathbf{x}-\mathbf{y}|^2+\frac{5}{2}\delta^2}{\left(|\mathbf{x}-\mathbf{y}|^2+\delta^2\right)^{5/2}}(\mathbf{x}-\mathbf{y})$$

$$\mathbf{K}_\delta^{WL}(\mathbf{x},\mathbf{y})=\mathbf{K}_\delta^{RM}(\mathbf{x},\mathbf{y})+\mathbf{K}_\delta^{\mathrm{cor}}(\mathbf{x},\mathbf{y}),\text{ where }\ \mathbf{K}_\delta^{\mathrm{cor}}(\mathbf{x},\mathbf{y})=-\frac{3\delta^2}{8\pi}\frac{\mathbf{x}-\mathbf{y}}{\left(|\mathbf{x}-\mathbf{y}|^2+\delta^2\right)^{5/2}}$$

$$\mathbf{u}(\mathbf{x})=\sum_{i=1}^{N_c}\sum_{\mathbf{p}}\frac{1}{\mathbf{p}!}D_{\mathbf{y}}^{\mathbf{p}}\mathbf{K}_\delta^{WL}(\mathbf{x},\mathbf{y}_c)(\mathbf{y}_i-\mathbf{y}_c)^{\mathbf{p}}\times[\omega dV]_i$$

$$=\sum_{i=1}^{N_c}\sum_{\mathbf{p}}\frac{1}{\mathbf{p}!}\Big(\underbrace{D_{\mathbf{y}}^{\mathbf{p}}\mathbf{K}_\delta^{RM}(\mathbf{x},\mathbf{y}_c)}_{\text{Taylor coefficients, computed with recurrence relation}}+\underbrace{D_{\mathbf{y}}^{\mathbf{p}}\mathbf{K}_\delta^{\mathrm{cor}}(\mathbf{x},\mathbf{y}_c)}_{\text{Taylor coefficients, computed with another recurrence relation}}\Big)(\mathbf{y}_i-\mathbf{y}_c)^{\mathbf{p}}\times[\omega dV]_i.$$

Estimated error btw SUMMATION and APPROXIMATION **Error control parameter**

$$\frac{M_p(c)}{4\pi R^{p+1}}\left(1+\frac{(p+2)(p+1)}{2}\frac{\delta^2}{R^2}\right)\le\varepsilon\ , \qquad \text{where} \qquad M_p(c)=\sum_i^{N_c}\|x_i-y_c\|^p\,|\omega_i|$$

Wee, D.H., Schlegel, F., Marzouk, Y. and Ghoniem, A.F., “A treecode algorithm for a high order algebraic kernel in vortex methods,” *SIAM J for Scientific Computing*, Vol. 31, No 4, 2009.

Parallel Implementation Using *k*-means Clustering

- Partition field into clusters:
  - Choose clusters and cluster centroids (processor work), and associated elements to minimize a cost function

$$J = \sum_{i}^{N} \min_{k} \left(\left\| x_i - y_k \right\|^2 \left| w_i \right| \right), \quad y_i \text{ is cluster centroid, } w_i \text{ is weight}$$

  - General scheme: update *centroids and clusters* based on previous time step's times, scaling.
  - Each processor computes field of its cluster on the entire fields.
  - Sum over all fields.

Marzouk, Y.M., and Ghoniem, A.F., "K-mean clustering for partition and dynamic load balance of parallel hierarchical n-body simulations" ***J. Comput. Phys.*****, Vol. 207, 2005, 493-528.**

Parallel domain decomposition for parallel implementation

cluster partition
N=157297, k=128

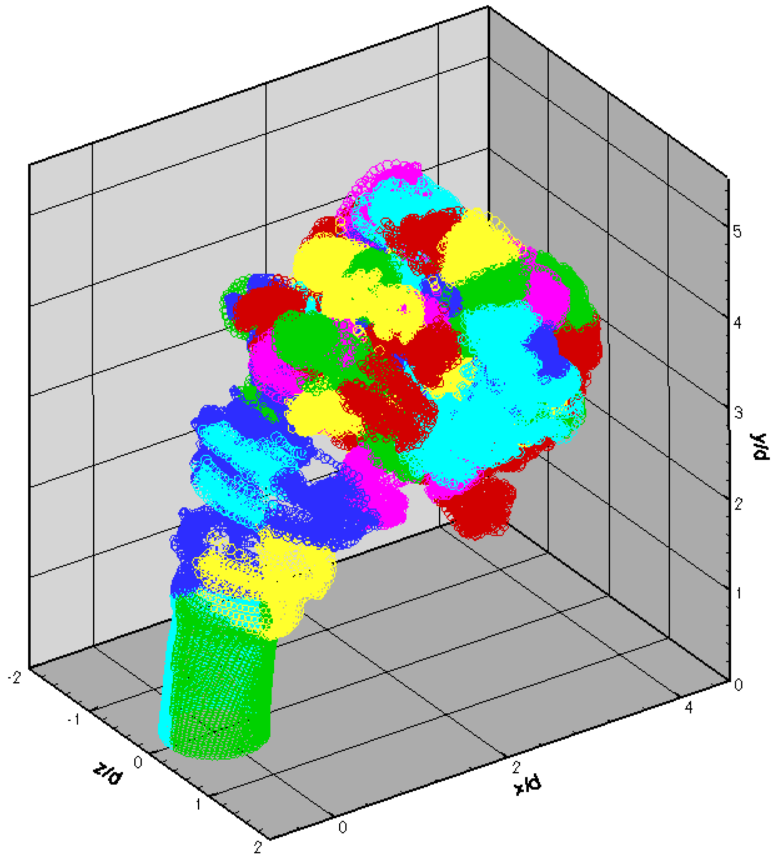

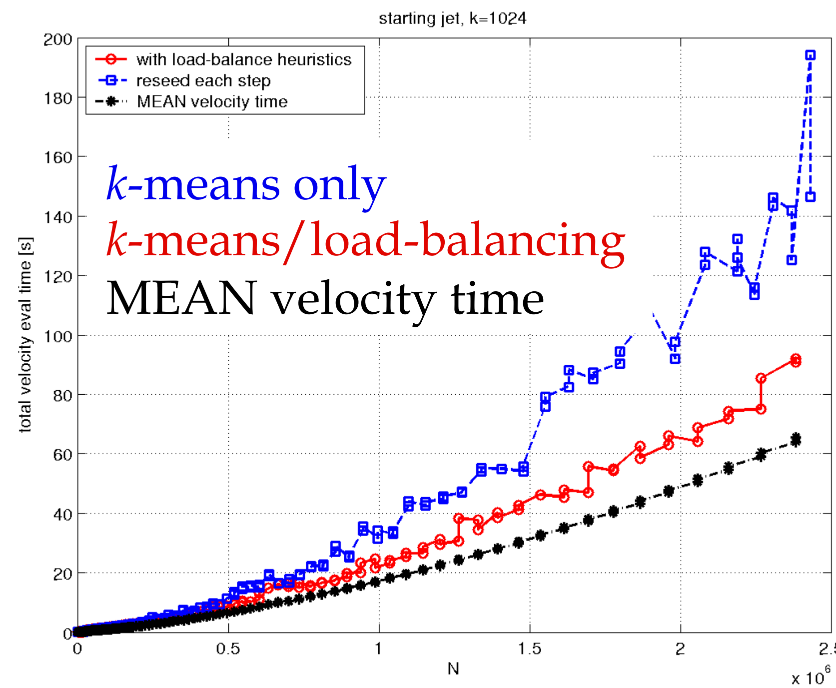

Wee, D.H., and Ghoniem, A.F., “Modified interpolation kernels and treating diffusion and remeshing in vortex methods,” *J. Comput. Phys.*, 213, 2006, pp. 239-263.

Diffusion

Grid-free Redistribution:

Shankar, RGD Internal Report (1999)

Lakkis, I. and Ghoniem, A.F., "Axisymmetric vortex method for low-Mach number, diffusion-controlled combustion," *J. Comput. Phys.*, Vol. 184: 435-475, 2003.

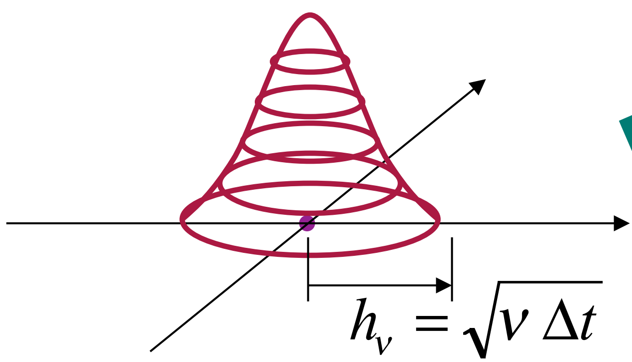

Fundamental solution

Matching moments

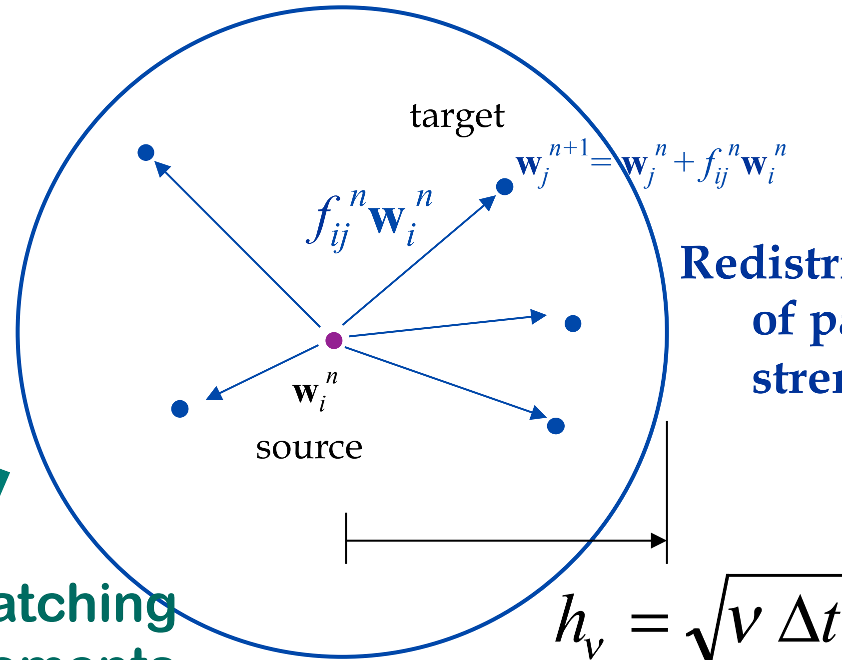

Redistribution of particle strength

Redistribution radius

Evolution equations for moments are discretized spatially with **Dirac measures** and temporally with **an explicit integration scheme**.

Galerkin formulation…

Redistribution formulae

$$\sum_j f_{ij}^n = 1$$

$$\sum_j f_{ij}^n (x_j^n - x_i^{n-1}) = 0$$

$$\sum_j f_{ij}^n (x_j^n - x_i^{n-1})^2 = 2\nu\Delta t_d$$

3D validation runs

- Evolution of a Vortex Ring at Re = 500
  vs. Stanaway *et al*. (1988)

  Intermediate Reynolds Number
  Convection & Diffusion

- Asymptotic Drift of a Vortex Ring
  vs. Rott & Cantwell (1993)

  Low Reynolds Number
  Diffusion-dominated Flow

- Vortex Reconnection
  vs. Kida *et al*. (1991)

  3D Flow Features

Schlegel, F., Wee, D.H, and Ghoniem, A.F., "A fast 3d particle method for simulations of buoyant flows", *J. Comput. Phys*, 227, 21, 2008, pp. 9063-9090.

Application to transverse jets

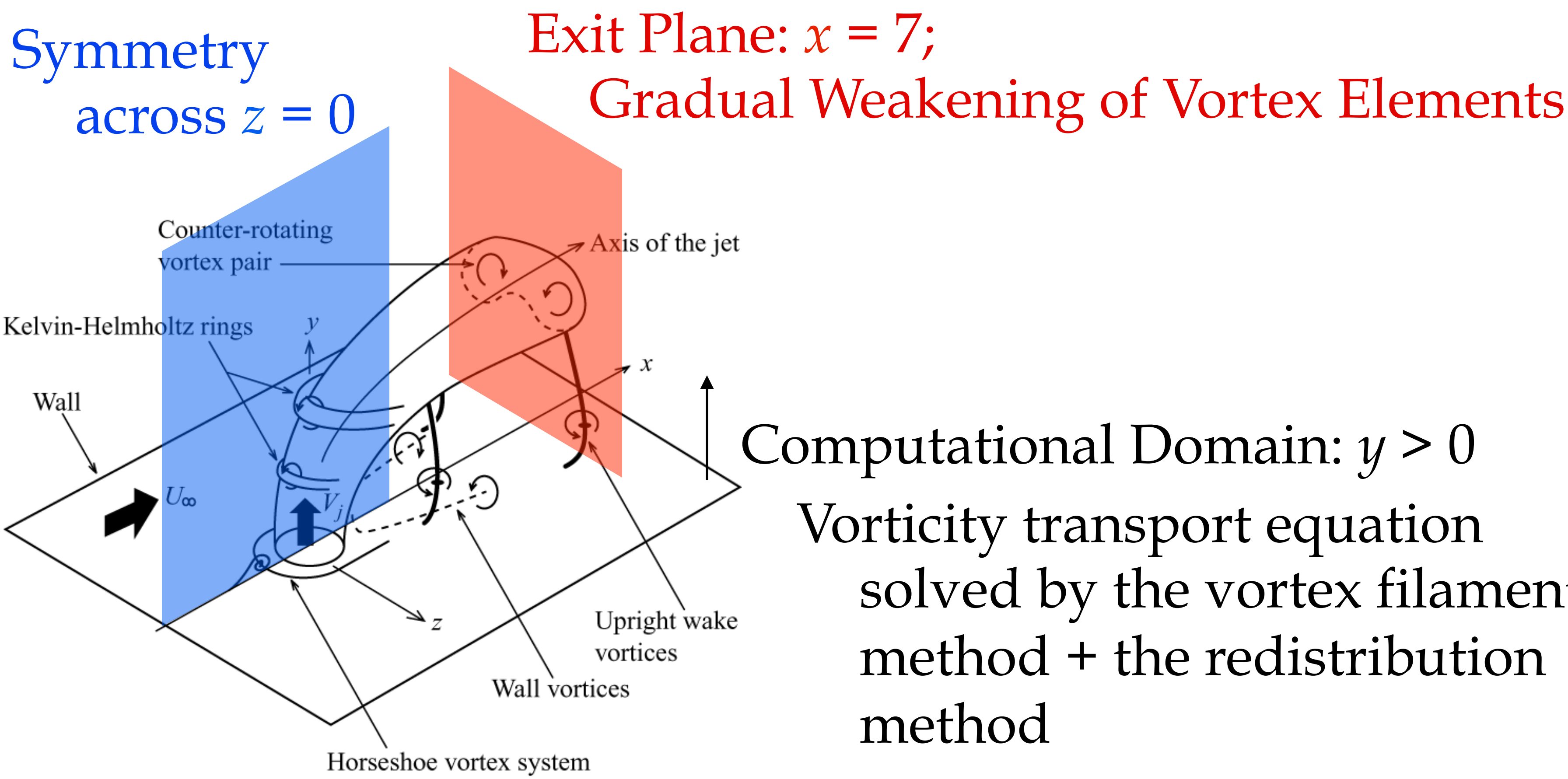

Computational Domain: $y > 0$

Vorticity transport equation solved by the vortex filament method + the redistribution method

Normalization based on U_∞, d

Boundary conditions in transverse jets

Imposing the boundary conditions in terms of vorticity generation at the walls

>> No-slip boundary condition γ_j

>> In-pipe boundary layer advected into the domain γ_c

>> Solenoidality ?

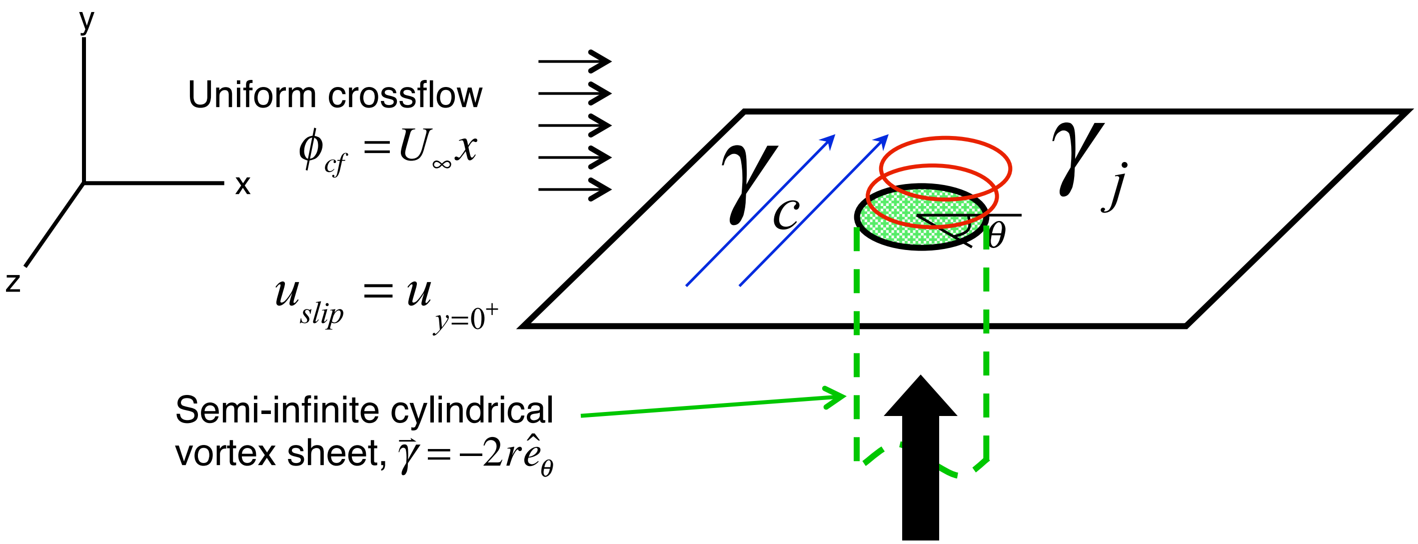

Two-way coupling

From Lagrangian field to the Eulerian field

- Vortex particles are used to compute the velocity on the faces of the finite volume in order to solve for the convective term on the grid

From the Eulerian field to the Lagrangian field

- The baroclinic generation of vorticity is computed on the grid, before being converted to vortex particles.
- Vortex particles are generated from the grid during the diffusion steps
- Expansion particles are generated from the grid as well and converted into expansion particles, used to compute the expansion velocity field

Scheme

- Time discretization: 2nd order predictor-corrector scheme
- Spatial discretization: 2nd order upwind Godunov scheme

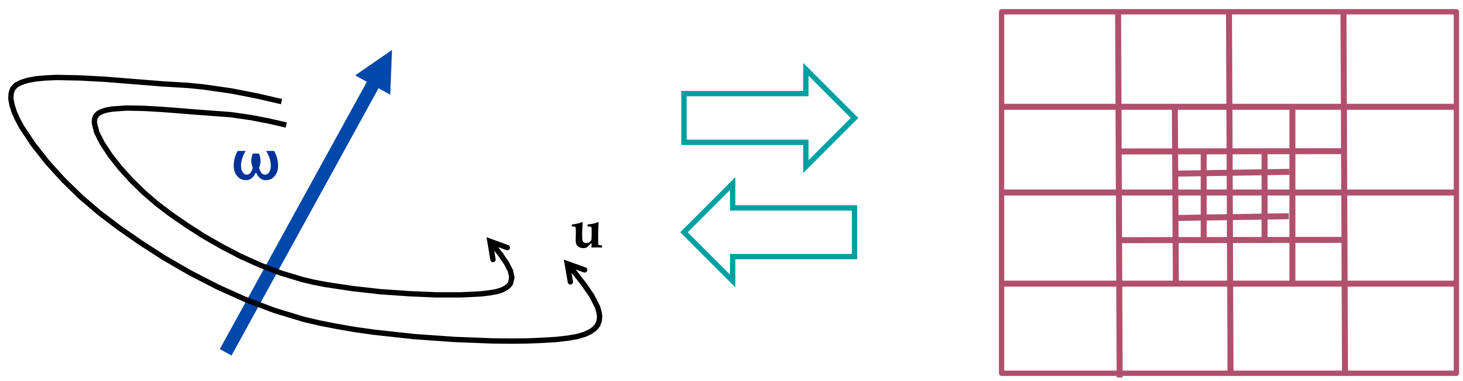

Data Structure and Parallelization

- **Lagrangian Scheme, Vortex Method**:
  - K-mean clustering of particles (Y Marzouk) for good load balancing, combined to a ring algorithm.
  - From a "Copy" to a "Ring" Algorithm
- **Eulerian Scheme, AMR:**
  - Peano-Hilbert space filling Curve, PARAMESH
- **Parallel library:** MPI
- **Hardware:**
  - Pharos
  - Shaheen (KAUST)

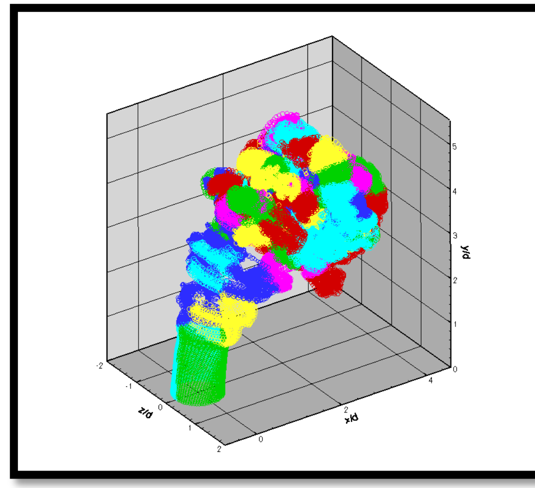

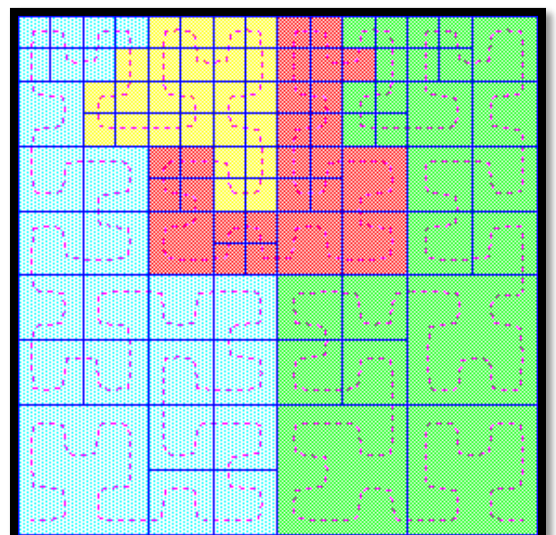

MITMECHE

Reactive Jet

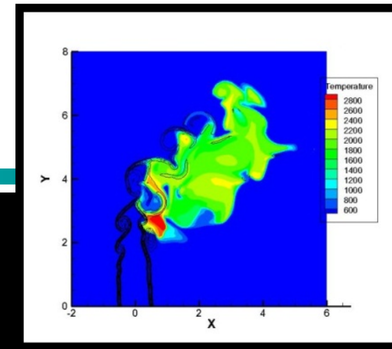

Temperature surfaces

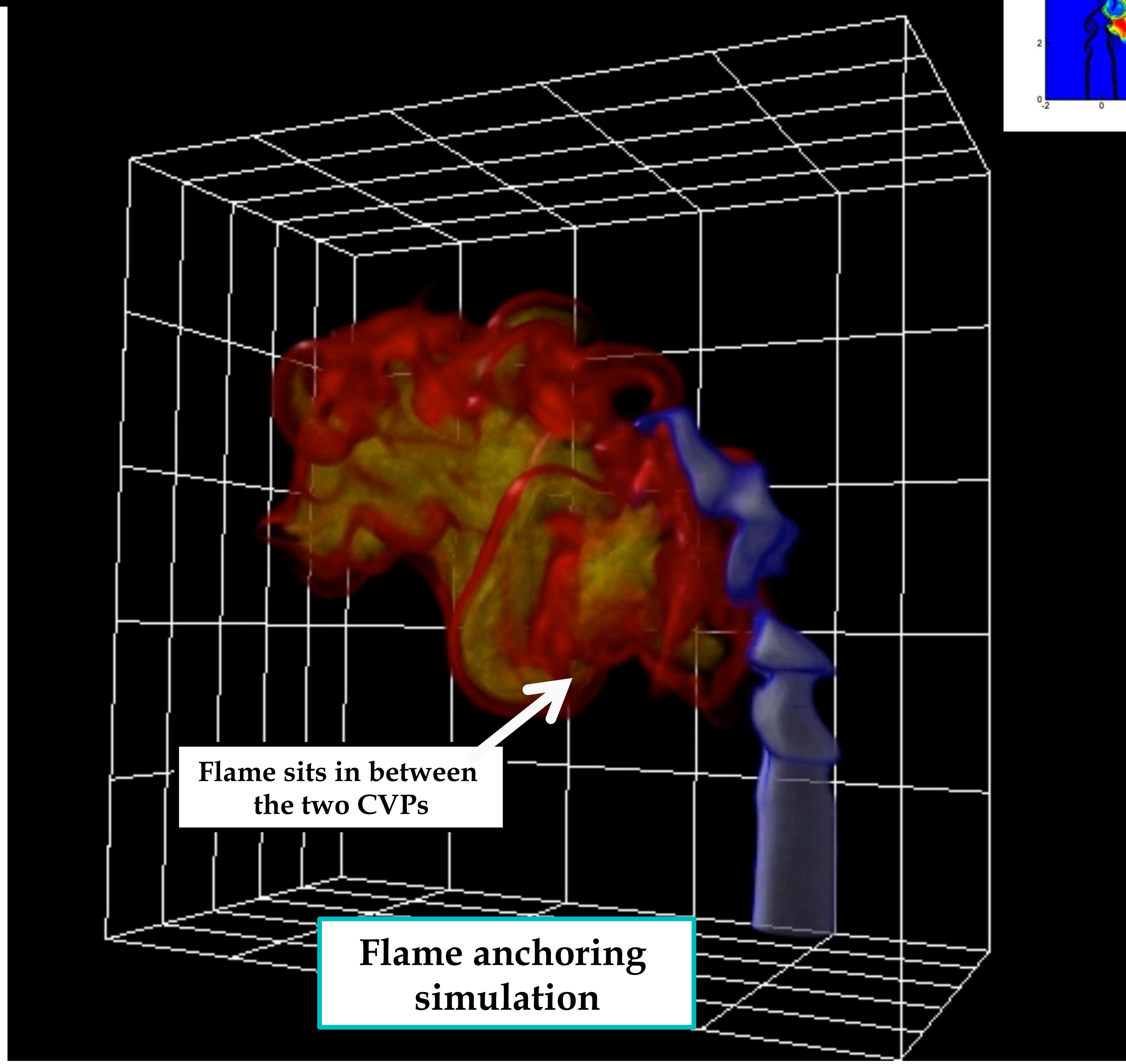

Cold vs. reactive flow comparison

Cold Flow

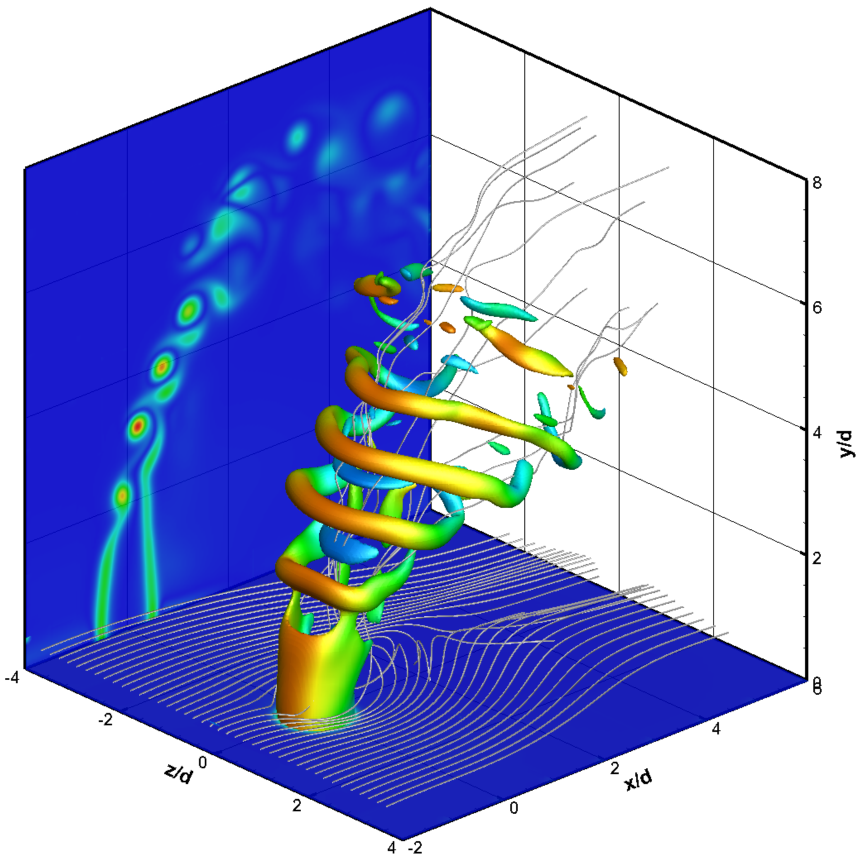

Reactive case

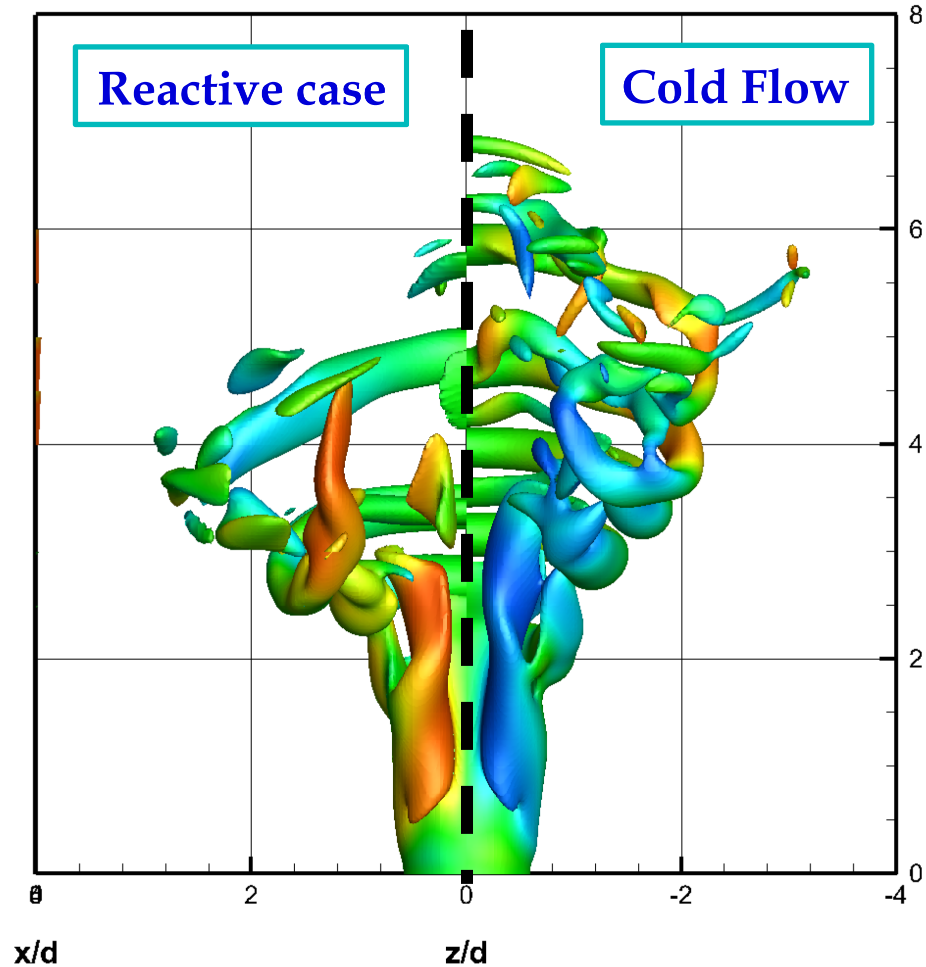

Cold vs. reactive flow comparison

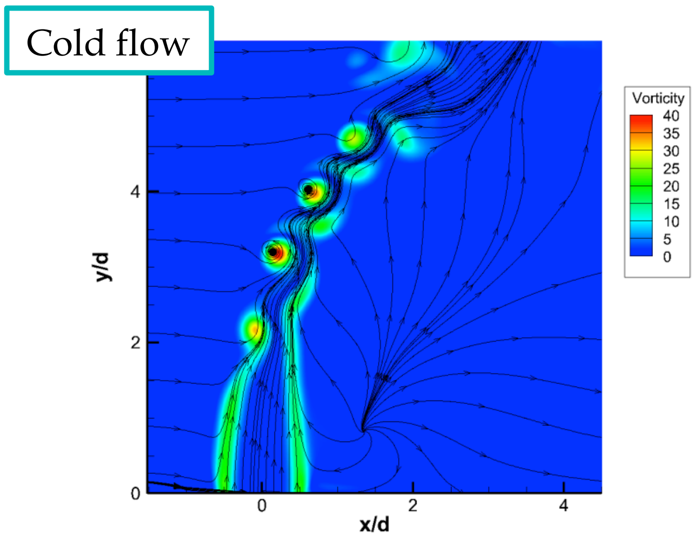

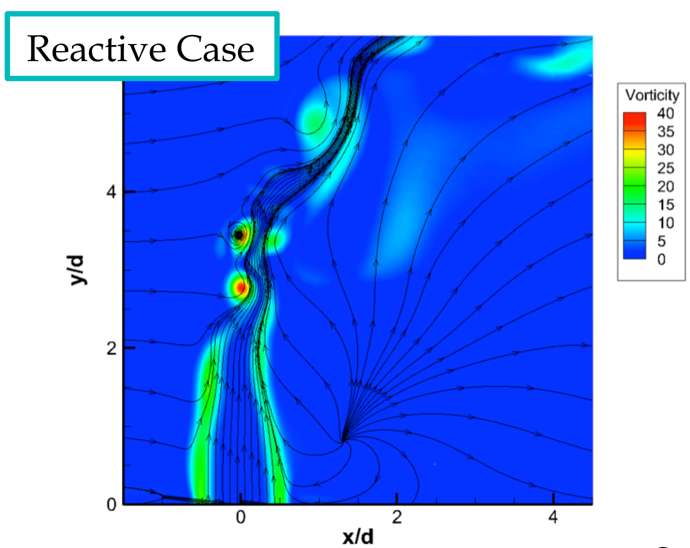

Hasselbrink and Mungal

⇨ Impact of expansion velocity

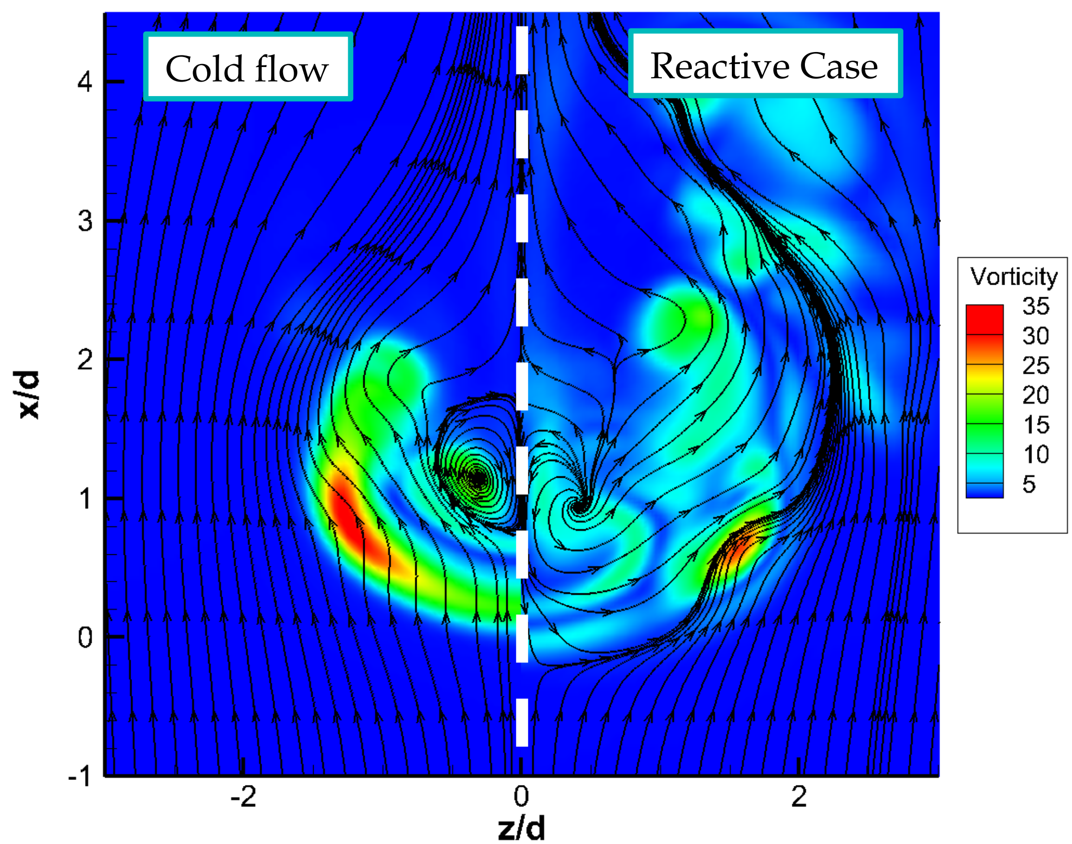

Streamlines and vorticity contours on the *y=3-plane*

Reactive jet analysis; where is the flame? where does it initiate? Needs tools to analyze data

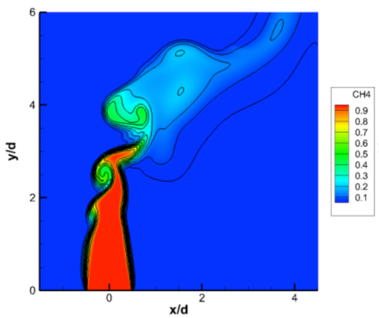

CH4

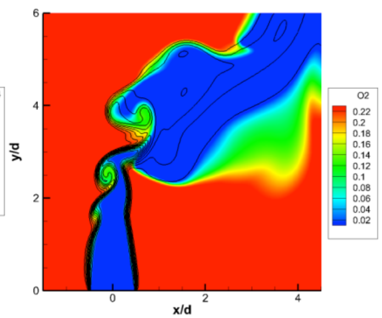

O2

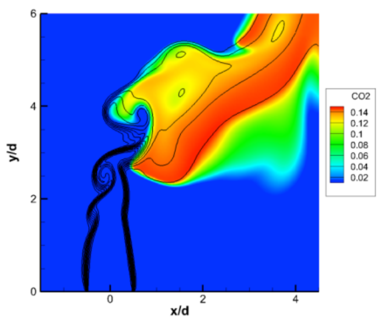

CO2

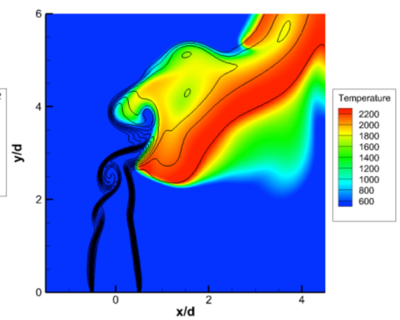

Temp.

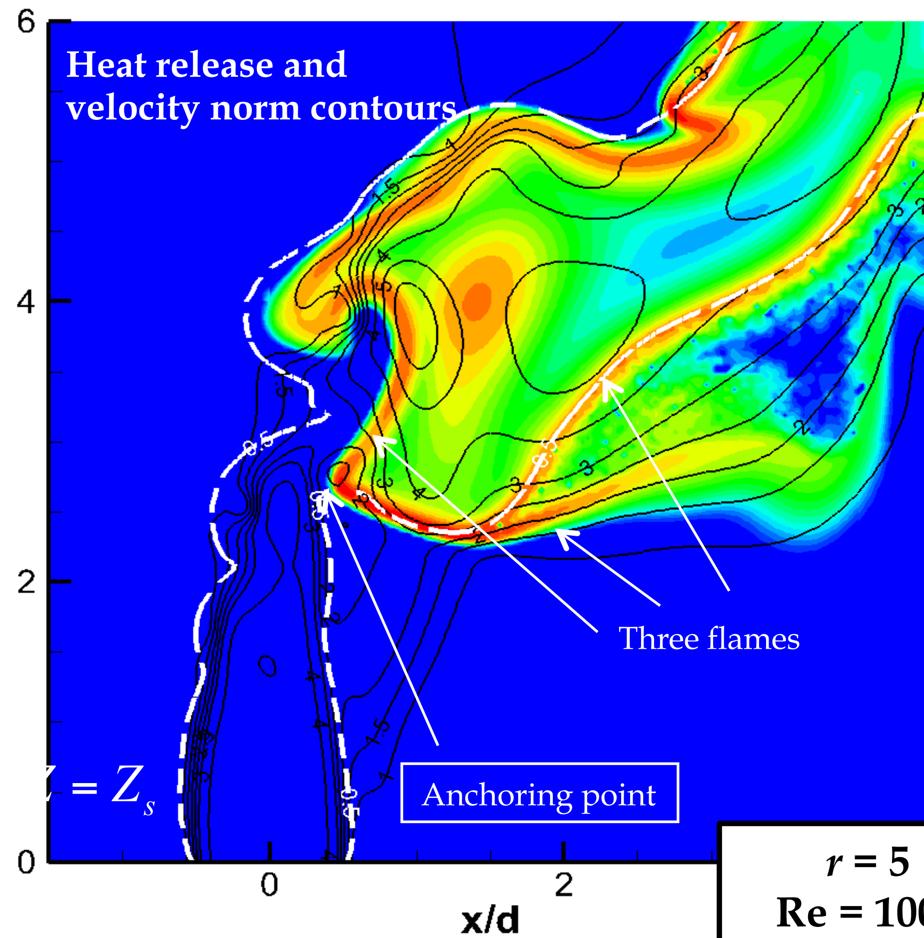

r = 5
Re = 1000
Da=42000
Fr=inf

According to stoichiometry, non premixed flames should be at stoichiometric contour Z_s but we see multiple flames??

What are they and why are they there?

Define another property to identify the flame (non premixed and premixed)

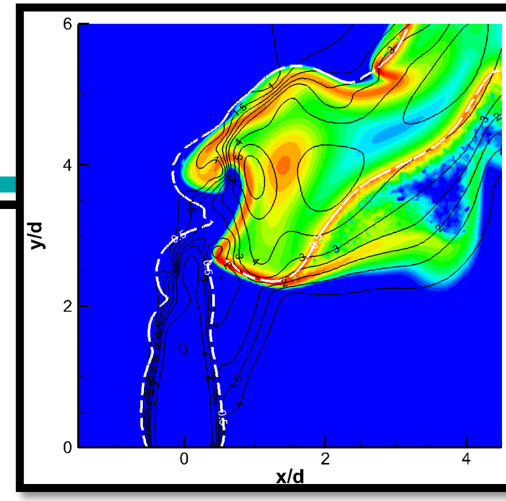

We observe the formation or A Triple Flame

- Plot Takeno's Flame Index and Heat Release Rate
- Where they coincide there is a flame
- But two types of flames exist!

$$FI_{Takeno} = \frac{\nabla Y_{CH_4} \cdot \nabla Y_{O_2}}{|\nabla Y_{CH_4}||\nabla Y_{O_2}|}$$

FI > 0 premixed flame (RED)

FI < 0 diffusion flame (BLUE)

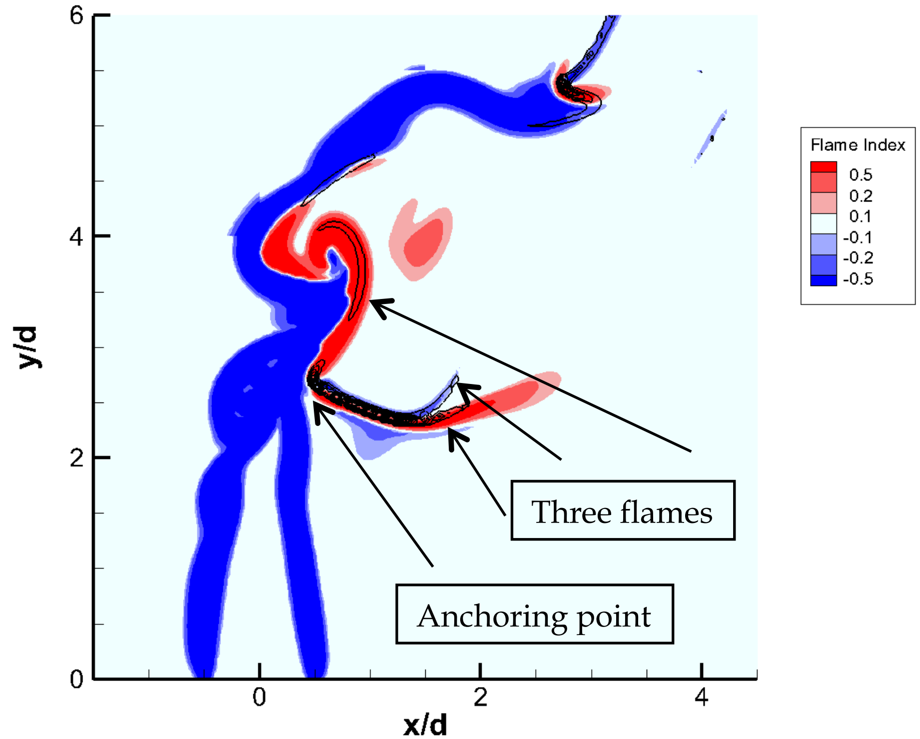

Expanded view of triple flame

$$FI_{Takeno} = \frac{\nabla Y_{CH_4} \cdot \nabla Y_{O_2}}{|\nabla Y_{CH_4}||\nabla Y_{O_2}|}$$

$FI > 0$ premixed flame (red)

$FI < 0$ diffusion flame (blue)

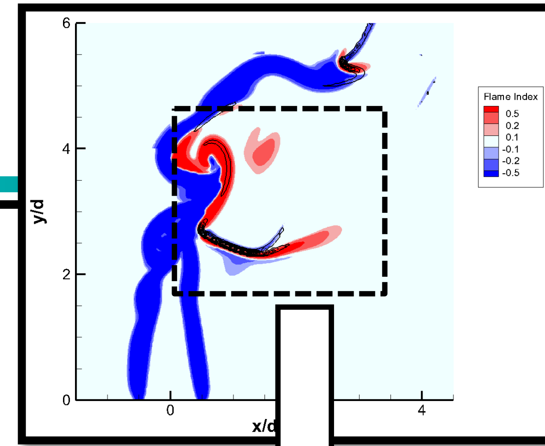

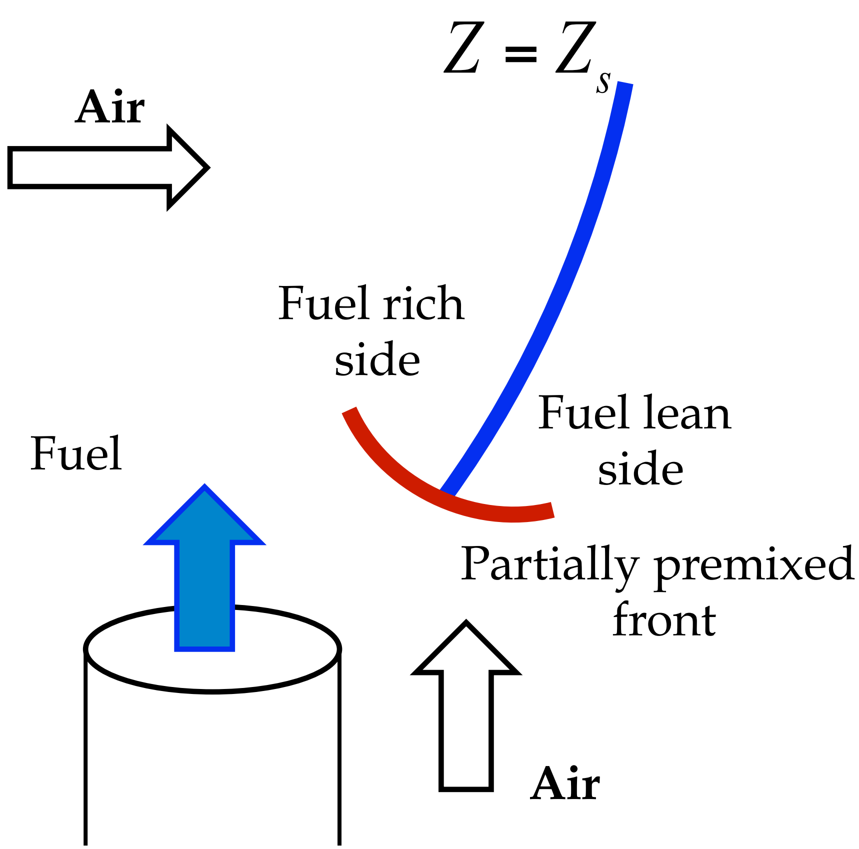

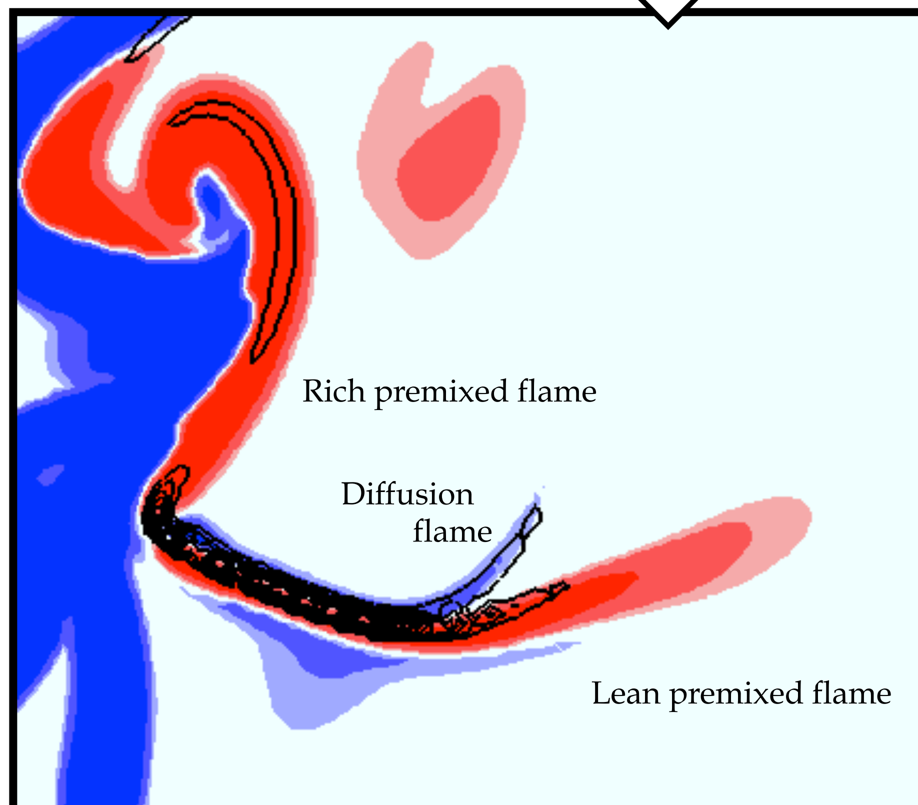

Flame structure in another view

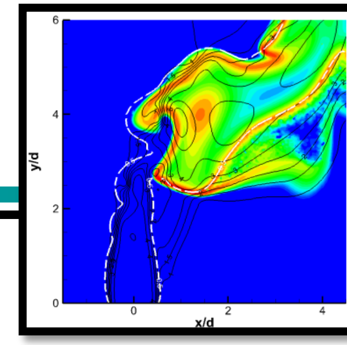

Premixed flames are almost parallel to velocity contours

Diffusion flame follows stoichiometric line (almost normal to vel. Contours)

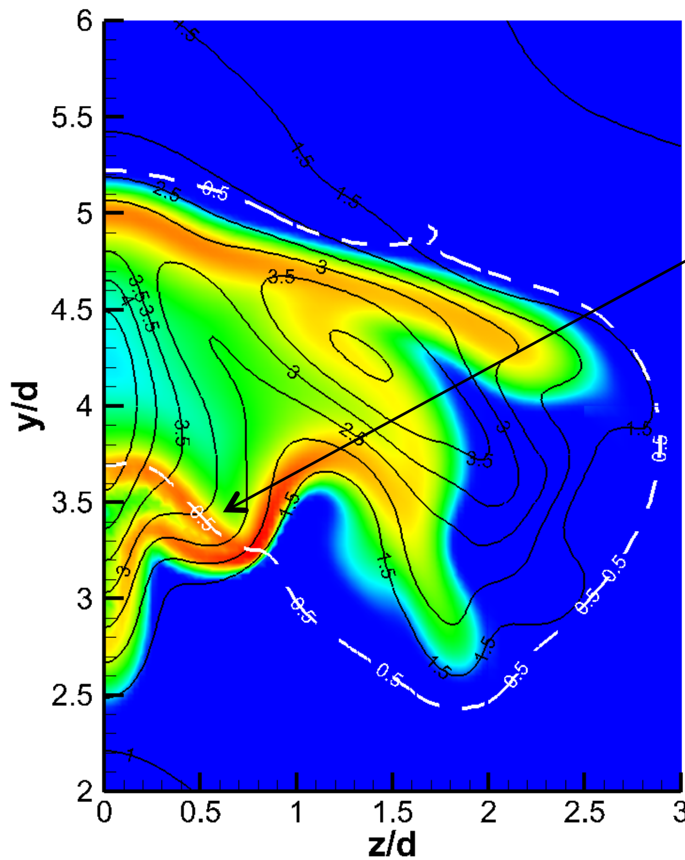

The triple flame

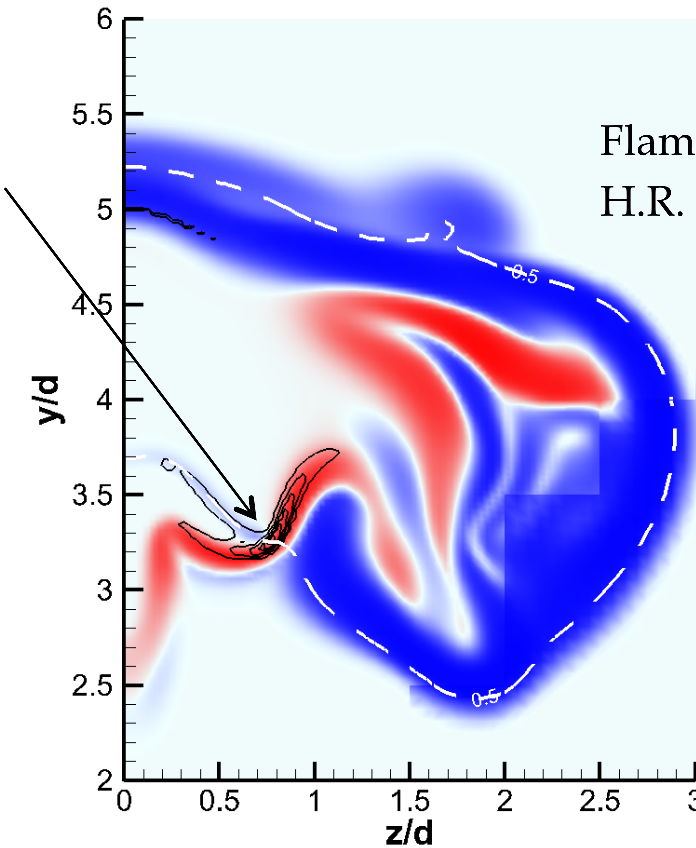

Flame index

H.R. contours

Flame structure and vorticity

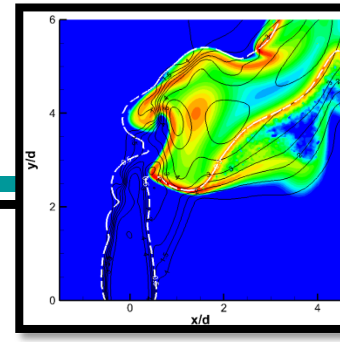

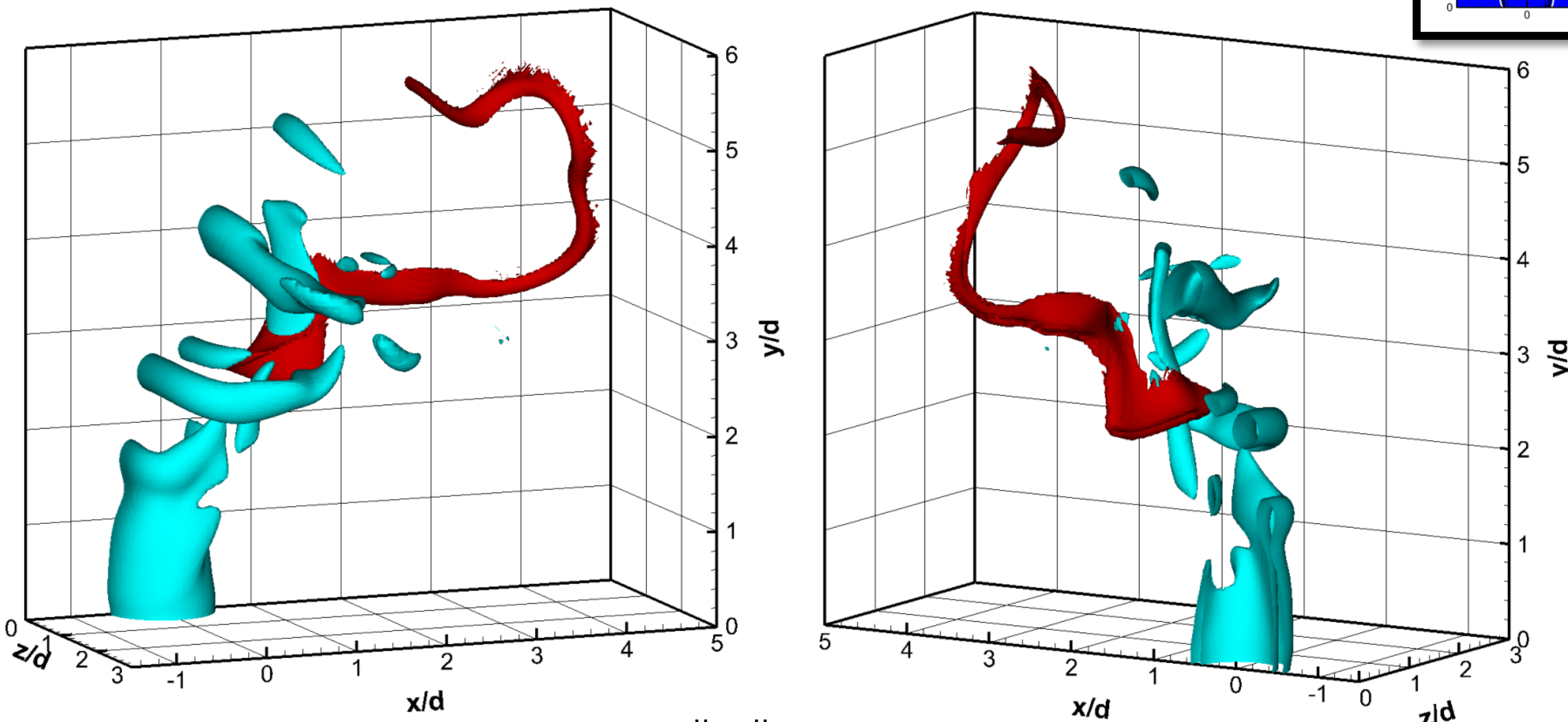

$$\|\omega\| = 15$$

$$q''' = 3.5\,10^8 \text{ W/m}^3$$

Vorticity isosurfaces, in cyan and heat release rate isosurfaces contours in red under to different perspectives.

Why is the flame stabilized at this point?

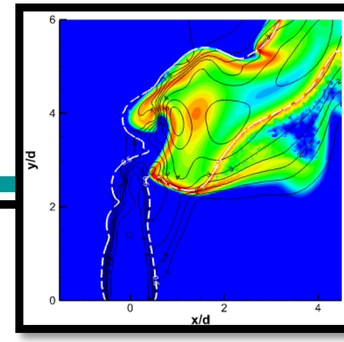

$$\chi = 2D\|\nabla Z\|^2$$

Scalar Dissipation Rate (SDR) (inverse of mixing time scale)
Fast mixing prevents diffusion flame from forming early

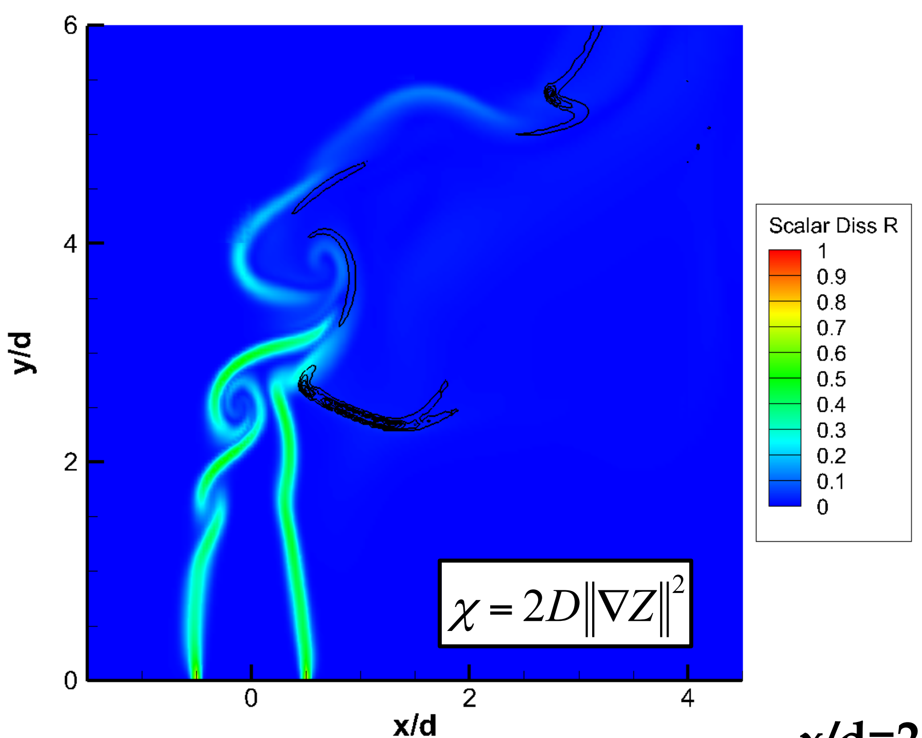

x/d=2.5

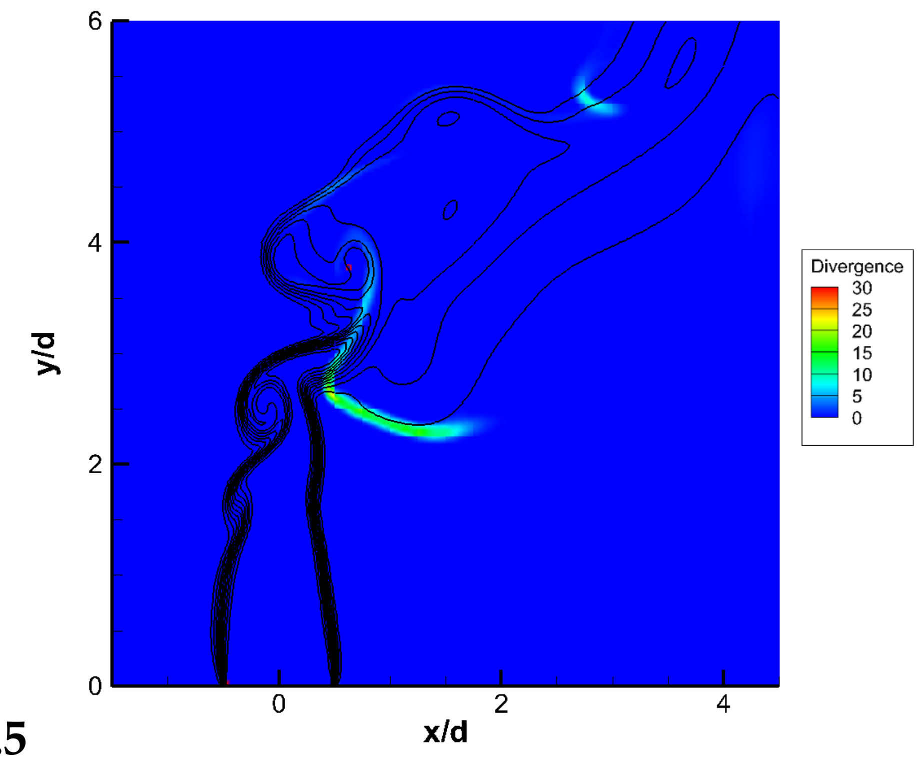

How flames stabilize/anchor near solid corners?

$Re_d = 500$

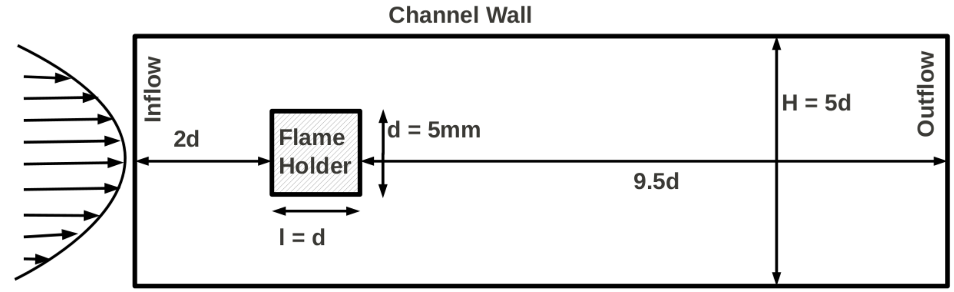

Fully-developed parabolic profile for a channel flow at inlet

C1 mechanism for methane: 16S/46R

Immersed boundary with dual buffer

4^{th} order space , 2^{nd} order time

AMR

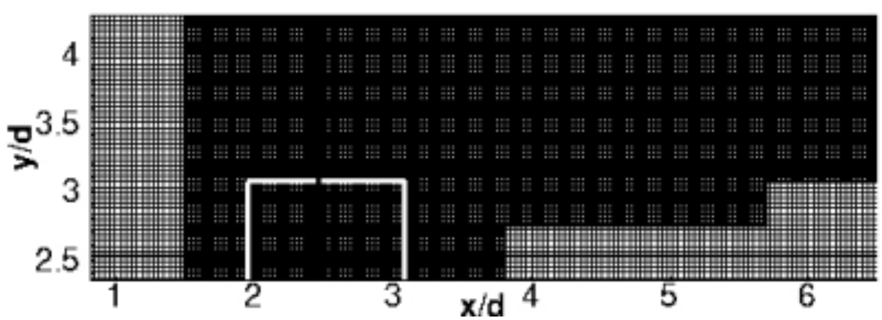

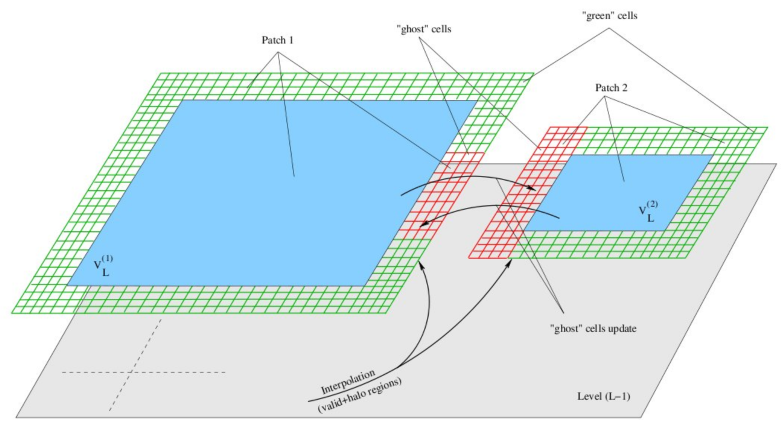

Kedia, et al. J. Comput. Phys, …

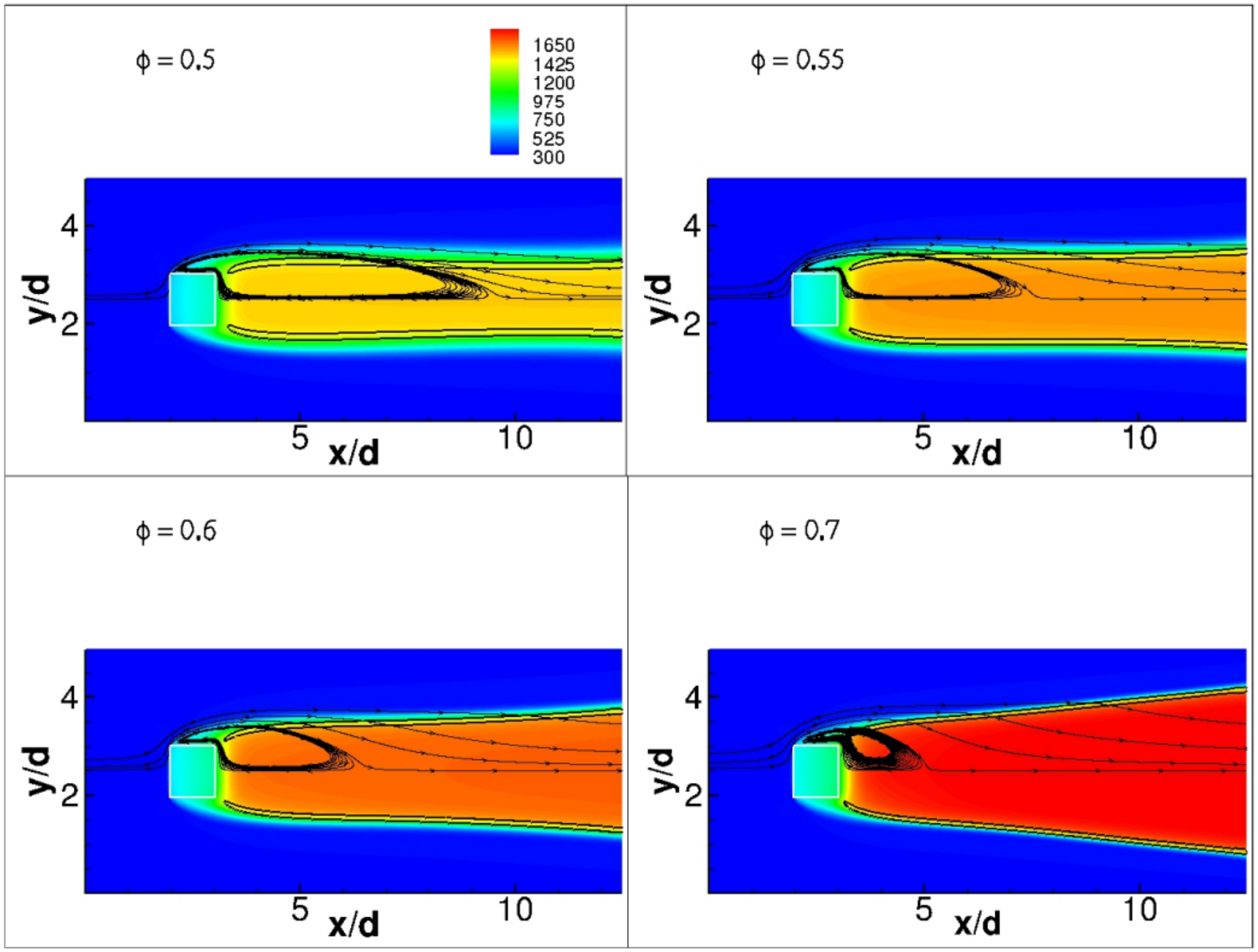

Kedia and Ghoniem, C&F, 2014, 2015

Flame-structure

Negative flame displacement speed at anchoring location

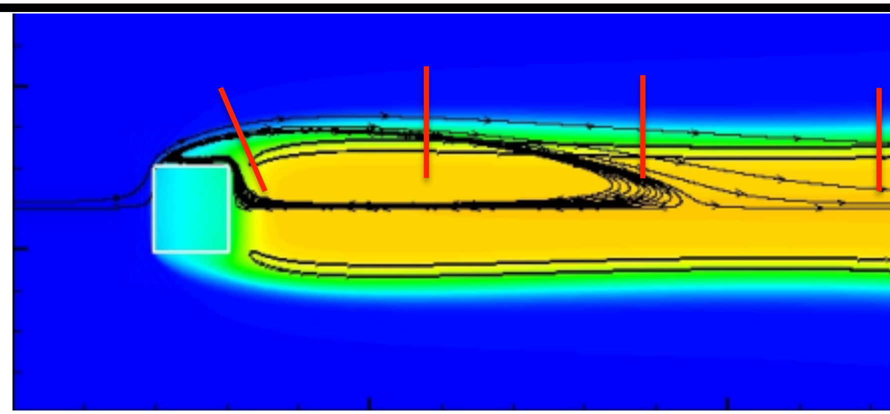

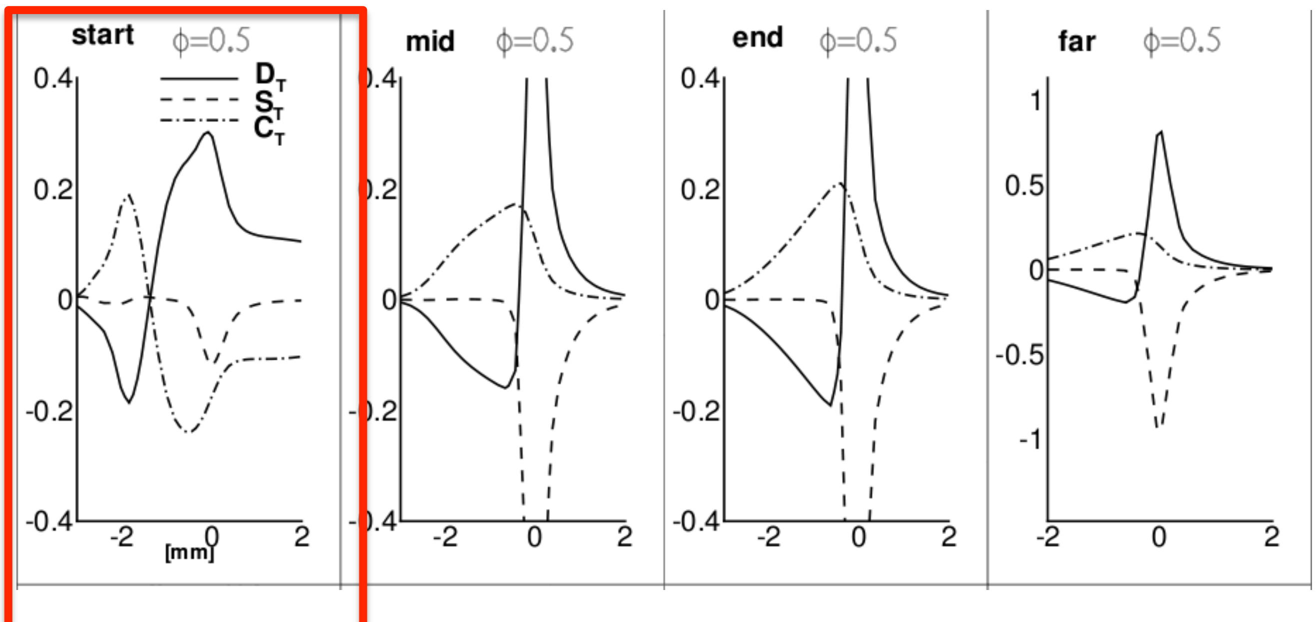

Conjugate-heat exchange

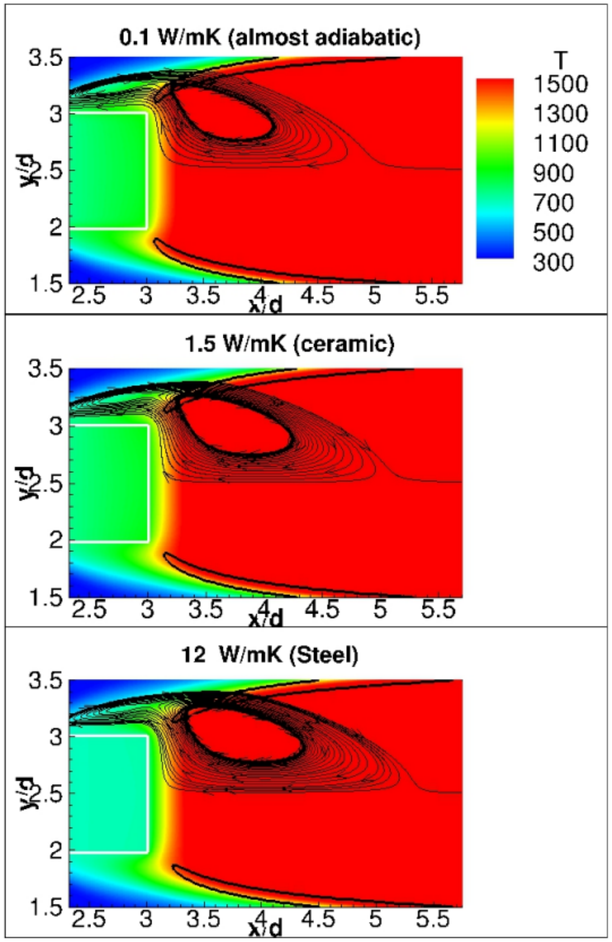

Conjugate heat exchange with the bluffbody plays a role at higher equivalence ratios

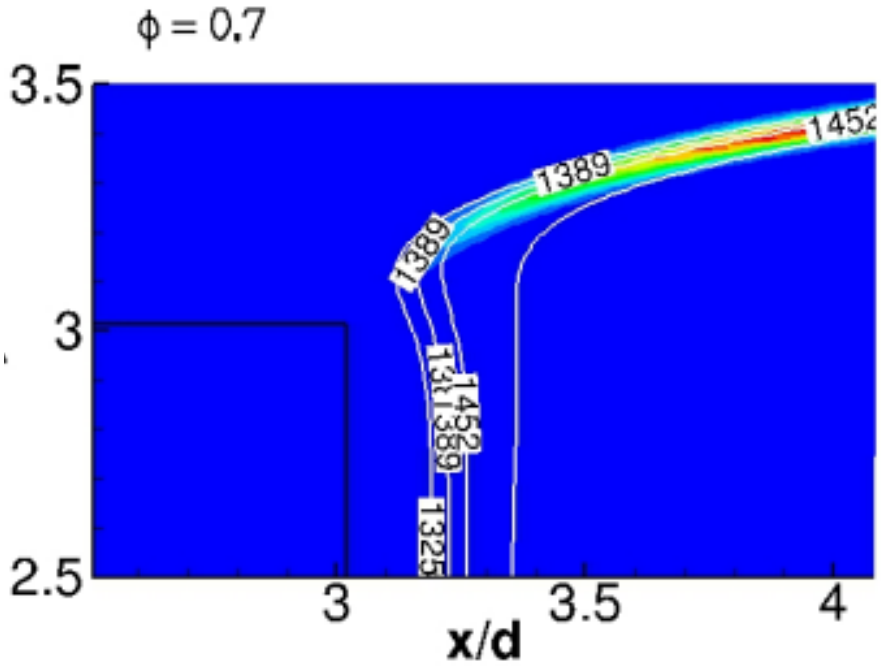

Anchoring location follows temperature contours

Preferential Diffusion

$$\phi_{local} = \frac{0.5(X_{H_2} + X_{H_2O}) + X_{CO_2} + X_{CO} + 2X_{CH_4}}{0.5(X_{CO} + X_{H_2O}) + X_{O_2} + X_{CO_2}}$$

(Barlow et al., 2012)

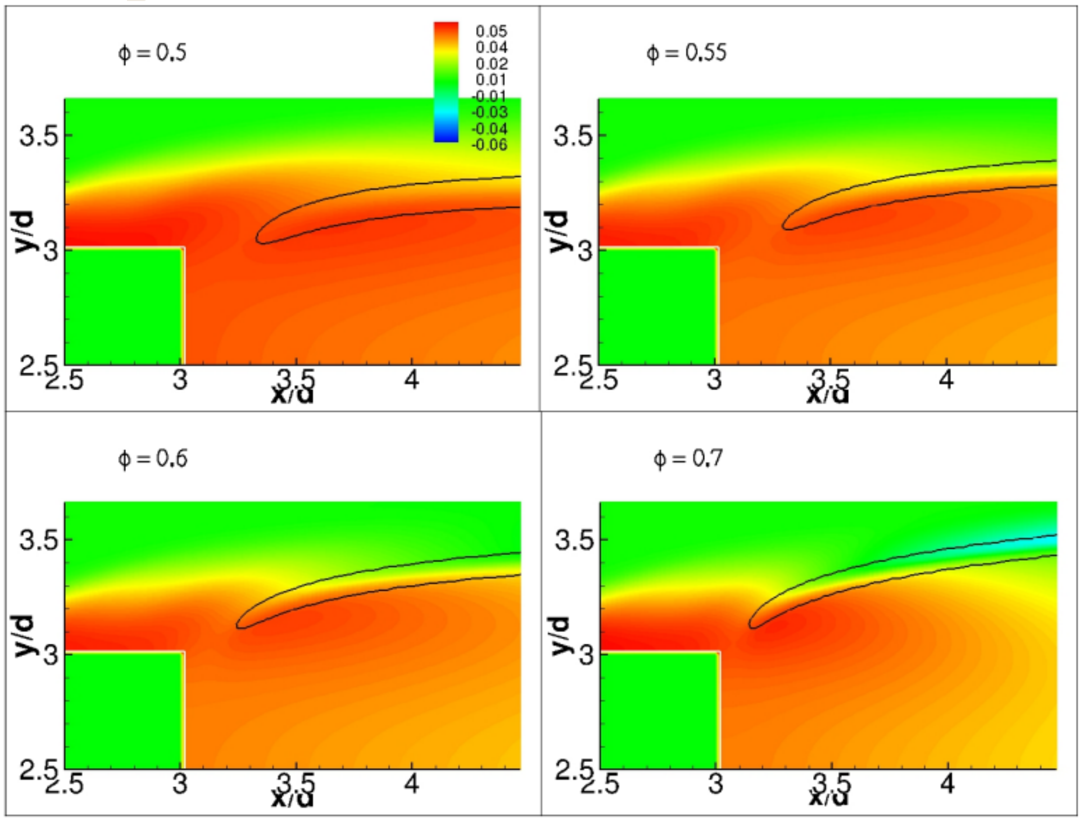

Flame leading edge finds the Locally maximum stoichiometry

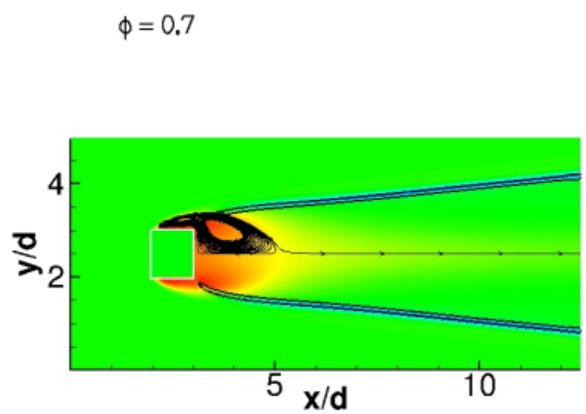

Kedia and Ghoniem, C&F, 2015 …

Residual Flames before complete blow-off

$\phi = 0.42$

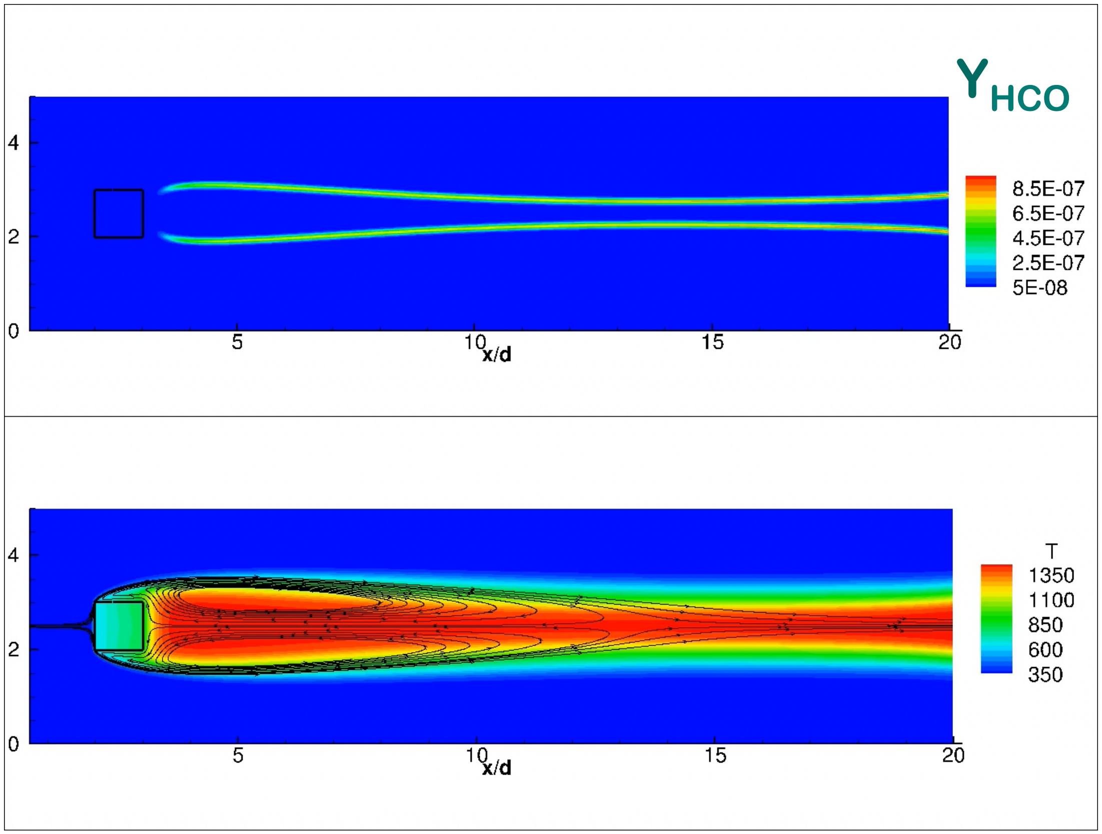

Stability Criteria

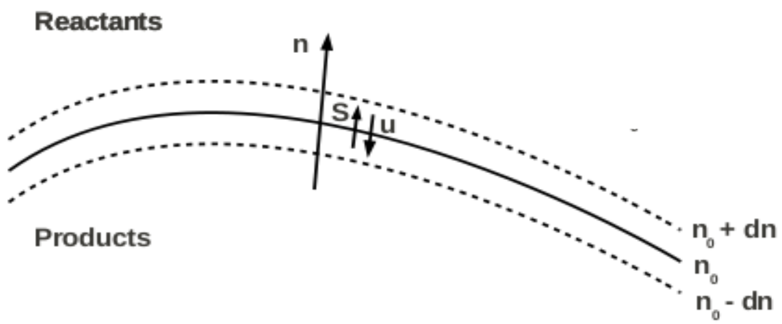

1. Static Stability: $$|S| = |v_n|$$

2. Dynamic Stability: $$\left|\frac{dS}{dn}\right| > \left|\frac{dv_n}{dn}\right|$$

(Kawamura et al. 1983)

$$S = S_u^0 - \mathcal{L}\kappa$$

$$\kappa = (\delta_{ij} - n_i n_j)\frac{\partial u_i}{\partial x_j} + S\frac{\partial n_i}{\partial x_i}$$

$$\mathcal{L}/\delta_T = \frac{1}{\gamma}\ln\frac{1}{1-\gamma} + \frac{\beta(\mathbf{Le}-1)}{2}\frac{1-\gamma}{\gamma}\int_0^{\gamma/1-\gamma}\frac{\ln(1+x)}{x}dx$$

Markstein Length **Flow property**

$$\left|\frac{dS}{dn}\right| = \left|\frac{dS}{d\kappa} \times \frac{d\kappa}{dn}\right|$$

Dynamic Stability Criterion

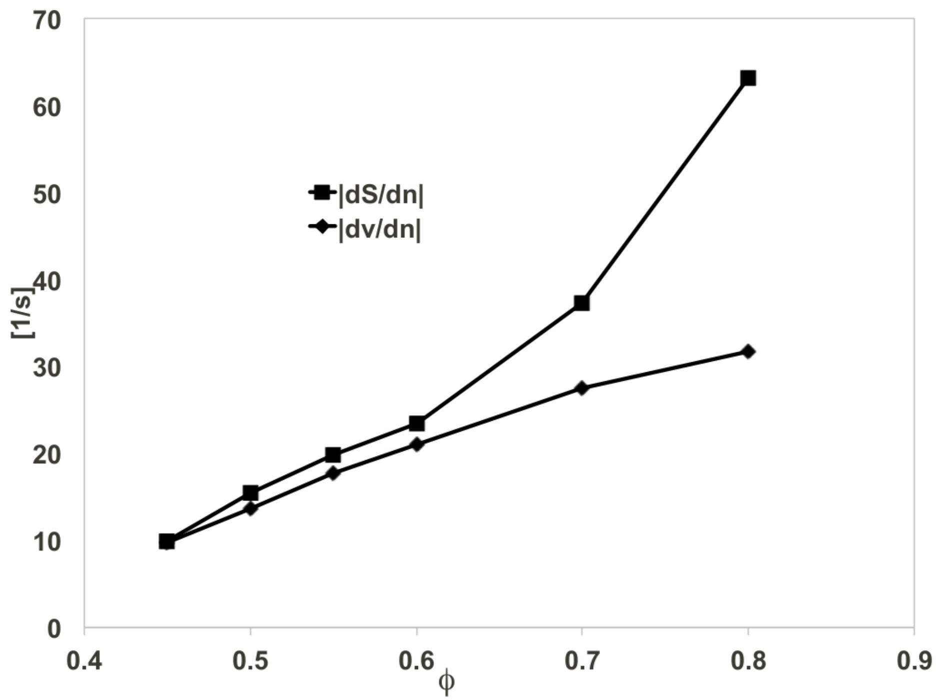

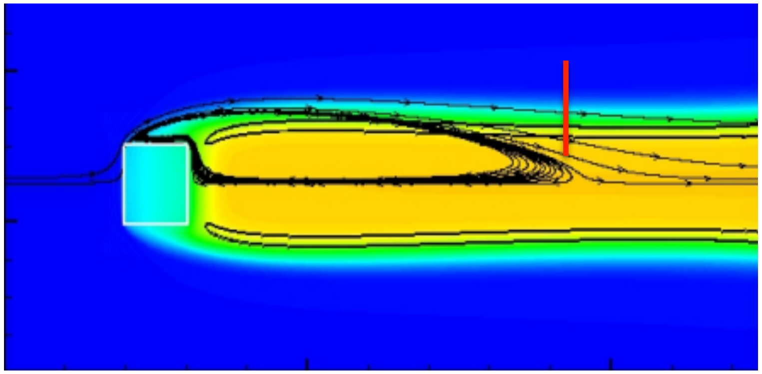

$$|\frac{dS}{dn}| = |\frac{dS}{d\kappa} \times \frac{d\kappa}{dn}|$$

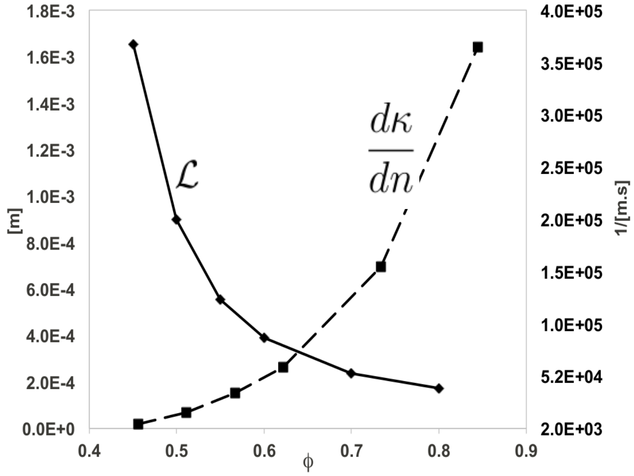

Approaching blow-off at fixed Re_d

Reference surface: 1 % methane consumption

Blow-off mechanism

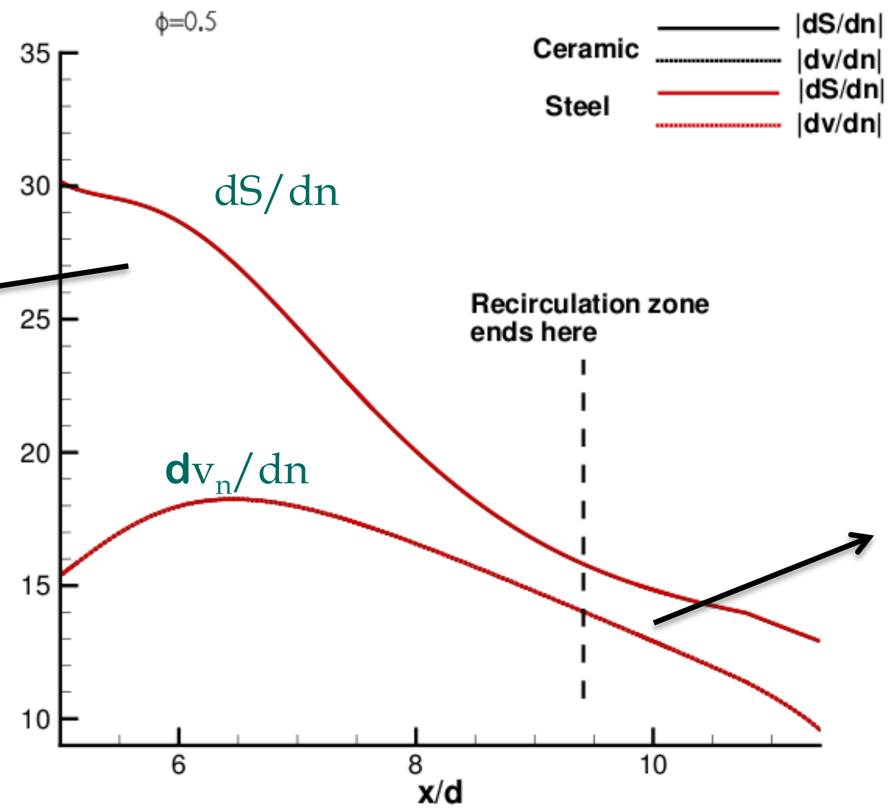

1. $|\frac{dS}{dn}| > |\frac{dv_n}{dn}|$

Strongly satisfied upstream leading to residual flames ***(Zukoski 1954)***

2. $|\frac{dS}{dn}| > |\frac{dv_n}{dn}|$

Weakest downstream leading to pinch-off

3. No impact of conjugate heat-exchange ***(Russi 1953)***

Blow-off mechanism

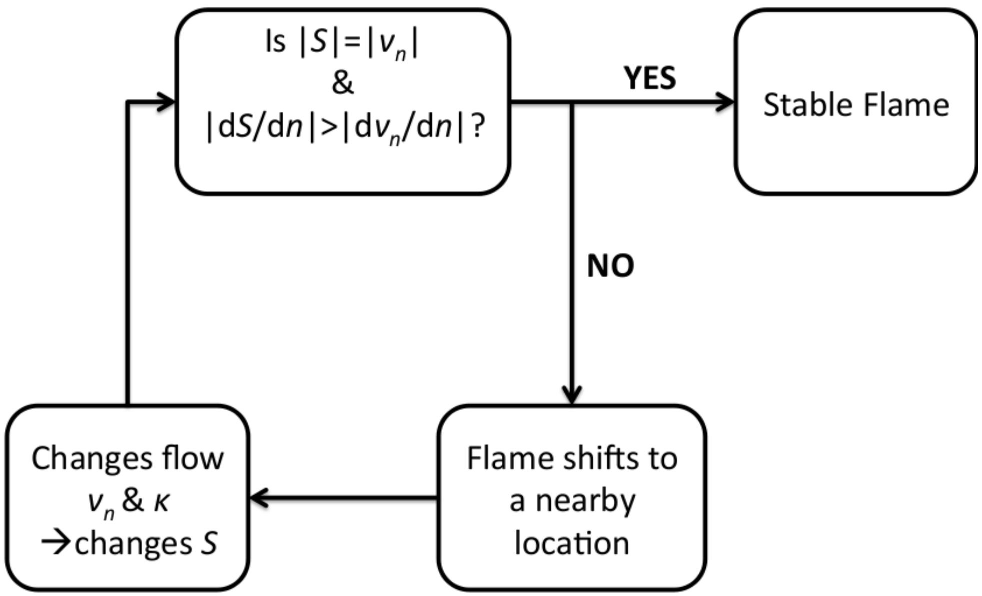

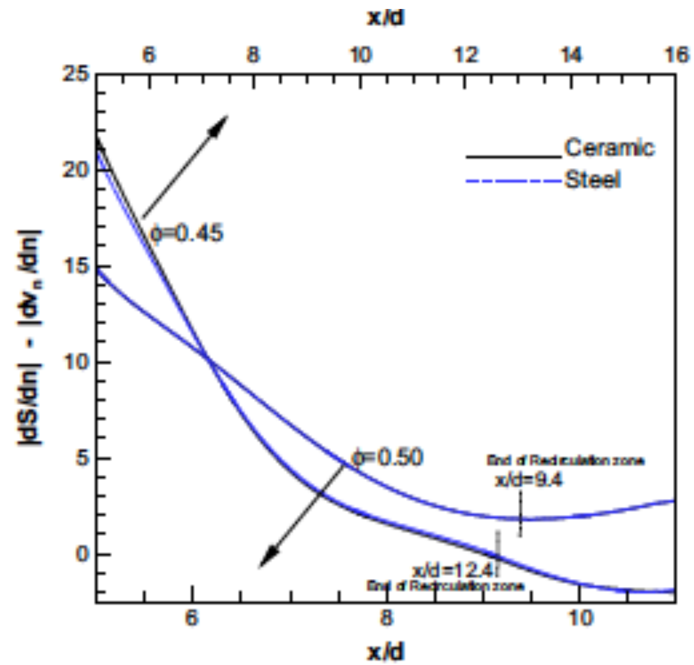

$$\mathbf{Da} = \tau_{flow}/\tau_{chem}$$

Explains the widely reported correlation ***(Shanbhogue et al. 2009)***

Wrap Up!

- Thanks for your attention
- Practical application in energy continue to push the frontier
- Challenges in CFD
  - complex fluid behavior (SCF)
  - Multiphase (dense!)simulations
  - Combustion
  - Thermochemistry and surface interactions
  - Multiscale ..